Jour. Sci. Hiroshima Univ., Ser. C, Vol. 10, No. 4, 519-582 (1996)

Geochemical Aspects of Fluid/rock Interaction in Hydrothermal Kaolinization at the Hiraki Mine, Hyogo Prefecture, Japan

By

KO KO MYINT

with 30 figures, 7 tables and 8 plates

(received, February 20, 1996)

Abstract: A kaolin deposit at the Hiraki mine, situated approximately 50 km northwest of Osaka, SW Japan, occurs in the rhyolitic non-welded tuff sandwiched between underlying rhyolite and overlying rhyolitic welded tuff of Late Cretaceous. Volcanostratigraphy of the mine area is designated as follows: (in ascending order) the rhyolite, the non-welded tuff (with three members) and the Hiraki rhyolitic vitritic welded tuff. The boundary between the rhyolite and the non-welded tuff is transitional, whereas that between the non-welded tuff and the Hiraki welded tuff is defined as unconformity. Chemically, these volcanic and pyroclastic rocks are all of low alkali and peraluminous. Variation diagrams for incompatible element pairs, both major and trace elements, suggest that the deposit was altered from a single precursor, the rhyolitic non-welded tuff. The deposit was formed by the interaction between the rhyolitic non-welded tuff and acidic fluids which passed mainly through the fracture zones formed after the emplacement of the overlying welded tuff. Mineralogically, it is composed exclusively of kaolin group with a few chlorite, illite, montmorillonite, mixed-layer clay minerals, sericite and pyrophyllite, confined to fracture zones, and ubiquitous occurrence of quartz throughout the deposit in varying degrees of abundance. Essentially, it is a kaolinite monomineralic deposit, showing no distinct zonal distribution of alteration mineral assemblages.

K-Ar ages were measured on the whole-rock samples of felsic volcanics and the clays from the Hiraki mine. The results are: (1) 70.0 ± 1.5 Ma for the underlying Kamogawa rhyolite; (2) 68.9 ± 1.6 Ma and 69.1 ± 1.6 Ma for the least-altered and altered rhyolitic non-welded tuff (= ore horizon), respectively; (3) 67.6 ± 1.5 Ma for the unconformably overlying rhyolitic Hiraki welded tuff; and (4) 63.8 ± 1.5 Ma for clays from the fracture zone crosscutting the whole volcanic sequence. These ages are fairly consistent with the volcanostratigraphy in the mine area, indicating that various volcanisms and mineralization took place within a time span of a few million years in the latest Cretaceous to the earliest Tertiary Periods. The unconformity recognized, therefore, means a minor time-gap, not a long cessation of volcanism, at least in the Hiraki mine area.

Immobility of element during the hydrothermal alteration was tested for Al_2O_3, TiO_2, Nb and Zr. Among them Zr and Nb show highest immobility throughout the deposit. Mass-transfer calculation, based on Zr as an immobile element monitor, and petrographic evidences reveal the followings: (1) dissolution of CaO, Na_2O, K_2O, Fe_2O_3 and MnO in the kaolinite zone; (2) slight enrichment of K_2O and Fe_2O_3 in the sericite "zone"** and chlorite "zone", respectively; (3) dissolution of silica at the initial stage and later precipitated as quartz from the fluid introduced to the system during alteration process; (4) immobility of Zr and Nb, as well as less immobility of TiO_2 and Al_2O_3 in the whole deposit; and (5) Al_2O_3 content in the non-welded tuff might vary within the range of 15 to 24 wt% .

Hydrogen and oxygen isotopic studies were carried out on the ore specimens and whole-rock samples to obtain information on the type of water responsible for alteration process and nature of water-rock interaction at the Hiraki mine. δD and $\delta^{18}O$ analyses, expressed as ‰ relative to SMOW, of the volcanic host rocks and ores (kaolinite+quartz) reveal that all the volcanic sequences display their magmatic $\delta^{18}O$ nature but with D-depleted nature except for the overlying rhyolitic welded tuff, while ores, exclusively localized in the underlying non-welded tuff, are much depleted in both D and $\delta^{18}O$ compared to a protolith, the non-welded tuff. Hydrothermal quartz shows $\delta^{18}O$ values of around 8 ‰. Kaolinite has a fairly consistent isotope values at δD of -94 ‰ and $\delta^{18}O$ of 0.9 ‰. Among alteration minerals, chlorite shows isotopically lowest value in δD of -138 ‰, probably due to its Fe-rich composition.

Equilibrium oxygen isotopic fractionation between quartz and kaolinite in ore is indicative of the formation temperature of about 150° C, which is consistent with the preservation of marcasite throughout the ore deposit. Pressure prevailing in the alteration process is estimated to be vapor pressure. The fluid-rock interaction is likely to have been isothermal and isobaric process. Isotope-shift and the presence of marcasite in the deposit indicate that the kaolin mineralization occurred under acidic condition (pH < 5).

Fluid flux, which passed through the system during the hydrothermal alteration, is calculated based on the material-balance of K^+ between fluid and precursor. The result reveals that the amount of fluid would be as much as 15000 times (in volume) of the host rock.

Infiltration metasomatism is a possible mechanism of the hydrothermal alteration at the Hiraki kaolin deposit. The fluid incurred the non-welded tuff at the inlet of metasomatic column was equilibrium with kaolinite and would have a concentration of log m_{K+} = -4.29 and log m_{Al3+} = -11.39 at assumed concentration of log m_{SiO2} = -2.8 and pH = 4.79. Most of time in the course of alteration, hydrothermal fluid would be slightly undersaturated with respect to muscovite. Non-stoichiometric clays were formed in place of muscovite. It is pointed out that the hydrothermal alteration process could be primarily controlled by composition, especially of a $H+$ (pH), of the fluid which reacted with the host rock.

Nature of the isotope shift between the host-rock and ores suggests that the water, i. e. ore fluid, reacted with the non-welded tuff would be a mixture of acidic meteoric water with isotope values of δD = -120‰ and $\delta^{18}O$ = -16‰, and magmatic water. Possible existence of meteoric water with such extremely light isotope values in the Hiraki mine area suggests that the Japanese island would be situated at much further north of the present location during the latest Cretaceous to the earliest Tertiary.

During the formation of kaolin deposit, the Hiraki welded tuff served as a cap-rock. Possible sources of magmatic water and heat would be the latest Cretaceous granite intrusions, though not exposed in the mine area, but crop out somewhere in the Hyogo Prefecture. A possible model of formation of the Hiraki kaolin deposit is presented.

** The word "zone" is used as an informal term for the mineral assemblages with indistinctive boundary in spatial distribution.

Contents

I. INTRODUCTION

The main purpose of the present research is to investigate the geochemical aspects of fluid/rock interaction being responsible for hydrothermal kaolin mineralization at the Hiraki mine. Major problems to be solved are: (1) re-establishment of volcanostratigraphic column according to field survey and K-Ar age determination; (2) nature of chemical and mass changes during alteration; (3) ambient physical condition in the formation of ore deposit; (4) physicochemical stability of alteration minerals, especially of mixed-layer clay minerals; (5) possible reaction path of alteration process and composition of fluid which interacted with rock; (6) fluid/rock ratio prevailing in fluid/rock interaction; (7) origin of ore fluid(s); and (8) most important controlling factor in the formation of hydrothermal kaolin deposit.

The Hiraki mine, a leading kaolin producing mine in Japan with annual production of about 50,000 tons of kaolinite concentrate (Taninami, 1991), is located at about 50 km northwest of Osaka, southwestern Japan. The kaolin deposit of the mine is of strata-bound with a bonanza occurring as a core of wedge-shaped hydrothermally altered non-welded tuff of about 100 m thick, sandwiched between the overlying latest Cretaceous rhyolitic welded tuff and the underlying vitritic rhyolite. Previous exploration works disclosed the nature of alteration and extension of mineralized zones, and rendered an opportunity to operate large-scale underground mining methods, such as sub level-stoping and mechanized cut and fill, now operating at the Hiraki mine. This is the first achievement that the large-scale truckless underground mining method has been applied well to a clay deposit in Japan (Taninami, 1991). The Hiraki ore, low in alkalis and iron contents, is suitable for raw materials for glass-fibers and hence, the mine is one of the leading suppliers of glass-fiber clays in Japan. Although the mine has been exploiting for nearly thirty years, previous explorations focused mainly on economic aspects. Therefore, little has been known about its detailed mineralogy and geochemistry, except for some publications on mixed-layer clay minerals (e.g. Kanaoka, 1980).

The stratigraphic position of the non-welded tuff, intervening the Hiraki welded tuff above and rhyolite (the Kamogawa Fm.) below, is somewhat controversial between Ozaki and Matsuura (1988) and Taninami (1991) in one hand, and Ko Ko Myint and Watanabe (1995) on the other. Ozaki and Matsuura (1988) and Taninami (1991) placed the non-welded tuff at the lower stratigraphic position than the rhyolite, whereas Ko Ko Myint and Watanabe (1995) designated it as a new lithostratigraphic unit and assigned at the upper stratigraphic position than the rhyolite lava. Thus volcanostratigraphic column of the lithologic units in the Hiraki mine area needs to be revised according to radiometric datings and field occurrences.

Timing of volcanism in the mine and its environs is generally agreed to be the Late Cretaceous on the basis of K-Ar datings on some minerals of the Hiraki welded tuff (Ozaki and Matsuura, 1988, and Shibata et al. 1984). However, no age data are available for the rhyolite and the non-welded tuff, two major lithologic units, and for ores of the Hiraki mine itself. Therefore, new age data will be presented for the whole lithologic sequence exposed in the mine area and for alteration minerals (clays) to clarify the above controversial stratigraphic sequence and temporal relationship between mineralization and volcanic events, as pointed out by Ko Ko Myint and Watanabe (1995).

Studies of hydrothermal alteration zones formed in homogeneous volcanic units (single precursor systems) associated with Canadian volcanogenic massive sulfide deposits such as those of Phelps Dodge deposit, Matagami (MacLean and Kranidiotis, 1987), Atik Lake, Manitoba (Bernier and MacLean, 1989), and some others in the Noranda district (Cattalani et al., 1989, and MacLean and Hoy, 1991) show that Al, Ti, Zr, Nb, Yb, and Lu are essentially immobile in hydrothermal alteration processes associated with massive sulfide deposition. Immobility of elements are tested for potential candidates (herein Al, Nb, Ti and Zr) and then most immobile elements or element-pair were used to adjust all other major elements. Correction procedure is based on the assumption that the changes in immobile element contents between precursor and altered rock are resulted from the gains and losses of mobile components in mass during volume constant alteration, where mechanical transfer is compensated by changes in porosity or specific gravity. Differences in the contents of these immobile elements between the altered rocks and the precursor are, thus, expressed as function of mass changes and can be used to calculate additions and depletion of the mobile elements in wall-rock alteration. Since alteration zones associated with massive sulfide deposits were formed by metasomatism, the principle used can also be applicable to the mass transfer process of any other hydrothermally altered rocks irrespective of whether they are related to massive sulfide mineralization or not.

It is emphasized that in the Hiraki deposit, unaltered precursor of the kaolin ores is partly exposed in the middle part of the orebody. Hence, the precursor composition can be determined exactly, resulting in better understanding of chemical and mass changes involved in hydrothermal alteration.

Although the Hiraki deposit is composed of quartz as a major alteration phase, hydrothermal quartz veins are completely absent in the outcrops possibly because of the disposal as gangue mineral in the early time of mine's history. Consequently, the present survey failed to find fluid inclusions consisting hydrothermal quartz. Estimation of formation temperature was done by use of oxygen isotopic method.

Despite major compilation efforts in the last two decades (e. g. Helgeson, 1969; Robie et al., 1978; Helgeson et al., 1978), basic thermodynamic data of adequate accuracy are still not readily available for many phases of geologic interest, such as interstratified mixed-layer minerals which are common alteration minerals in the hydrothermal clay deposits including Hiraki. Stability fields of these nonstoichiometric mineral are delineated in the activity diagrams by either hypothetical end-members or pseudostoichiometric analogs. But they rarely

represent the wide spectrum of composition observed in natural minerals. Thus, chemical stabilities of non-stoichiometric clay minerals are defined in the activity diagrams based on the assumption of solid-solution model proposed by Giggenbach, 1985.

Early studies of irreversible reaction in the water-rock interaction were started from empirical works of the hydrolysis of feldspars (e.g., Hemley and Jone, 1964; Hemley et al., 1971; Fisher and Zen, 1971; Gordon, 1973; Helgeson et al., 1975; Montaya and Hemley, 1975) and gained much progress by the mass transfer calculation (e. g.,.Helgeson, 1968; Helgeson, 1969; Helgeson et. al., 1970). Independent of mechanism, alteration of K-feldspar is theoretically predictable to form a zone sequence (from host-rock towards fluid) of K-feldspar / muscovite / kaolinite / fluid. Although an apparent lack of certain alteration mineral zone in a normal metasomatic column has been pointed out by some author (e.g., Korzhinskii, 1970) and mathematical approach to solve this problem is proposed by some (e.g.. Lichtner and Balashov, 1993), satisfactory explanation is not available, yet. The Hiraki deposit is characterized by its kaolinite monomineralic zone and almost absence of pure muscovite zone between the orebody (kaolinite) and precursor (K-feldspar). In the present study, alteration zone sequence in the Hiraki kaolin deposit is firstly considered under feldspar hydrolysis process and infiltration metasomatism, and then the absence of muscovite zone between K-feldspar and kaolinite zones is explained with the aid of solid-solution of clay mineral hypothesis proposed by Aagaard and Helgeson (1983), and Giggenbach (1985). This hypothesis expresses the formation of non-stoichiometric dioctahedral clay minerals instead of muscovite when activities of muscovite and pyrophyllite decrease. Also estimated are the possible reaction path during alteration process and the composition of inlet fluid responsible for the alteration zonal arrangement in the Hiraki deposit.

By use of analyzed precursor composition and estimated inlet fluids composition, water/.rock ratio prevailing at the time of hydrothermal alteration is calculated by the material-balance of K^+ between fluids and rock.

Inasmuch as H_2O is the dominant constituent in fluid-rock interaction, a knowledge of light stable isotope systematics are of fundamental importance in the understanding of a source of ore fluid(s) and alteration mechanism (e.g., Taylor, 1979).

However, there have so far been very few studies on the origin of ore fluids responsible for so-called hydrothermal clay deposits in Japan (e.g., Watanabe et al., 1994). The presence of unaltered precursor gives also a good opportunity to examine isotopic relationships among the precursor, altered rock (ores) and fluid(s). Based on hydrogen and oxygen isotopic ratio measurements of host rocks, ore samples and quartz, the evaluation on nature and role of ore fluids, conceivably H_2O, responsible for the hydrothermal kaolin deposit at the Hiraki mine will be described and discussed.

Finally, a genetic model for the formation of kaolin deposit at the Hiraki mine is presented.

II. GEOLOGY

1. Regional setting

Geologically, the Hiraki mine is located in the Sanda area (Southwest Japan), situated in the Inner Zone delineated by the Medium Tectonic Line. The oldest rock unit exposed in the area is of Late Cretaceous acidic volcanic rocks of the Arima Group (Fig. 1), which in turn is overlain unconformably by the Tertiary and Quaternary sedimentary units, viz. the Kobe Group (Eocene - Oligocene), the Osaka Group (Pleistocene), and younger terrace deposits. Dikes of granite porphyry, porphyrite and quartz porphyrite of probably latest Cretaceous intruded into the Arima Group and other younger units especially in the eastern-half of the area.

Earliest descriptions on the geology of the Hiraki mine and its environs are those of Tanaka et al., (1963), who divided the Arima Group of Late Cretaceous into two formations: Lower — rhyolitic tuff, tuff breccia, and welded tuff; and Upper — dacitic welded tuff (Taninami,1991). Ozaki and Matsuura (1988) reinvestigated this area and correlated the Tanaka's Lower formation to the Kamogawa formation and the Upper formation to the Hiraki Welded Tuff. The Kamogawa formation consists of four units: (in ascending order) (1) tuffaceous mud stone, sandstone and conglomerate; (2) rhyolite non-welded tuff, pumice tuff and stratified tuff; (3) rhyolite welded vitric tuff; and (4) rhyolite lava. The Hiraki Welded Tuff lies unconformably over the Kamogawa formation and it can be subdivided into two parts; Upper - Rhyolite welded vitric-crystal tuff (with basal non-welded crystal vitric tuff and vitric tuff), and Lower - Rhyolite welded vitric-crystal tuff and tuff breccia (with tuffaceous mud stone and sandstone) (Ozaki and Matsuura, 1988). At the Hiraki mine area, the Hiraki Welded Tuff comprises rhyolitic welded vitric-crystal tuff often showing flow texture. K-Ar datings on biotite and K-feldspar of the Hiraki Welded Tuff gave 70 ± 3.5 Ma (Ozaki and Matsuura, 1988) and 72.7 ± 2.3 Ma (Shibata et. al., 1984), respectively. Because of its limited areal extent, complete sequence of the above units cannot be detectable in the Hiraki mine, exposing only the upper part of the Hiraki welded tuff, the non-welded tuff, and the Kamogawa rhyolite (Fig. 2).

Major regional structural trend developed in the Sanda area can be subdivided into two; ones developed in the Mesozoic units have a N - S general trend, whereas the Cenozoic units show general trend of E - W. Compared to the Mesozoic units, the Cenozoic units were weakly affected by structural disturbances, since NEE - SWW trending major faults, well developed in the Arima group are relatively absent in the younger units. This fact is consistent with the geological history of Japanese islands, in which the Cretaceous is the period with strongest diastrophism and igneous activity (Tanaka, 1977).

The most prominent fracture system having an alignment of N 70° E developed in the mine area is very likely to have been formed prior to the hydrothermal alteration and served as channel ways for fluids to invade

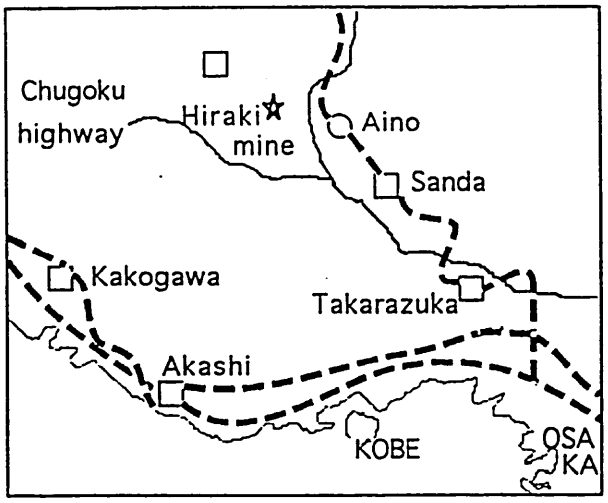

(a)

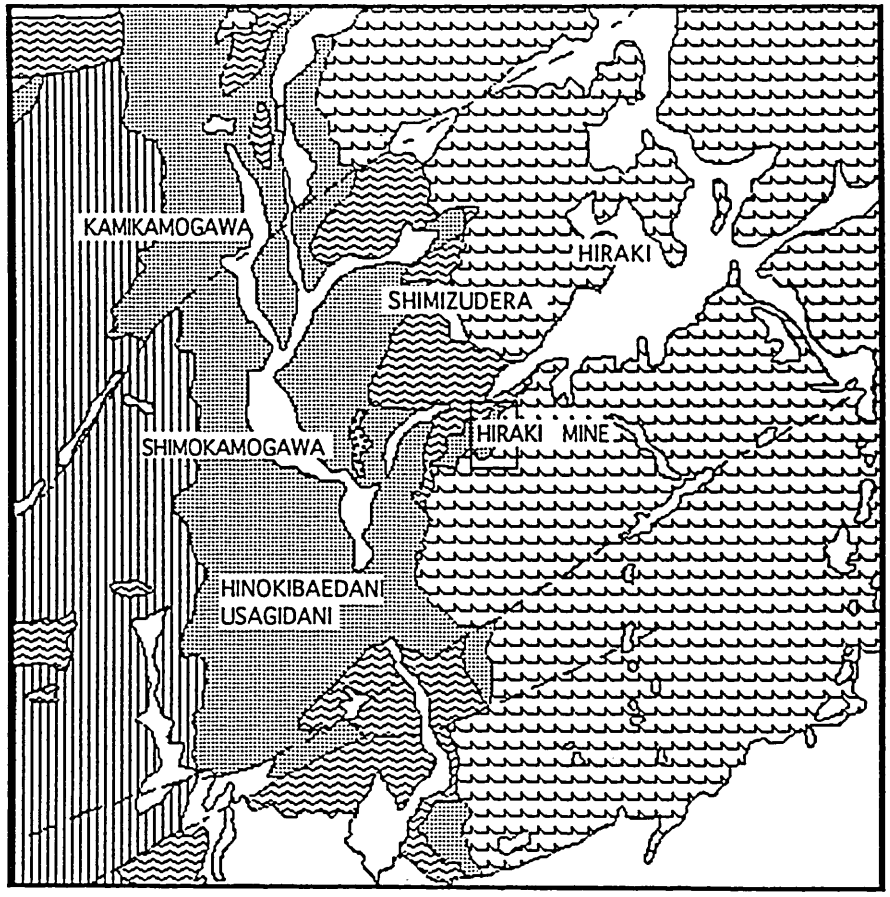

(b)

(modified after Ozaki and Matsuura, 1988) 0 1 2 km

Late Cretaceous

- Tertiary and Quaternary sediments
- Hiraki welded tuff (Upper part)
- Rhyolite
- Welded tuff
- Non-welded tuff
- Tuffaceous mudstone, sandstone and conglomerate

Fault

Fig. 1 (a) Location and (b) regional geologic setting of the Hiraki mine and its environs.

Fig. 2 (a) Outcrop map and (b) cross-section along A-B of the ore deposit in the Hiraki mine. (c) Generalized cross-section of volcanic sequences and orebody. ((a) and (b) are modified after Taninami, 1991.)

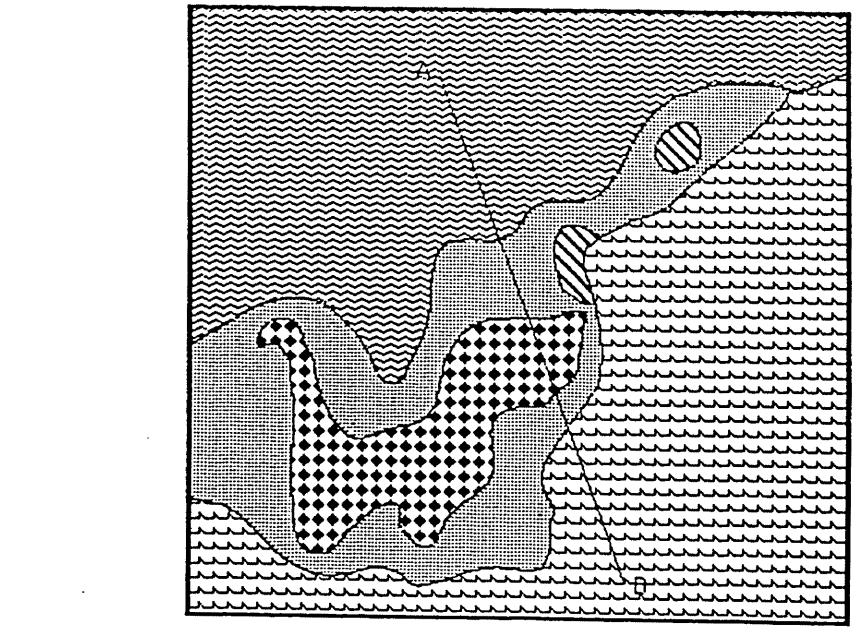

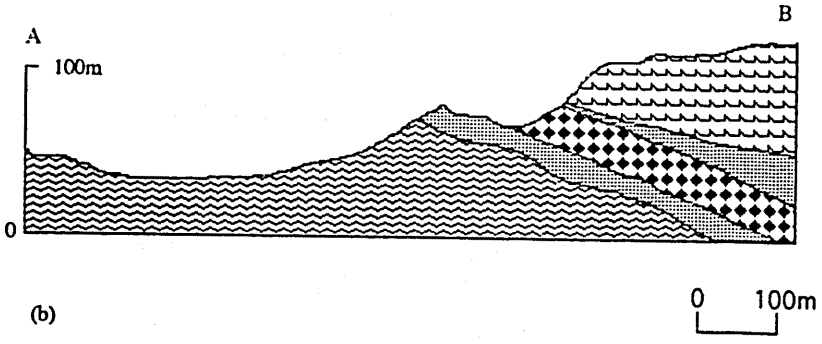

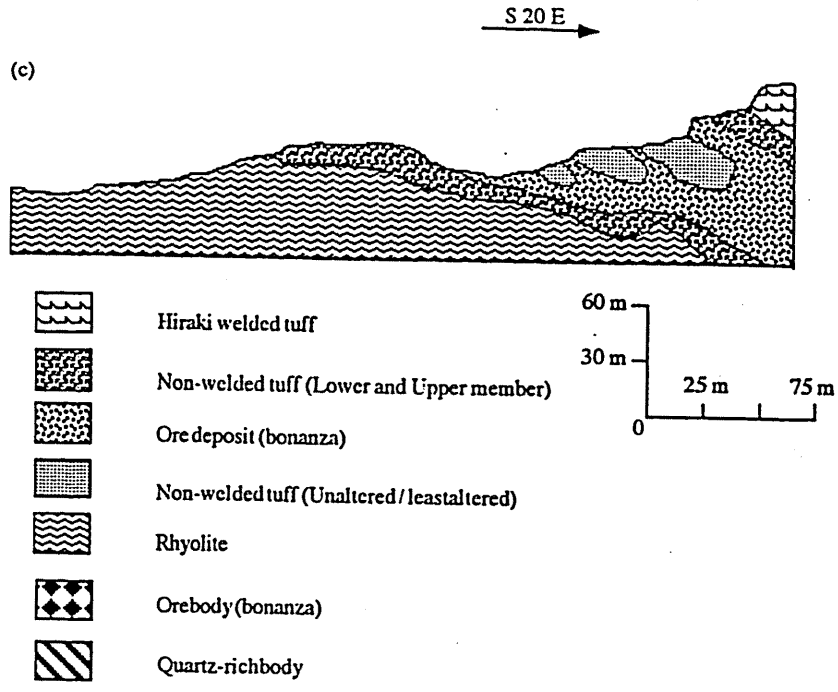

host rocks. At least four large fractures, one of which exceeds 10 m in width, and numerous small ones are found to occur in the open-pit. Since the traces of these fractures are continuing into and vanish inside the Hiraki Welded Tuff, timing of deformation and mineralization could be estimated as at least after the Hiraki Welded Tuff, 73 ~ 70 Ma. However, it is noted that the cross-cutting relationship becomes obscured in the underlying non-welded tuff (ore zone) possibly due to the extensive alteration. Thus, mineralization age should be known based on dating of ore sample themselves, which will be discussed in detailed elsewhere.

2. Volcanostratigraphy

At the Hiraki mine , the volcanic sequence can be subdivided into three formations: (in ascending order) the rhyolite lava flow; the non-welded tuff; and the Hiraki welded tuff (Fig. 3). Both the lower boundary of the rhyolites and the upper limit of the Hiraki welded tuff cannot be defined in the mine area. The Hiraki welded tuff, corresponding to the Hiraki Welded Tuff defined by Ozaki and Matsuura (1988), lies unconformably over the non-welded tuff. Their contact is demarcated at the boundary where. the strongly altered non-welded tuff meets the hard and compact Hiraki welded tuff. On the contrary, the rhyolite grades conformably upwards to the non-welded tuff. The boundary between the rhyolite and non-welded tuff is defined at first appearance of spherulitic parts of the rhyolite or reddish brown rhyolite with flow structure. Chloritization and sericitization in the uppermost part of the rhyolite somewhat obliterate boundary characters and sometimes it is impossible to distinguish one from another.

Rhyolite

The rhyolite, forming the basement rock in the mine area, can be divided into two units: (1) the lower unit consisting of reddish, massive vitric flow-structured rhyolite; and (2) the upper unit composed of alternated sequence of massive, flow-structured rhyolite layer (3 ~ 10 cm thick) and rhyolitic spherulitic (mostly feldspars) layers (3 ~ 10 cm). Due to the alteration, the uppermost part changes into the kaolinite-chlorite "zone" with a small amount of sericite, while the massive portion results sometimes in quartz rich kaolinite-sericite "zone". Both zones never exceed a few meters in thickness.

Non-welded tuff

According to the exploration up to the present, non-welded tuff, striking about N 20° E with dip of 20° SE, has an average vertical thickness of 100 m with 300 m in length and about 250 m in width (NE - SW) in the mine area (Taninami, 1991). On the basis of its texture, structure and nature of alteration products, this unit, being composed essentially of rhyolitic lapilli-tuff, can be divided into three members as lower, middle and upper. These three members are considered as individual, distinct bedding sets within a single pyroclastic co-set, non-welded tuff. Since contacts between these members are obliterated due to the alteration and not detectable in the field, the individual thicknesses are estimated from borehole data and lithostratigraphic characteristics used to define individual members.

The lower member is a massive pyroclastic bed characterized by internally structureless, ill-sorted lapilli-tuff to lapillistone in which lapillus autoclasts are randomly embedded in the matrix tuff. Most of lapilli are less affected by the alteration, whereas tuff altered to quartz and kaolinite assemblage. This member has a varying thickness of 10 ~ 30 m and more extensively develops at the marginal portion of the orebody.

The middle member is an alternation of medium-bedded fine tuff, ash layer and lapilli-tuff, in which laminations shown by oriented fragments are well developed. At the alteration front, this member merges laterally into a massive unit with ghost bedding made up of trains of lapilli which fade out away from the least-altered portion to the altered one (ore zone). Within this bedding set, there occur numerous subsets decorated as many repeated sequences of 10 ~ 20 cm thick fine tuff intervened by 0.5 ~ 2 cm ash layers. Although most of these have been altered, some relic bodies of unaltered portion can be observable in the middle part of the ore deposit. This member is about 50 m thick and mainly developed in the central portion of the non-welded tuff which was later transformed to bonanza.

The Upper member is medium-bedded lapilli-tuff unit, in which beddings are marked by alignments of discontinuous planar tracks of lapilli. Even after the alteration, these lithic trains are traceable, while ash turned to kaolinite and quartz. This member has an approximate thickness of 20 m.

Based on the above characteristics observed in the least-altered bodies exposed in the middle part of the ore zone, the depositional sequences of the non-welded tuff can be deduced as poorly sorted, massive lapilli-tuff in the lower part, through alternated sequences of bedded fine tuff and lapilli-tuff in its middle part and medium bedded lapilli-tuff in the upper. Major differences between the lower and upper members, both of lapilli-tuff, are the size and alignment of lapillus. Lapilli in the lower member are large (3 ~ 6cm) and randomly embedded, whereas those in the upper member are small (rarely exceeding 4 cm) and well oriented. In the upper member the ash content predominates over the lapillus content, but opposite nature is true in the lower member.

The above deduced sequence suggests that during the initial stage of eruption, the volcano gave out a huge mass of various size of pyroclasts, which is too much to be sorted out, and thus, resulted in the formation of basal surge or pyroclastic flow deposit, i.e. the lower member. In the course of time, pyroclasts would be changed to mostly ash and fine lapilli and, rested as fallout deposits, i.e. the middle and upper members.

It is very difficult to describe the detailed lithologic characters of pre-altered non-welded tuff, since it was intensively altered and leaving a few evidences of syndepositional structure. However, on the basis of lithostratigraphic, structural and chronological relationships, the author designate this unit as a new lithostratigraphic unit, which places at the uppermost part of the Kamogawa formation (Fig. 3). It can be lithologically correlated with the Rhyolite non-welded tuff, pumice tuff and stratified tuff of Ozaki and Matsuura (1988), but stratigraphically not.

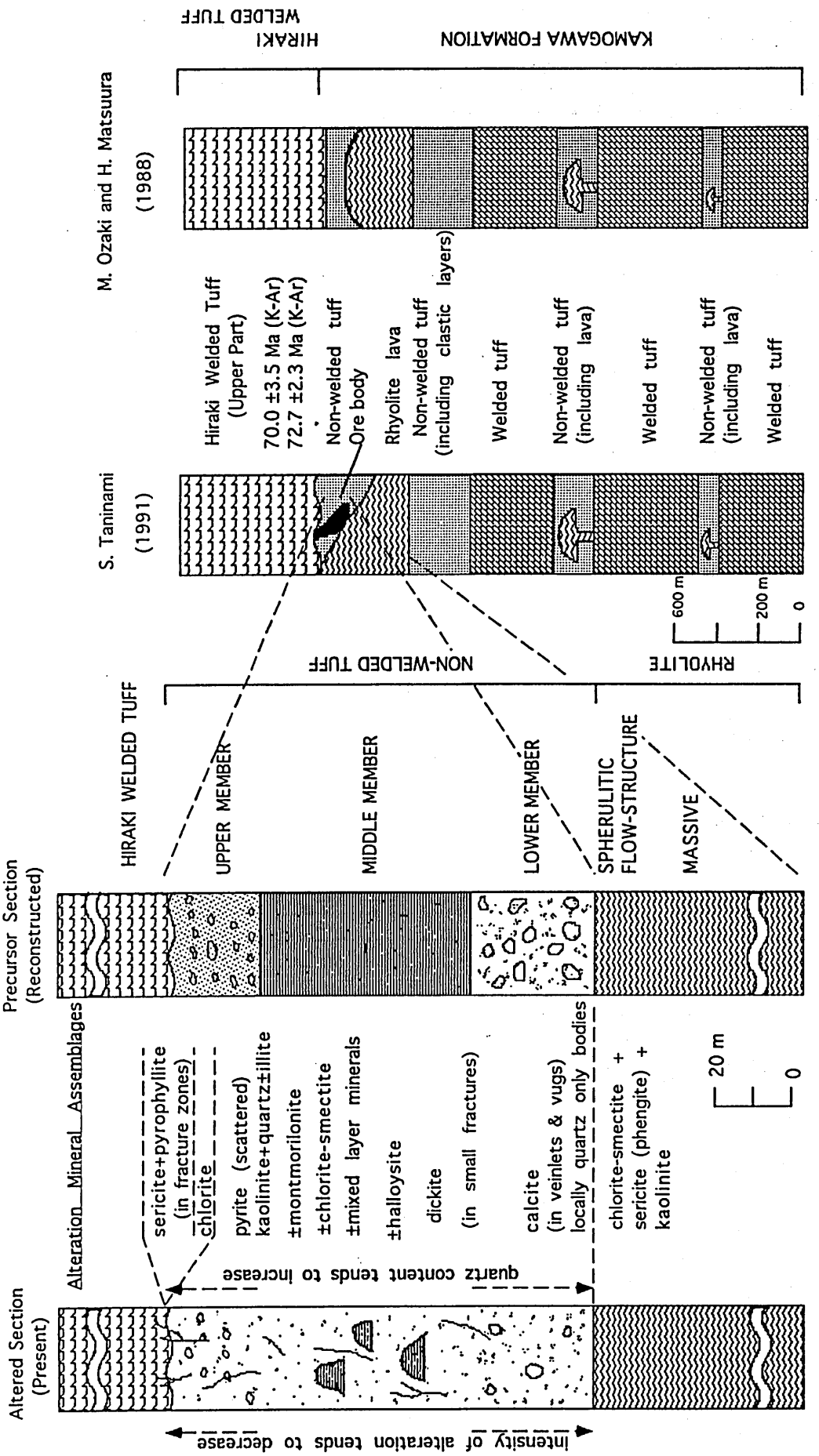

Fig. 3 Volcanostratigraphic column of the lithologic unit exposed in the Hiraki mine area established by present work (two columns in the left) in comparison with those of previous works. Note that the non-welded tuff of present work is a newly established unit and is not correlatable with the non-welded tuff of Ozaki and Matsuura (1988).

Hiraki welded tuff

The Hiraki welded tuff in the mine is correlative with the Upper part (without basal portion) of the Hiraki Welded Tuff defined by Ozaki and Matsuura (1988). Since the mine's non-welded tuff can be delineated from the overlying welded tuff by unconformity, it cannot be correlated with the basal portion of Ozaki and Matsuura (1988).

Since the present investigation is restricted to the mine area, most of which is covered by the non-welded tuff and hence, no further description on the Hiraki welded tuff and rhyolite can be possible.

3. Petrography

In this section petrography, mainly microscopic characteristics, of representative rock specimens of all volcanics and volcaniclastics cropping out in the mine area are described together with brief discussion on petrochemistry. Inasmuch as the whole volcanostratigraphic sequence underwent alteration lesser to a greater extent, petrographic studies, especially for non-welded tuff, were largely based on altered specimens and thus their pre-altered characteristics and petrogenesis are of a little conjectural.

Rhyolite

Microscopically rhyolite has hypocrystalline texture in which crystals and spherulites of feldspars (mostly K-feldspar and albite) and chalcedonic quartz, and biotite are embedded in cryptocrystalline groundmass of quartz and feldspars. Spherules are mainly composed of a dense mass of very fine intergrown needles of both alkali feldspars and quartz radiating from a common nucleus, and some of them exhibit various textures such as hollow spherulites, lithophysa and axiolites (Plate I & II). There are also aggregates of quartz crystals displaying spherulitic texture and they resisted to the alteration. Some specimens often show granophyric texture formed by intergrown quartz and alkali feldspar microlites. In the uppermost part of the alternate sequence, all of feldspar phenocrysts are altered to sericite (Plate III) and locally, biotite changes to chlorite.

Under the ore microscope, opaque minerals consist of small grains (0.05 to 0.1 mm) of euhedral ilmenite and sub- to euhedral pyrite. Some of ilmenite are oxidized. Euhedral pyrite often shows cubic form and less commonly aggregates of tiny globules and colloform-like texture. Co-existence of subhedral marcasite and pyrite is also observable.

Non-welded tuff

Under the microscope the non-welded tuff shows fragmental matrix supported texture in which quartz, feldspars, and rock and glassy fragments are embedded in cryptocrystalline glassy matrix. The glassy fragments in the rock are not welded to one another, but banded and slightly flattened fragments are not uncommon. Almost entire portion of the non-welded tuff suffered alteration, resulting in interstitial replacement of kaolinite, sericite and other clay minerals in the matrix. Feldspar crystals are altered to kaolinite. Sometimes, an apparent discontinuous laminations of glassy matrix, together with regular alignment of flattened fragments, form eutaxic texture. There are at least three types of quartz observed in the altered non-welded tuff; (1) large single crystals of igneous quartz invariably show a dissolved grain boundary embayed by kaolinite cryptocrystallites (Plate IV), (2) chalcedonic quartz spherules with no dissolved boundary which are considered as igneous spherules resistant to alteration (Plate I), and (3) amygloidal and veinlet quartz which are those precipitated from silica saturated fluids introduced into the system in the later stage of alteration. The rock fragments, although some of them were replaced by kaolinite, usually withstand to alteration. Glassy fragments were mostly devitrified and are considered to have served as a major contributor to the silica content of some specimens.

Among the opaque minerals ilmenite and magnetite show their euhedral form whereas pyrite and marcasite have mostly subhedral outline under reflected light (Plate V & VI). Usually, ilmenite grains are small (~ 0.05 mm) tabular-shaped compared to large (~ 0.3 mm) anhedral pyrite and marcasite.

Hiraki welded tuff

Microscopically the Hiraki welded tuff shows a hypohyaline texture formed by hypautomorphic to automorphic plagioclase and alkali feldspars, biotite and quartz embedded in cryptocrystalline groundmass of the same minerals and devitrified glass. Feldspars occur as crystals with various size ranging from 2.5 mm to cryptocrystalline and form seriate texture. Fibrous glassy fragments welded together and, incorporated with microlaths of feldspars, form well defined crenulated laminations (Plate VII). Composition of plagioclase ranges from albite to andesine. The welded tuff, in the fracture zones and adjacent to the altered welded tuff, consists of sericite replacing feldspar crystals and interstitial cryptocrystalline matrix forming the same alignment with tabular, elongated glass materials. Some biotites are altered to chlorite. It exhibits also granophyric texture of intergrown quartz-feldspar microlites.

Minor opaque minerals identified under ore microscope are consists of tiny (0.02 ~ 0.05 mm) sub- to euhedral ilmenite, relatively large (~1.5 mm) sub- to euhedral magnetite and very small (*Ca.* 0.01 mm) mostly euhedral pyrite. Most of ilmenite grains occur along the cleavages of large biotite crystals and sometimes embedded in large feldspar crystals. Very fine-grained pyrite is scattered through the rock and rarely together with subhedral marcasite.

4. Petrochemistry

Pressed powder pellets of all rock samples were analyzed for their major and trace elements by X-ray flourescence spectrometer using calibration curves established by Okudira et al. (1993). Note that the bulk samples used for analyses were collected from the whole alteration zones, i.e. not from veins, in order to represent a general alteration pattern and in order to avoid unnecessary high concentration of one component. Chemical data are listed in Table.1. Bulk rock analyses indicate that the volcanogenic rocks exposed in the Hiraki

Table 1. Major and trace elements contents of the volcanic rocks and ores of the Hiraki mine.

Serial No.	Specimen	SiO2	TiO2	Al2O3	*Fe2O3	MnO	MgO	CaO	Na2O	K2O	P2O5	Nb	Zr	Y	Sr	Rb	Th	Th	Zn	Cu
1	1012	76.74	0.11	14.93	1.66	0.05	n.d.	0.44	0.52	5.27	0	6	78	29	24	167	12	21	25	n.d.
2	1013	64.92	0.15	21.18	1.76	0.05	0.27	0.65	0.12	5.79	0	10	115	34	24	180	16	24	48	22
3	1014	71.28	0.13	14.56	1.87	0.06	0.32	2.78	1.96	3.21	0	8	101	27	483	90	14	19	36	n.d.
4	1015	74.57	0.11	13.65	1.64	0.05	0.07	2.14	2.53	3.64	0	7	92	24	199	116	11	18	30	n.d.
5	2017	70.63	0.12	14.23	1.59	0.05	0.09	2.87	3.55	3.13	0.02	9	105	24	572	89	16	18	32	n.d.
6	1004	71.93	0.16	22.41	0.27	0.01	n.d.	0.36	0.01	n.d.	0.01	15	290	16	18	7	10	19	4	n.d.
7	1006	76.94	0.11	16.21	0.71	0.01	n.d.	0.39	0.03	0.04	0.01	4	189	25	18	10	102	17	9	n.d.
8	1007	77.66	0.12	18.58	0.41	0.01	n.d.	0.41	0	0.12	0.01	10	193	18	12	10	11	8	7	n.d.
9	1008	71.61	0.16	22.45	0.36	0.01	n.d.	0.38	0.01	n.d.	0.01	15	275	23	15	8	13	22	7	n.d.
10	1010	62.96	0.17	23.87	3.96	0.02	n.d.	0.61	0.06	2.19	0	18	342	77	21	122	20	111	103	n.d.
11	2012	69.34	0.21	22.86	1.91	0.01	n.d.	0.39	0.05	0.06	0	14	250	10	26	8	12	23	4	n.d.
12	2021	68.31	0.14	25.15	0.43	0.01	n.d.	0.44	0.09	0.72	0.01	14	267	16	26	30	18	17	12	n.d.
13	2023	75.25	0.12	19.87	0.04	0.01	n.d.	0.41	0.13	n.d.	0.01	12	199	6	19	4	9	20	5	n.d.
14	2024	69.94	0.14	23.87	0.37	0.01	n.d.	0.42	0.14	n.d.	0.01	12	220	16	12	3	14	10	5	n.d.
15	2025	76.19	0.11	18.31	0.04	0.01	n.d.	0.41	0.13	n.d.	0	10	168	11	15	1	8	8	5	n.d.
16	2049	72.12	0.16	21.04	1.21	0.01	n.d.	0.38	0.14	0.01	0.01	16	273	29	16	10	9	20	6	n.d.
17	2050	74.21	0.11	19.96	0.24	0.01	n.d.	1.25	0.23	n.d.	0.01	11	200	7	52	6	12	24	5	n.d.
18	2005	72.26	0.16	23.28	0.07	0.01	0	0.42	0.08	n.d.	0.01	14	269	12	20	8	16	24	5	n.d.
19	2014	66.59	0.15	20.72	2.27	0.06	0.51	0.74	1.55	6.17	0.04	11	116	27	50	208	17	20	26	n.d.
20	2015	77.01	0.07	13.59	0.86	0.03	0	1.03	1.17	5.01	0.01	8	72	21	22	154	11	19	21	n.d.
21	2016	66.67	0.15	20.66	0.72	0.03	0.21	0.99	0.58	6.78	0.02	10	104	32	20	195	18	7	26	n.d.
22	2018	72.43	0.14	16.03	1.82	0.06	0.65	1.41	2.59	2.98	0.03	9	102	29	103	116	16	20	35	n.d.
23	2019	70.55	0.14	19.01	1.57	0.04	0.43	0.62	1.11	5.14	0.03	9	101	27	26	213	18	7	16	n.d.
24	1000	71.36	0.11	23.27	0.06	0.01	n.d.	0.51	0.01	n.d.	0.01	9	161	3	45	2	6	16	3	n.d.
25	1001	70.61	0.11	23.28	0.03	0.01	n.d.	0.61	0.01	n.d.	0.01	8	163	5	40	2	8	20	5	n.d.
26	1005	70.91	0.15	23.44	0.22	0.01	n.d.	0.33	0	n.d.	0.01	13	236	6	29	4	10	16	4	n.d.
27	2007	73.83	0.15	19.78	0.24	0.02	n.d.	0.55	0.21	n.d.	0.01	11	200	6	23	6	12	12	5	n.d.
28	2008	79.06	0.11	15.16	1.55	0.01	n.d.	0.91	0.38	1.61	0.01	12	177	50	33	91	11	10	57	n.d.
29	2010	65.93	0.22	23.76	1.31	0.01	n.d.	0.91	0.25	0.21	0.01	16	277	20	22	27	14	26	7	n.d.
30	2011	68.51	0.18	25.27	0.79	0.01	n.d.	0.41	0.17	0.01	0.01	18	330	26	14	8	13	10	10	n.d.
31	2026	69.28	0.14	24.74	0.43	0.01	n.d.	0.43	0.04	n.d.	0.01	10	200	27	19	9	12	16	10	n.d.
32	2027	76.62	0.12	16.14	1.55	0.02	n.d.	1.26	2.06	2.29	0.01	12	239	68	62	113	14	22	48	n.d.
33	2028	74.67	0.14	21.16	0.07	0.01	n.d.	0.41	0.06	n.d.	0	11	214	14	14	7	17	8	6	n.d.
34	2291	73.29	0.15	16.64	1.86	0.06	0.73	1.24	1.91	3.22	0.03	8	97	25	80	154	15	23	61	n.d.
35	2292	74.39	0.14	21.94	0.11	0.01	n.d.	0.41	0.05	n.d.	0.01	13	231	13	17	6	14	16	6	n.d.
36	2030	74.61	0.15	19.37	0.44	0.01	n.d.	0.54	0.18	0.31	0.01	12	218	29	19	29	13	16	16	n.d.
37	2031	65.86	0.21	25.32	1.29	0.01	n.d.	1.04	0.32	1.07	0.01	20	374	60	45	64	24	18	25	n.d.
38	2035	64.14	0.11	28.62	0.01	0.01	n.d.	0.48	0.07	n.d.	0.01	10	180	2	69	2	17	24	6	n.d.
39	3085	73.58	0.12	17.91	1.58	0.01	n.d.	0.96	0.44	1.71	0.01	12	208	61	32	80	13	11	47	n.d.
40	3086	68.54	0.14	19.56	2.83	0.02	n.d.	1.02	0.35	3.83	0.01	17	293	74	33	218	15	41	156	2
41	3087	75.75	0.11	18.81	2.15	0.01	n.d.	0.44	0.07	0	0.01	11	192	35	15	9	11	15	28	n.d.
42	2041	71.59	0.16	22.62	0.01	0.01	n.d.	0.96	0.08	n.d.	0.01	12	245	1	46	2	18	22	4	n.d.
43	2042	73.91	0.15	18.56	2.01	0.02	n.d.	1.16	1.15	2.08	0.01	16	245	72	53	134	16	19	34	n.d.
44	2043	82.27	0.07	14.03	0.65	0.01	n.d.	0.45	0.21	n.d.	0.02	6	107	19	15	7	11	17	14	n.d.
45	2044	77.22	0.12	16.16	1.58	0.01	n.d.	1.19	0.94	1.46	0.01	12	194	61	50	99	11	32	38	n.d.
46	2045	76.25	0.17	19.44	0.28	0.01	n.d.	0.42	0.25	0.12	0.01	11	185	10	29	19	10	25	6	n.d.
47	2046	83.54	0.08	13.93	n.d.	0.01	n.d.	0.41	0.14	n.d.	0.01	7	132	10	19	3	11	8	5	n.d.
48	2047	78.68	0.12	18.98	n.d.	0	n.d.	0.43	0.08	n.d.	0.01	12	223	5	29	2	9	18	4	n.d.
49	2048	64.06	0.21	28.75	0.24	0.01	n.d.	0.43	0.03	n.d.	0.02	18	351	16	56	2	23	42	3	n.d.
50	2051	74.11	0.12	21.59	n.d.	0.01	n.d.	0.42	0.12	0.16	0	12	190	15	34	11	13	20	7	n.d.
51	2052	68.46	0.12	24.86	n.d.	0.01	n.d.	0.51	0.08	0.09	0.01	13	217	7	19	11	13	24	10	n.d.
52	3064	78.46	0.11	18.22	n.d.	0.01	n.d.	0.38	0.74	n.d.	0.01	9	172	9	35	1	10	9	4	n.d.
53	3065	61.54	0.13	30.23	0.14	0	n.d.	0.42	0.08	n.d.	0.01	11	208	12	24	3	12	22	10	n.d.

Note: Serial no. 1 ~ 5 = Hiraki welded tuff, 6 ~ 17 = Upper ore zone, 18 ~ 23 = Fracture zone, 24 ~ 61 = Bonanza, 62 ~ 100 = Lower ore zone, 101 ~ 106 = Rhyolite, 32, 34, 37, 39, 40, 45, 58 and 59 = Non-welded tuff.

mine are of alkali deficient and strongly peraluminous type, and consequently most of them do not fall into any rock type in chemical classification scheme used for common igneous rocks. Aluminum Saturation Index (ASI = moles Al_2O_3/moles [CaO+Na_2O+K_2O]) of the rhyolite, the non-welded tuff and the Hiraki welded tuff are 1.5 ~ 3.0 (with mean value of 2.0), 2.6 ~ 6.5 (with mean value of 3.0) and 1.4 ~ 3.2 respectively.

Component-element plots of igneous compatible-incompatible pair (SiO_2 - Zr) and incompatible-incompatible pairs (Nb - Zr and TiO_2 - Zr) (Fig. 4) show differences in both fractionation and alteration trends for the Hiraki welded tuff in one hand and the underlying non-welded tuff and rhyolite in the other. This fact suggests that two volcanic units emplaced during separate volcanic activities or series. It agrees also with the age

Table 1 (contd.)

Serial No.	Specimen	SiO2	TiO2	Al2O3	*Fe2O3	MnO	MgO	CaO	Na2O	K2O	P2O5	Nb	Zr	Y	Sr	Rb	Th	Pb	Zn	Cu
54	3066	78.26	0.21	18.03	n.d.	0.01	n.d.	0.38	0.15	n.d.	0.01	9	160	4	38	2	10	17	4	n.d.
55	3067	47.42	0.28	38.21	0.42	0.01	n.d.	0.48	0.08	n.d.	0.02	18	322	2	185	3	16	64	5	n.d.
56	3068	58.27	0.09	31.19	n.d.	0.01	n.d.	0.61	0.05	n.d.	0	8	162	11	21	1	7	13	4	n.d.
57	3069	88.42	0.11	11.05	n.d.	0	n.d.	0.37	0.08	n.d.	0.01	10	187	8	22	0	5	22	3	n.d.
58	3070	70.63	0.13	19.09	3.46	0.01	n.d.	0.44	0.09	n.d.	0.02	15	251	29	37	4	13	48	10	n.d.
59	3071	74.51	0.14	16.57	3.29	0.01	n.d.	0.75	0.21	3.02	0.01	14	263	70	44	102	16	22	15	1
60	2006	72.77	0.12	23.06	n.d.	0	n.d.	0.37	0.05	n.d.	0.01	12	216	5	34	1	8	16	4	n.d.
61	2009	65.81	0.18	23.69	3.71	0.03	n.d.	0.75	0.12	0.84	0.01	20	336	70	25	61	15	31	28	n.d.
62	2000	78.97	0.13	17.55	0.04	0.01	n.d.	0.38	0.09	0.08	0	12	235	20	16	9	12	6	4	n.d.
63	2001	66.65	0.16	25.07	0.72	0.01	n.d.	0.37	0.03	n.d.	0.01	15	269	39	13	10	17	23	8	n.d.
64	1002	81.83	0.12	15.76	0.07	0.01	n.d.	0.41	0.03	0.03	0.01	11	209	7	39	7	10	21	7	n.d.
65	1003	71.36	0.14	22.62	0.18	0.01	n.d.	0.38	0	n.d.	0.01	11	210	6	26	8	7	14	9	n.d.
66	1009	72.46	0.17	21.96	n.d.	0.01	n.d.	0.45	0.02	0.43	0.01	13	233	9	21	21	11	12	4	n.d.
67	1017	66.41	0.13	23.01	2.48	0.02	n.d.	0.32	0.01	1.75	0	13	241	60	11	85	15	13	32	n.d.
68	2003	73.75	0.17	21.29	0.2	0	n.d.	0.37	0.12	n.d.	0.01	15	270	15	18	8	13	24	7	n.d.
69	2032	56.74	0.16	33.13	n.d.	0	n.d.	0.36	0.06	n.d.	0.01	13	257	9	11	3	11	14	6	n.d.
70	2004	75.64	0.11	18.32	1.64	0.02	n.d.	0.61	0.12	1.17	0.01	11	186	30	23	59	13	16	39	n.d.
71	2038	74.93	0.12	20.82	0.06	0.01	n.d.	0.41	0.08	n.d.	0.01	10	180	11	16	6	14	15	7	n.d.
72	2039	64.32	0.15	26.77	1.98	0.01	n.d.	0.44	0.06	0.2	0.01	15	234	18	22	16	18	62	30	n.d.
73	2040	69.31	0.17	24.12	0	0.01	n.d.	0.55	0.29	0.07	0.01	13	241	13	42	9	30	22	20	n.d.
74	3056	75.74	0.11	15.76	2.06	0.04	n.d.	0.79	1.04	2.62	0.01	12	178	35	39	134	11	22	47	n.d.
75	3057	64.06	0.12	27.65	0.02	0.01	n.d.	0.67	0.04	1.08	0.02	11	189	3	72	40	10	45	4	n.d.
76	3058	76.32	0.09	16.05	1.53	0.01	n.d.	0.64	0.31	3.07	0.01	10	174	12	35	92	10	23	10	n.d.
77	3059	65.05	0.12	25.26	2.13	0.01	n.d.	0.51	0.08	0.15	0	12	201	15	25	7	11	19	10	n.d.
78	3060	68.24	0.16	25.82	n.d.	0.01	n.d.	0.41	0.06	n.d.	0.01	14	232	18	27	3	18	27	6	n.d.
79	3061	78.68	0.09	18.47	n.d.	0.01	n.d.	0.43	0.11	n.d.	0.01	9	153	8	35	5	7	7	4	n.d.
80	3062	56.08	0.23	32.01	1.01	0.01	n.d.	0.64	0.16	0.9	0.01	22	378	70	32	46	25	35	10	n.d.
81	3072	69.78	0.12	25.14	n.d.	0.01	n.d.	0.45	0.89	n.d.	0.01	11	222	3	44	n.d.	11	22	4	n.d.
82	3073	74.44	0.31	19.46	0.36	0.01	n.d.	0.56	0.55	0.08	0.03	13	245	18	47	12	14	47	6	n.d.
83	3074	74.75	0.09	19.65	n.d.	0.01	n.d.	0.86	0.22	n.d.	0.01	10	175	25	59	5	16	22	5	n.d.
84	3075	62.23	0.15	24.22	2.73	0.02	n.d.	0.83	1.22	6.07	0.01	20	312	66	47	194	21	32	51	n.d.
85	3076	72.42	0.09	19.38	1.01	0.01	n.d.	0.79	1.01	5.16	0.01	11	173	37	46	138	13	25	14	n.d.
86	3077	61.68	0.19	29.46	0.04	0.01	n.d.	0.49	0.11	n.d.	0	16	257	5	20	1	7	10	4	n.d.
87	3078	76.34	0.11	20.61	n.d.	0	n.d.	0.38	0.11	n.d.	0.01	10	182	5	110	n.d.	8	18	4	n.d.
88	3079	89.26	0.12	9.71	n.d.	0.01	n.d.	0.41	0.14	n.d.	0.01	10	207	4	28	n.d.	7	28	3	n.d.
89	3080	75.37	0.14	19.65	n.d.	0	n.d.	0.75	0.28	n.d.	0.01	11	218	8	32	5	10	11	4	n.d.
90	3081	70.97	0.13	23.26	n.d.	0.01	n.d.	0.43	0.16	n.d.	0.01	10	186	14	31	4	20	13	5	n.d.
91	3082	84.86	0.11	11.97	n.d.	0.01	n.d.	0.51	0.16	n.d.	0.01	9	162	10	42	2	15	13	4	n.d.
92	3083	78.74	0.13	18.05	n.d.	0.01	n.d.	0.39	0.13	n.d.	0.01	12	223	12	30	2	19	46	4	n.d.
93	3084	73.51	0.11	21.33	0.2	0.01	n.d.	0.37	0.06	0.01	0.01	7	154	11	20	6	23	10	7	n.d.
94	3842	71.17	0.09	23.61	0.19	0.01	n.d.	0.37	0.05	0.03	0.01	6	148	13	21	7	23	8	6	n.d.
95	2033	75.46	0.09	19.97	0.08	0.01	n.d.	0.39	0.13	n.d.	0.01	7	135	12	17	11	13	11	6	n.d.
96	2036	73.61	0.25	20.62	0.23	0.01	n.d.	0.37	0.05	0.06	0.01	16	316	8	53	10	26	23	4	n.d.
97	2037	69.92	0.21	22.55	0.43	0.01	n.d.	0.37	0.12	0.31	0.02	12	250	18	56	19	30	25	5	n.d.
98	2053	67.03	0.24	25.79	0.01	0.01	n.d.	0.51	0.08	n.d.	0.02	18	290	4	15	n.d.	8	29	5	n.d.
99	2054	82.99	0.08	14.31	n.d.	0.01	n.d.	0.38	0.44	n.d.	0.01	9	137	2	24	n.d.	4	13	5	n.d.
100	2055	79.75	0.22	15.92	0.43	0.01	n.d.	0.46	0.25	0.06	0.01	17	288	10	17	8	12	26	5	2
101	1011	76.63	0.11	14.57	1.41	0.03	n.d.	0.57	4.58	1.38	0	9	148	37	74	49	12	14	21	n.d.
102	1016	82.39	0.09	12.56	0.46	0.02	n.d.	0.44	0.94	3.84	0.02	9	182	57	30	113	16	15	12	n.d.
103	1018	65.09	0.15	21.41	3.02	0.04	0.24	1.01	3.22	3.65	0.01	14	253	45	65	136	21	25	94	6
104	1019	67.39	0.11	17.25	6.81	0.04	n.d.	0.71	0.21	3.94	0.01	11	181	46	28	186	20	32	58	2
105	2341	67.24	0.12	19.33	2.74	0.03	n.d.	0.81	2.91	3.01	0.01	11	195	42	81	116	22	19	61	n.d.
106	2342	79.38	0.09	11.81	0.68	0.01	n.d.	0.86	3.41	4.37	0.01	10	152	33	34	134	12	31	23	1
	* Total Fe as Fe+++			Concentration in wt%				n.d. = not detected							Concentration in ppm					

data of Ko Ko Myint et al., 1995, who showed evidence of the presence of unconformity between the Hiraki welded tuff and the non-welded tuff. The Hiraki welded tuff contains less silica than non-welded tuff and rhyolite at constant Zr. However, it is not an unambiguous evidence for different time of formation, since a volcano can emit volcanic materials of different rock types without time break. Even under such circumstance, it can be suggested that the whole non-welded tuff is considered as a single volcanic series, although it might show some compositional variation.

III. K-Ar DATINGS ON THE VOLCANOSTRATIGRAPHIC COLUMN

As described above the geology of the Hiraki mine area has partly been revised and proposed a new

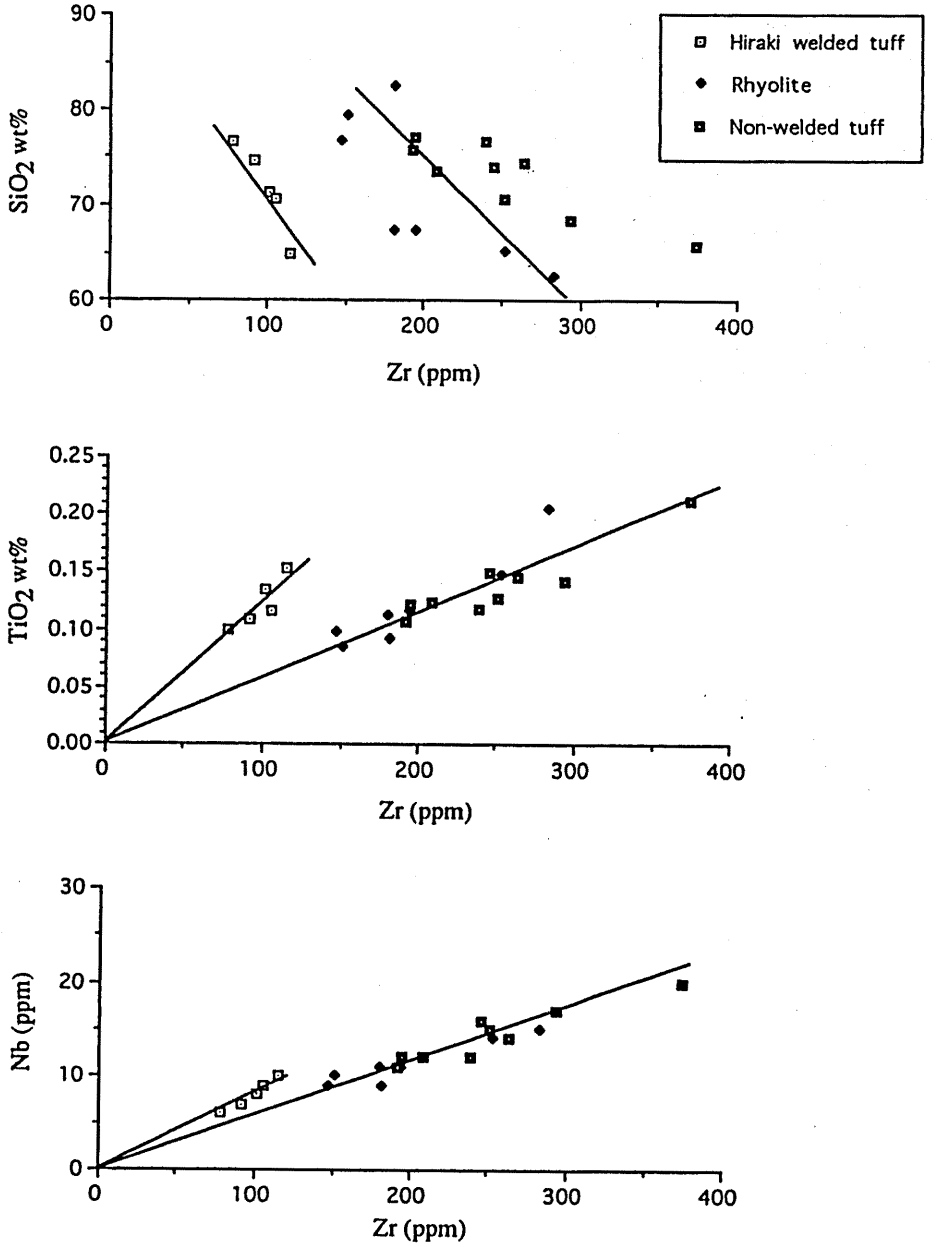

Fig. 4 Fractionation (upper) and alteration (lower two) lines of the volcanic rocks in the mine area showing two different series.

volcanostratigraphic sequence of the Kamogawa formation in the Hiraki mine area by assuming a normal sequence, introducing the rhyolitic non-welded tuff (later altered to ore deposit) as a new lithostratigraphic unit overlying the rhyolite lava, at least in the mine area. This relation is based on the field observations which strongly against the sequential order of Ozaki and Matsuura (1988), who described the Kamogawa formation as an overturned sequence in the Hiraki mine area. This assumption of Ozaki and Matsuura (1988) is stratigraphically irrelevant unless there is any structural or stratigraphical disturbances described. But they have never mentioned these facts in their report. Consequently, the stratigraphic sequence of the Hiraki mine area needs a serious re-establishment in accordance with its field occurrences and radiometric datings. Also the time of formation of ore deposit (i. e. hydrothermal alteration) still remains undetermined, yet. Hence, to clarify the controversy over the stratigraphic order and to establish the mineralization time, representative rock specimens for lithologic units exposed in the Hiraki mine and ores were analyzed for their radiometric ages by K-Ar dating method.

1. Sampling and analytical method

Samples collected are: (1) the fresh foot-wall rhyolite lava (sp. no. 1001); (2) the least-altered and altered non-welded tuff which formed the kaolin deposit (sp. no. 1002 and 3056); (3) the hanging-wall Hiraki welded tuff (sp. no. 1003); (4) the sericite-pyrophyllite

clay from the fracture zone cutting across the whole volcanic sequence in the Hiraki mine (sp. no. 1014). To get the highly sensitive information about time of formation, samples were taken from the basal part of the Hiraki welded tuff and from the uppermost part of the rhyolite. For the non-welded tuff, sample is available only from the least altered part of the relict body of middle member exposed in the open-pit. In order to avoid the effect of alteration, whole-rock samples were checked carefully under microscope for their freshness before analysis. These samples were then crushed and sieved between mesh no. 80 and 100, and later powder specimens were used for K-Ar dating of whole rocks. K-Ar age determination was made by use of a 30 cm radius sector-type mass spectrometer with a single collector system installed at the Okayama University of Science by the isotopic dilution method described by Nagao et al.(1984) and Itaya et al.(1966). The physical constants used are: $40K/K=1.167 \times 10^{-4}$ mole/mole; $\lambda_\beta = 4.962 \times 10^{-10}$/y; $\lambda_\varepsilon+\lambda_{\varepsilon'} = 0.581 \times 10^{-10}$/y (Steiger and Jäger, 1977).

2. Analytical results

K - Ar ages along with the K and Ar analytical data, are given in Table 2 in stratigraphical order. As shown in the table, sample from the fracture zone which includes alteration minerals, sericite and pyrophyllite, has the youngest age of 63.8 ± 1.5 Ma. The underlying rhyolite (the Kamogawa formation) is the oldest with 70.0 ± 1.5 Ma, while the Hiraki welded tuff is the youngest with 67.6 ± 1.5 Ma among the volcanic sequence. Samples of the non-welded tuff are of 69 ± 1.6 Ma and 68.9 ± 1.6 for altered and least-altered parts respectively. Altered specimen of non-welded tuff (no. 3056) possibly did not lose its K of igneous origin during hydrothermal alteration inasmuch as it gave out radiometric age in good agreement with that of the least-altered non-welded tuff. This fact points out that both the least-altered and altered non-welded tuff specimens can safely be taken as the fresh non-welded tuff for further geochemical purposes.

As shown in the Table 2, resulted dates match well with actual stratigraphic column established in the Fig. 2, i. e. the non-welded tuff is younger than the rhyolite and thus is different from the rhyolitic non-welded tuff of Ozaki and Matsuura, 1988. The newly established volcanostratigraphic column composes of (from older to younger): the rhyolite, the non-welded tuff, and the Hiraki welded tuff, with cessation of volcanic activity during 68.9 ± 1.5 to 67.6 ± 1.5 Ma. This fact points out that Ozaki and Matsuura improperly assigned the non-welded tuff stratigraphically below the rhyolite and then repeatedly placed above the rhyolite without giving any reliable reason, such as structural disturbances, lateral facies changes, etc..

A possible reason for this misplacing might be that they considered only on lithologic similarity between these two non-welded tuff units, one above and one below the Kamogawa rhyolite. Very delicate age differences between lithologic units elucidate that the stratigraphic column cropping out in the Hiraki mine is a normal sequences and can be depicted as in Fig. 5.

Formation of fractures, also major deformation, occurred after cessation of all volcanic events in the Hiraki mine area, since they are cutting through the Hiraki welded tuff, the youngest unit. The age of alteration minerals from the fracture zone unravels that the mineralization (hydrothermal alteration) took place about 3.8 m. y. after the emplacement of the Hiraki welded tuff being formed as a cap-rock during alteration. Since there are no evidences for multiple mineralizations such as existence of mineral assemblages stable under different physicochemical conditions, and intervening zonal array, it is assumed that the mineralization in the Hiraki mine took place in single episode. Timing of deformation is considered as prior to mineralization, although there also has a possibility of that the deformation was contemporaneous with mineralization. Exact temporal relation between deformation and mineralization cannot be justified, however.

All the above findings indicate that the whole sequence of volcanogenic rocks in the Hiraki mine area were emplaced during a relatively short duration (about 2.4 m. y.) in the latest Cretaceous to the early Tertiary Periods (67.6 ± 1.5 Ma) , and mineralization (63.8 ± 1.5 Ma) occurred after volcanic activities.

In comparison with the K - Ar ages reported by Shibata et al. (1984) and Ozaki and Matsuura (1988) for the Hiraki welded tuff, the present ages are slightly young. This is probably due to the fact that their data are for the basal part of the Hiraki welded tuff, which is not exposed in the Hiraki mine area, whereas the present data are for the upper part of the Hiraki welded tuff (for details see in Ko Ko Myint and Watanabe, 1995). Another possible cause is that they analyzed minerals, while the present study used whole-rock analyses.. In any case, present ages data show a high accuracy compared to Shibata et al. (1984) and Ozaki and Matsuura (1988).

IV. ALTERATION MINERAL ASSEMBLAGES AND THEIR DISTRIBUTION

Mineral identifications were done under petrographic microscope, with powder X-ray diffractometer for clay minerals, and with electron probe microanalyzer for individual mineral composition. Samples showing mixed-layer clays peaks in diffractograms were reinvestigated after treated with ethylene glycol and shifting in *d* spacings were used to verify the individual minerals.

The non-welded tuff of the Hiraki mine was altered to an essentially monomineralic zone of kaolinite and quartz with a few mixed-layer clay minerals contaminations in irregular distribution. In the Hiraki welded tuff, sericite occurs in the fractures, and chlorite with or without sericite at the boundary with the orebody. On the other hand, the rhyolite contacts with the orebody by thin sericite and chlorite "zones", but sometimes by quartz-rich body. Although the orebody shows no distinct mineral zonations, both the lower and the upper bounded rocks, i.e. rhyolite and welded tuff, tend to display a general order of appearance of sericite "zone"

Table 2 Analytical results of K-Ar dating for volcanic rocks and ore specimens of the Hiraki mine. Note that K-Ar ages are consistent with present established stratigraphic column, not with those of Ozaki and Matsuura (1988) and Taninami (1991).

Specimen no.	Material analyses	Major mineral assemblages	K (wt%)	^{40}Ar (rad) (10^{-8} ccSTP/g)	^{40}Ar % (atmos.)	Age (Ma)	Remarks
1014	Clay from fracture zone	pyrophyllite, sericite, qtz	2.45	617.3±7.8	18.2	63.8±1.5	
1003	Hiraki welded tuff	biot., K-f, pl., qtz	2.89	772.5±8.3	6.2	67.6±1.5	70±3.5* 72.7±2.3#
1002	Non-welded tuff (least-altered)	K-f, pl., qtz	1.06	288.8±3.6	17.4	68.9±1.5	
3056	Non-welded tuff (altered)	K-f, pl., qtz musc.	1.78	486.6±5.8	10.7	69.1±1.6	
1001	Rhyolite (Kamogawa fm.)	K-f, pl., qtz	4.49	1244±13	3.5	70.0±1.5	

* Ozaki and Matsuura, 1988, on biotite. # Shibata et al., 1984, on K-feldspar.

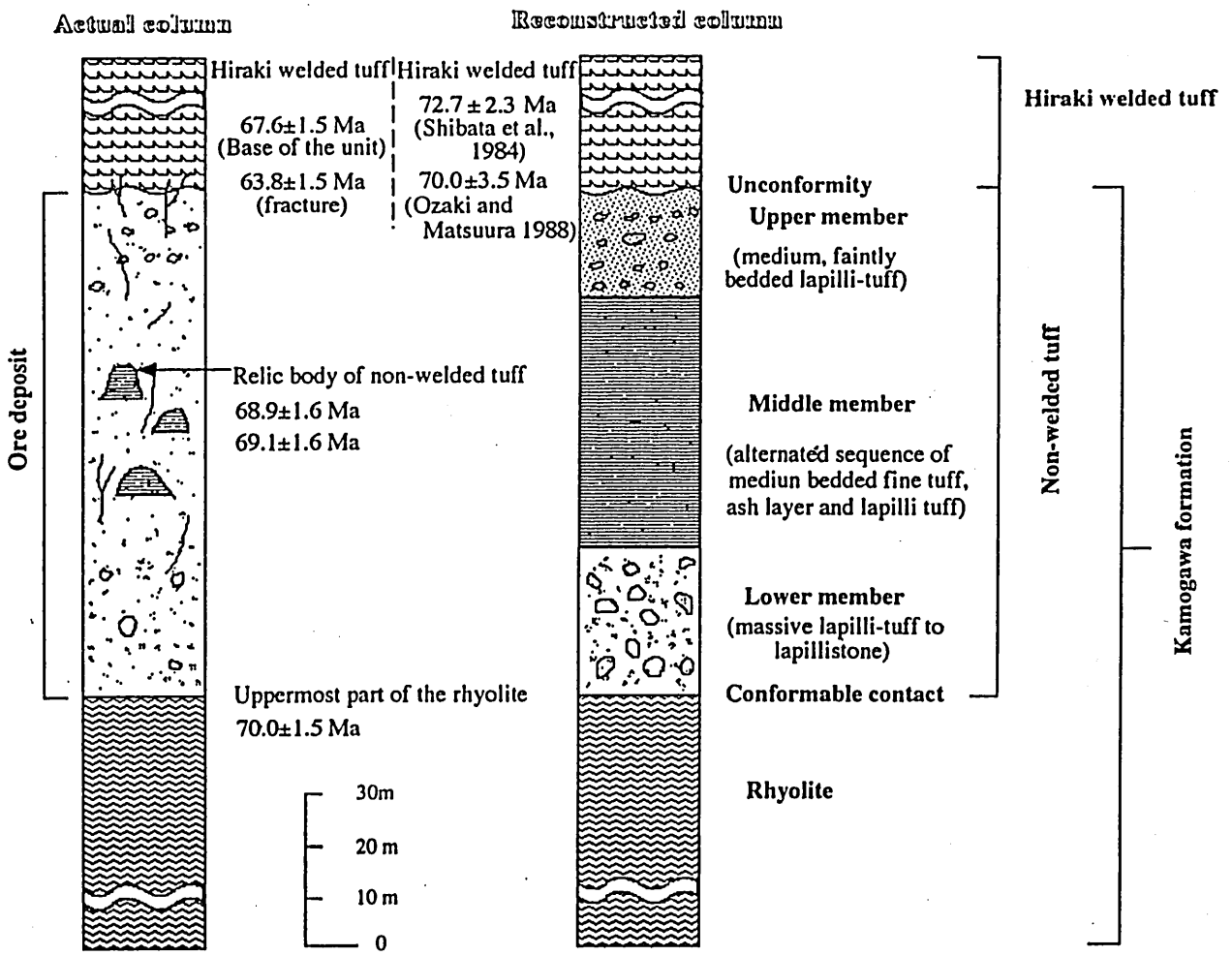

Fig. 5 Volcanostratigraphic column in together with their respective K-Ar ages on the whole-rocks and ore samples.

and chlorite "zone" in the direction towards the orebody, in which kaolinite dominates in the central portion. Nevertheless, the boundary between these "zones" is somewhat obscured and, in many occasions, impossible to demarcate, and thicknesses of the sericite and chlorite "zones" are negligible compared to the main kaolinite zone of about 100m thick. In some fractures, the alteration pattern cuts across the volcanic stratigraphy. However, it is, generally, more or less conformable to the planar structures in the rest of the ore deposit. Degree of alteration appears to decrease significantly towards NE and SW directions of the ore zone. General pattern of distribution and abundance of alteration mineral assemblages are shown in Fig. 6 & 7.

1. Kaolinite

Kaolinite, the major hydrothermal alteration product due to interaction between invading acid fluids and feldspars of the Hiraki non-welded tuff, is accompanied by a variable proportion of quartz, and usually concentrated in the central portion of the ore deposit. In general, kaolinite decreases and quartz increases in amount towards the peripheral of the ore deposit, but the change in proportion is ungradational and irregular, and seldom disturbed by the presence of extremely quartz-rich bodies. Small amounts of illite, montmorillonite, illite-smectite and chlorite-smectite mixed-layer clay minerals are found to occur unsystematically with kaolinite and thus, no common zone can be defined for these minerals.

Kaolinite, under microscope, is replacing feldspars phenocrysts and groundmass feldspars, and being interstitial to the rock and glassy fragments. Some lithophysa were altered to kaolinite in the central part initially occupied by feldspar, whereas quartz bands remain unchanged. Mineral composition of the ore deposit varies as widely as kaolinite 70%-quartz 30% to vice versa, but not transitional as aforementioned. Normative calculation, based on the assumption of conserved Al_2O_3 for the kaolinite zone, and modal abundance result in quartz/kaolinite ratio of the ore zone as within the range of 1.5 to 3 with mean value of 2.2.

2. Pyrophyllite

In the Hiraki mine, pyrophyllite has never been reported to date. It occurs rarely, only in fracture zone which cuts through the ore deposit and the overlying welded tuff in common association with sericite and quartz. Some specimens from the fracture zone contain kaolinite and illite-smectite mixed-layer minerals accompanied to pyrophyllite. Pyrophyllite always occurs in together with quartz and clays other than kaolinite, never as pyrophyllite-only or pyrophyllite-quartz assemblage.

3. Sericite

Sericite is detectable at the margins of the unaltered non-welded tuff, the welded tuff, and the rhyolite. Width of sericite "zone" is usually no more than a few centimeters, but sometimes exceeds a meter in the uppermost part of the rhyolite. Sericite accompanies chlorite very often at these margins, while in the fracture zone, it occurs together with pyrophyllite. Its precursor mineral can be defined as feldspars, since sericite is found to replace feldspar phenocrysts and interstitial groundmass feldspars of original rocks. This fact points out that sericite was formed in equilibrium with the feldspars. Sericitization Index ($S.I = K_2O/K_2O+Na_2O$) of the uppermost part of the rhyolite is 80-90 and thus it falls in the hydrothermal alteration field (MacLean, 1984). Electron microprobe analyses (Table. 3) reveal that some of sericite in the uppermost part of the rhyolite have a composition of phengite.

4. Chlorite

Zones of intense chloritization with negligible thickness are restricted to the spherulitic portion of the uppermost rhyolite, the contact between the least-altered non-welded tuff and the ore deposit, and the sharp contact between the Hiraki welded tuff and the ore deposit. There are some continuous laminations of chlorite with thickness of approximately 5 cm at the hanging wall contact, while it occurs with phengite and chlorite-smectite mixed-layer in other portions of the orebody. In fact, chlorite-smectite mixed layer is more abundant than pure Fe-chlorite. After treatment with HCl for 1 hour at 100°C, chlorite peak of octahedral site (14 A°) apparently disappeared from the diffractograms. In general, the chlorite "zone" of varying thickness and scattered distribution envelopes the outer fringe of the ore deposit with an irregular pattern. Chlorite in the Hiraki mine is of Fe rich-type formed probably by alteration of biotite in the non-welded tuff.

5. Other minerals

There are some accessory minerals, found to occur with major alteration minerals, in the mine. These are dickite, illite, illite-smectite mixed-layer, chlorite-smectite mixed-layer, halloysite, pyrite, marcasite, hematite and calcite. So far as it is known that dickite and halloysite occur only in the fissures and fractures, whereas the occurrences of illite and mixed-layer minerals have no definite locality in the ore deposit. All these minerals accompany to kaolinite in very negligible amounts. Some pyrite crystals of about 2~4 mm are sparsely scattered throughout the upper part of the ore deposit. In some ore specimens, marcasite occurs together with pyrite. Under reflected-light microscope, marcasite can be easily differentiated from pyrite by its pale creamy color and strong anisotrophism. Co-existence of marcasite and pyrite strongly points out that the deposit was formed under acidic condition. Small veins of drusy calcite can be found somewhere in its lower part. Minor amounts of hematite occur in the margin of unaltered tuff body observed in the ore deposit.

V. CHEMICAL CHANGES

The essence of metasomatism is that bulk compositional changes take place during water-rock interaction which is evident by change in stable mineral

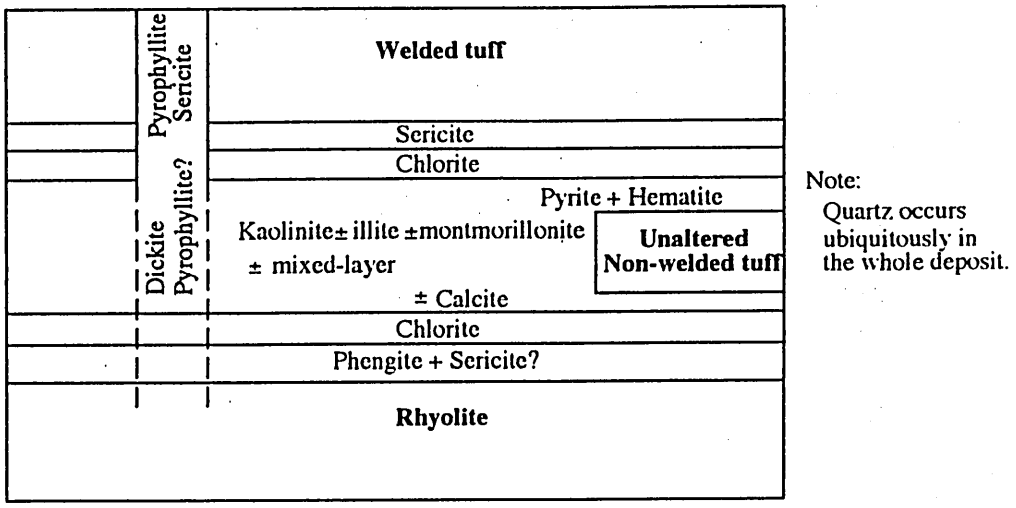

Fig. 6 Schematic diagram illustrating spatial relation between alteration mineral "zones" and respective mineral assemblages in the Hiraki deposit.

Mineral	Rhyolite (uppermost part)	Bonanza and lower part	Orebody (upper part)	Fracture	Welded tuff (boundary)
Phengite	———				
Kaolinite		———	———	———	
Illite		- - - - -	- - - - -		
Montmorillonite		- - - - -	- - - - -		
Mixed-layer		- - - - -	- - - - -		
Calcite		- - - - -			
Pyrite			- - - - -		
Hematite			- - - - -		
Chlorite					- - - - -
Pyrophyllite				———	
Sericite				———	- - - - -
Dickite				- - - - -	
Quartz	———	———	———	———	———
Thickness	few centimeter	80 m	20 m	a few cm to 10 m	a few cm

Fig. 7 Diagram showing areal distribution and relative abundance of alteration minerals in the mine.

assemblages. Although multiple approaches have been proposed to link the final state to the initial state of the system, i.e. to determine gains and losses of components, the fundamental relation can be expressed in terms of masses by:

$$m_i^o + \Delta m_i = m_i^f \qquad \text{V-1,}$$

where m_i is the mass of the ith species, the superscripts, o and f, refer to initial and final states, and Δm_i is the change of mass. Although the relation V. 1 reflects what actually happens in a rock during hydrothermal alteration, working principle still needs further assumptions.. Since the chemical analyses data are usually available in geological investigation , the operative relationship for mass balance becomes:

$$\Sigma m^o[X_i^o] + [\Delta m_i] = \Sigma m^f[X_i^f] \qquad \text{V-2,}$$

or because we can arbitrarily set our initial mass (say to 100 gm):

$$[X_i^o] + [\Delta m_i]/\Sigma m^o = (\Sigma m_i^f/\Sigma m_i^o)[X_i^f] \qquad \text{V-3,}$$

where Σm and X_i represent total mass and concentration fraction of subscribed species.

It is appeared in the relationship (V- 3) that the

Table 3 Chemical composition of phengite from the uppermost part of rhyolite.

Sample no.	1	2	3	4
Element	wt %	wt%	wt%	wt%
SiO_2	53.71	54.43	52.17	53.02
TiO_2	0.26	0.17	0.02	0.22
Al_2O_3	31.98	31.81	37.58	33.50
FeO	4.93	4.67	2.20	4.27
MnO	0.02	0.05	0.02	0.05
MgO	0.40	0.40	0.24	0.32
CaO	0.31	0.28	0.60	0.48
Na_2O	0.08	0.08	0.11	0.10
K_2O	8.28	8.06	7.01	7.99

EPMA analysess

Sample no.	1	2	3	4
Element	Cation	Cation	Cation	Cation
SiO_2	7.001	7.0965	6.7299	6.8911
TiO_2	0.26	0.0168	0.0026	0.0224
Al_2O_3	4.913	4.8883	5.7137	5.1329
FeO	0.538	0.5097	0.2383	0.4647
MnO	0.002	0.0056	0.0024	0.0063
MgO	0.08	0.0787	0.0469	0.0632
CaO	0.043	0.04	0.0841	0.0672
Na_2O	0.02	0.0223	0.0278	0.0268
K_2O	1.377	1.3418	1.1537	1.3249

Mineral general formula

1. Muscovite	K_2	Al_4	Si_6Al_4
3. Illite	K_{2-x}	Al_4	$Si_{6+x}Al_{2-x}$
4. Phengite	K_2	$Al_{4-x}(Mg,Fe^{2+})_x$	$Si_{6+x}Al_{2-x}$

from "An Introduction to the Rock Forming Minerals" Deer, Howie & Zussman, 1970.

solving for Δm_i involves in determining of Σm_i^f, as pointed out by some authors e. g., Brady (1975). This double-standard problem can be eliminated if the mass of some component is assumed or proved by independent method to be constant and thus, the change in the total mass can be determined from a relationship such as:

$$X^o_{c.c.}\Sigma m_i^o = X_{c.c.}{}^f\Sigma m_i^f, \text{ or}$$

$$\Sigma m_i^f/\Sigma m_i^o = X^o_{c.c.}/X^f_{c.c.} \qquad \text{V-4,}$$

where subscript c. c. represents constant component.

1 Hydrothermal mass transfer

As a matter of fact, mass itself is a dependent factor on the volume and density by the expression:

$$V^o{}_r{}^o = \Sigma m^o,\ V^f{}_{rf} = \Sigma m^f,$$

$$\text{thus } \Sigma m^f/\Sigma m^o = V^f{}_{rf}/V^o{}_r{}^o \qquad \text{V-5.}$$

Thus alternative resolution can be achieved if volume is concerned or known to be changed to a certain amount.

To a practical matter then, one need to decide what is conserved volume or component, and hence provide the reference for mass transfer. Early approaches emphasized

on constant volumes (e. g., Lindgren, 1925) or fixed numbers of anions (e. g., Barth, 1948). These approaches should be justified on the basis of field evidences, but offer poor approximations when net transfer reactions are insignificant. Alternatively one can assume that a component is conserved or that volume varies in a known way (Gressens, 1967; Brimhall and Dietrich, 1987). A conserved component can be chosen on geological or experimental evidence for minimum mobility under the conditions of interest. Grant (1986) described a simple approach to this where altered compositions are plotted against fresh compositions, then components that are conserved fall on a line (isocon) passing through the origin. For this purpose Al_2O_3 is normally chosen as immobile a priori, although it clearly move in some aureoles (e.g., Barton, 1987; Giere, 1990) and moderate solubility is indicated by experiment (e. g., Pascal and Anderson, 1989).

From the above discussions it is cleared that one must be sure or assumed one of the two necessities, i. e., volume-constant or no net change in mass of one component. If volume is constant, $\Sigma m_i^f/\Sigma m_i^o = rf/r^o$, if not, the ratio V^f/V^o is a measure of the strain during mass transfer (cf. Brimhall and Dietrich, 1987). Thus measurement of strain (e. g., from changes in bedding thickness) can yield a normalizing factor. If both factors, volume-conserved and component-conserved, can be estimated or proved, then mass transfer in hydrothermal process will lead to changes in porosity or density between initial and final rocks,

In general, metasomatism occurs without any changes of volume. At the Hiraki mine, field observations show no evidence of volume changes, such as sudden disappearance or shrinkage of beddings, discontinuity of exposure at fault plane, etc.. Consequently, as pointed out above, mass changes of chemical components were compensated by specific gravity changes between original non-welded tuff and altered counterparts (ore) by the relationship: $m^o = V^o r^o$.

The effects of hydrothermal alteration on each chemical elements can be best understood by disclosure of variation in their concentrations either with distance from the center of the alteration (fracture zone) to the original (host) rock or individual mineral zone, when the location of center is not evident. These variations due to dilutions or additions need to be corrected for most immobile element monitor.

Method of calculation

The method used here to evaluate precursor compositions together with gains and losses of mass during hydrothermal alteration is a modified version of calculations initiated by Finlow-Bates and Stumpfl (1981), later developed by MacLean and Kranidiotis (1987) and MacLean (1990). It is based on the assumption that in a series of hydrothermally altered rocks, best-fit lines to binary plots of magmatic incompatible elements pass through the origin and precursor composition. If these elements are immobile during alteration, reduction or addition of their concentration factors is determined by increase (as by precipitation) or decrease (as by dissolution) in mass of other materials in the system. And, this phenomenon can be represented by their plots close to or farther away from the origin along best-fit line for element pair concerned as shown in the Fig. 8. Thus, immobile elements in both protolith and altered rock plot on a common regression line; i. e., they retain constant interelement ratios.

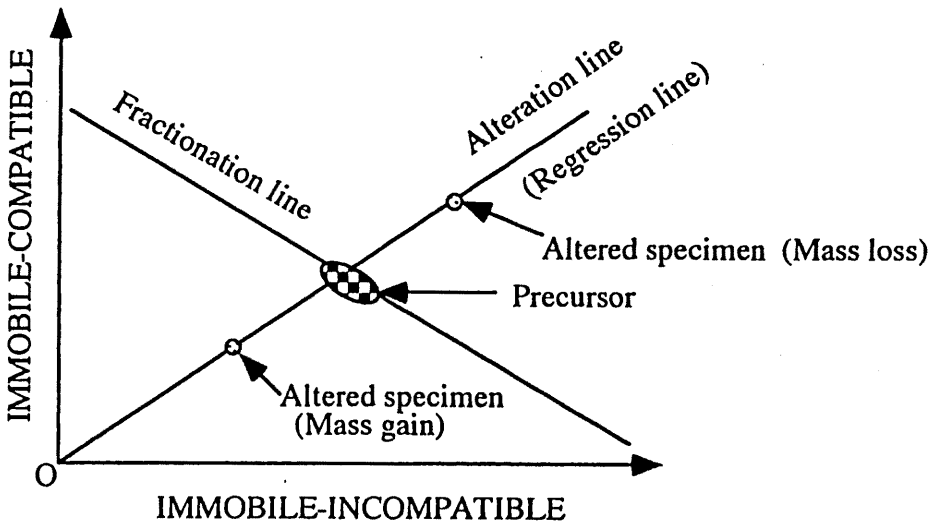

Fig. 8 Graphical presentation of the nature of fractionation and alteration lines defined by immobile-incompatible and immobile-compatible elements. (Modified after MacLean, 1990)

Correlation coefficients,

$$R=\frac{\sum_{i=1}^{n}(x_i-\bar{x})(y_i-\bar{y})}{\sqrt{\sum_{i=1}^{n}(x_i-\bar{x})^2}\sqrt{\sum_{i=1}^{n}(y_i-\bar{y})^2}},$$ for regression lines that pass through precursor's composition and the origin can be used to test the most immobile element pair; the higher the value, the more immobile the elements. The error associated with accuracy of the method applied for chemical analyses in addition to some heterogeneities in protolith's composition, which are common in most pyroclastics, can reduce the values of the coefficient. Based on the evidences of its structural continuity and gradational contact with the orebody, the unaltered and least-altered rhyolitic non-welded tuff is assumed as a precursor in the Hiraki mine.

To ascertain a single homogeneous precursor system, widely accepted incompatible immobile element pair, Nb-Zr, is applied to determine an alteration trend for the Hiraki deposit. It shows single best-fit line for the whole ore deposit with R =0.911 (not shown in here) and that for kaolinite concentrated part (bonanza) with R = 0.958 (Fig. 9). From this result it can be concluded that the Hiraki deposit was altered from a single precursor, i. e. the non-welded tuff.

Mass change calculations for the major components of the non-welded tuff to those of the ore deposit are done by use of concentration (mass) relation of a pre-determined immobile component between protolith and its altered counterparts. Thus, the gains and losses of every mobile components during alteration can be calculated by the following relation (on the basis of 100 g of precursor):

$$G/L_c=Conc._c wt\%(p)-\left[Conc._c wt\%(a.r.)X\frac{Conc._{I.M}(p)}{Conc._{I.M}(a.r.)}\right] \quad V-6$$

where,

G/L_c = Gain or loss of subscribed component, c, in mass (gram); $Conc._c$ wt% (p) = Concentration in wt% of subscribed component, c, in precursor; $Conc._c$ wt%(a.r.) = Concentration in wt% of subscribed component, c, in the altered rock; $Conc._{I.M}$(a.r.) = Concentration of immobile element monitor in altered rock; and $Conc._{I.M}$(p) = Concentration of immobile element monitor in precursor.

Note that the unit of $Conc._{I.M}$(a.r.) and $Conc._{I.M}$(p) must be the same, although it will not appear in normalized factor. By using the 100 g basis of specimens, concentrations in wt% can be converted directly to gram equivalents. Therefore, gain or loss of each component has an unit of gram.

Several previous studies (e. g., Pearce and Cann, 1971, 1973; Winchester and Floyd, 1976, 1977; Humphris and Thompson, 1978a, b; Valsami et al., 1994) have indicated that certain chemical elements can safely be regarded as immobile in sea floor hydrothermal alteration environments, and thus can be used as geochemical indicators in mass balance calculations. Al, Ti, Nb and Zr have been shown for their extreme immobility also in the hydrothermal alteration of host volcanic rocks in the Canadian massive sulfide deposits. In the present study, these elements were tested for their immobility by the method described above, resulting in Zr-Nb pair with highest R value of 0.956 and other element pairs with poor relation (R < 0.7) (Fig. 9). Zr also shows good correlation with other components as Zr-Ti pair (R = 0.688) and Zr-Al pair (R = 0.471). Therefore, Zr was chosen as an immobile element monitor because of its most immobility among other elements and its concentration of 208 ppm. in the middle member of non-welded tuff is used as normalizing factor for mass change calculations.

Caution should be taken in application of above method in concerning with following points. (1) Precursor should be defined accurately with field evidences. Taking the nearby rock or least-altered rock, presumed to have same composition with precursor, would lead to unrelated results. (2) Use of the element pair of similar chemical affinity, such as K-Rb and Zr-Hf, as monitor should be avoided. Such a pair always show in high correlation coefficient because of their constant relative solubility in common solvent, not because of immobility. However, in some case this phenomenon can be sorted out by other reasoning (will be discussed later). (3) This method implicitly is applicable only for single alteration or final alteration stage. For multiple episodes of alteration it is needed to modify as changes in precursor's composition, accordingly.

Reconstructed concentration (second term in the right hand side of the Eq. (V- 6))and gains and losses in mass of major oxides other than Zr of the altered specimens from bonanza are listed in Table.4. Gains or losses of individual components are calculated by subtracting the reconstructed values from the precursor composition. The -ve or +ve appeared in the G/L_c calculated by Eq. (V- 6) indicates the gain or loss in mass of that component, respectively. With an assumption of volume-conserved, mass changes are calculated for 1 liter of original rock and are shown in Table. 5.

Since the Zr/Nb ratios were always found to be almost similar between the two, regardless of degree of alteration, these elements were used as monitors in countercheck for mass fluxes in the highly altered samples. The average of the ratios $Nb_{protolith}/Nb_{altered}$ was taken to represent the dilution factor (values > 1 indicate mass dilution). Other elements were then normalized with this factor to calculate their abundance within the altered rocks, thus providing an estimate of their dilution-corrected concentrations. Dilution factors for specimens of bonanza are shown in Table. 4 to compare the data between qualitative gains and losses and quantitative mass balance calculations based on Zr-conserved frame. The results show strong agreement between two methods..

2. Calculated results

Based on the assumption of constant mass of Zr and constant volume, mass changes of other major

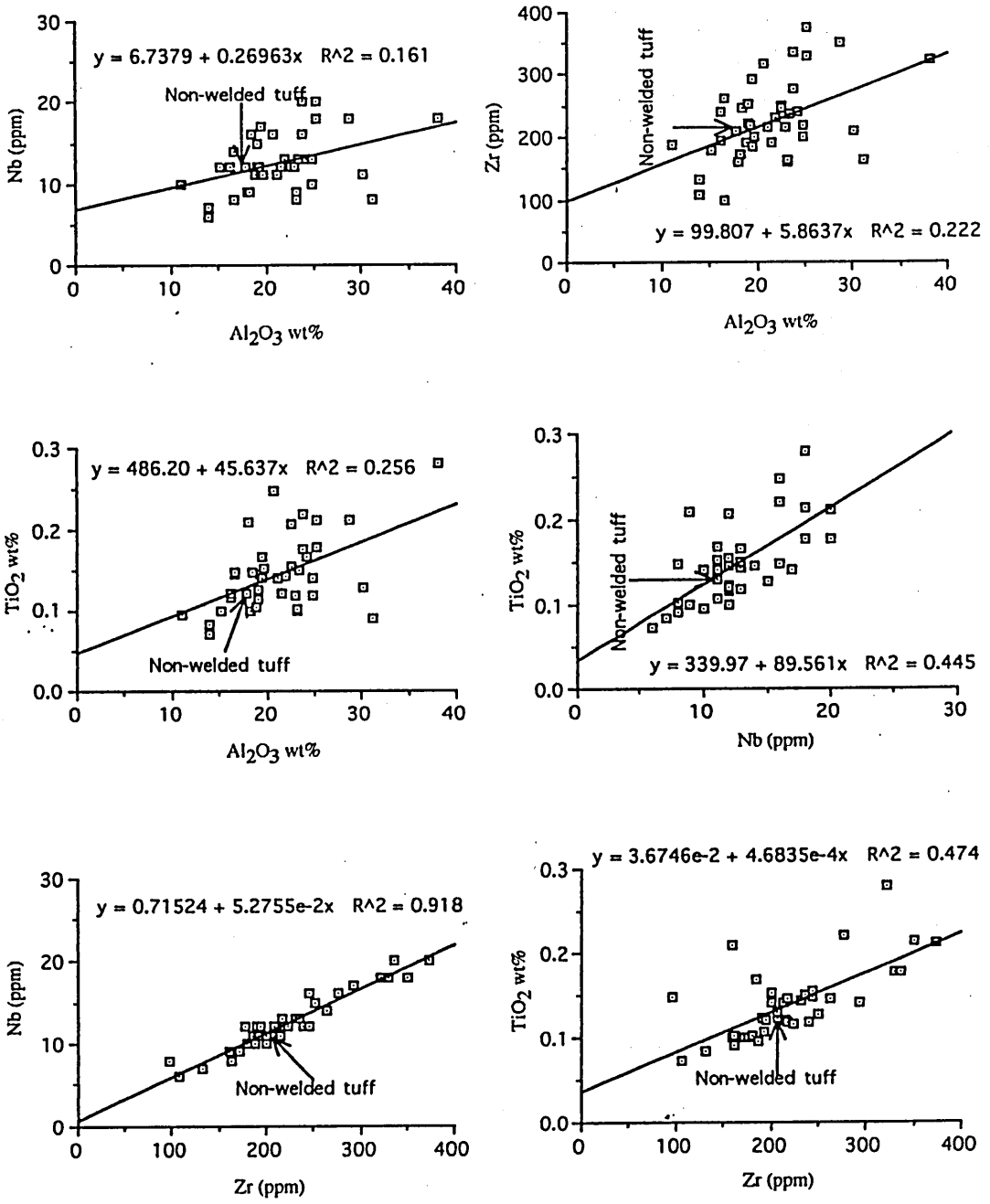

Fig. 9 Binary plots of element-pairs showing interelement correlation among elements and components. Higher "R" value indicates higher immobility of element-pair concerned.

components associated with hydrothermal alteration at the Hiraki mine resulted in the followings: (1) dissolution of Na_2O, K_2O, Fe_2O_3, CaO and MnO in the kaolinite zone; (2) slight enrichment of Fe_2O_3 (up to 1 wt%) in the chlorite "zone"; and (3) enrichment of K_2O (1.5 to 6.5 wt%) and Fe_2O_3 (1.0 to 6.0 wt%) in the sericite "zone". Mass change in SiO_2 occurred locally in the wide range from 86% gain to 58% loss of original concentration, but mean gain and loss are 25% and 15%. It can be the effect of total dissolution of silica in the initial stage of alteration and these solution pits were later filled by amygdaloidal and interstitial quartz deposited from hydrothermal solution. The above interpretation is in agreement with the occurrences of quartz phenocrysts with dissolved boundary and void-filling microcrystalline quartz under microscope. Likewise, irregularly occurring

Table 4 Reconstructed concentration (R.C.) and gain/loss (G/L) in mass of major oxides components for ores from bonanza calculated on the basis of Zr constant. Also shown is the correction factor (Corr. factor).

Sample	R.C. SiO2	R.C.TiO2	R.C. Al2O3	R.C. Fe2O3	R.C. MnO	R.C. CaO	R.C. Na2O	R.C. K2O	G/L SiO2	G/L TiO2	G/L Al2O3	G/L Fe2O3	G/L MnO	G/L CaO	G/L Na2O	G/L K2O	Corr. Factor
1000	92.20	0.13	30.06	0.08	0.01	0.64	0.02	0.00	-18.62	-0.01	-12.15	1.50	0.00	0.32	0.42	1.70	1.31
1001	90.10	0.13	29.70	0.03	0.01	0.78	0.02	0.00	-16.52	-0.01	-11.79	1.55	0.00	0.18	0.42	1.70	1.39
1005	62.50	0.13	20.66	0.20	0.01	0.29	0.00	0.00	11.08	-0.01	-2.75	1.38	0.00	0.67	0.44	1.70	0.90
2007	76.79	0.16	20.57	0.25	0.02	0.57	0.20	0.00	-3.21	-0.04	-2.66	1.33	-0.01	0.39	0.24	1.70	1.07
2008	92.90	0.12	17.82	1.83	0.01	1.06	0.45	1.98	-19.32	0.00	0.09	-0.25	0.00	-0.10	-0.01	-0.28	1.09
2010	49.51	0.17	17.84	0.99	0.01	0.68	0.19	0.15	24.07	-0.05	0.07	0.59	0.00	0.28	0.25	1.55	0.75
2011	43.18	0.11	15.93	0.50	0.01	0.26	0.11	0.01	30.40	0.01	1.98	1.08	0.00	0.70	0.33	1.69	0.65
2026	72.05	0.15	25.73	0.45	0.01	0.45	0.04	0.00	1.53	-0.03	-7.82	1.13	0.00	0.51	0.40	1.70	1.12
2027	66.68	0.10	14.04	1.35	0.01	1.10	1.79	2.00	6.90	0.02	3.87	0.23	0.00	-0.14	-1.35	-0.30	0.94
2028	72.58	0.14	20.57	0.07	0.01	0.40	0.06	0.00	1.00	-0.02	-2.66	1.51	0.00	0.56	0.38	1.70	1.03
2291	157.17	0.32	35.69	3.98	0.12	2.66	4.08	6.90	-83.59	-0.20	-17.78	-2.40	-0.11	-1.70	-3.64	-5.20	1.82
2292	66.98	0.13	19.75	0.09	0.01	0.36	0.05	0.00	6.60	-0.01	-1.84	1.49	0.00	0.60	0.39	1.70	0.91
2030	71.18	0.14	18.48	0.42	0.01	0.51	0.18	0.30	2.40	-0.02	-0.57	1.16	0.00	0.45	0.26	1.40	0.98
2031	36.63	0.12	14.08	0.72	0.01	0.58	0.18	0.60	36.95	0.00	3.83	0.86	0.00	0.38	0.26	1.10	0.58
2035	74.12	0.12	33.07	0.01	0.01	0.56	0.08	0.00	-0.54	0.00	-15.16	1.57	0.00	0.40	0.36	1.70	1.18
3085	73.58	0.12	17.91	1.58	0.01	0.96	0.44	1.70	0.00	0.00	0.00	0.00	0.00	0.00	0.00	0.00	1.00
3086	48.66	0.10	13.89	2.01	0.01	0.72	0.25	2.71	24.92	0.02	4.02	-0.43	0.00	0.24	0.19	-1.01	0.71
3087	82.06	0.11	20.38	2.33	0.01	0.47	0.07	0.00	-8.48	0.01	-2.47	-0.75	0.00	0.49	0.37	1.70	1.09
2041	60.78	0.13	19.21	0.00	0.01	0.82	0.06	0.00	12.80	-0.01	-1.30	1.58	0.00	0.14	0.38	1.70	0.92
2042	62.74	0.13	15.76	1.70	0.02	0.99	0.97	1.76	10.84	-0.01	2.15	-0.12	-0.01	-0.03	-0.53	-0.06	0.80
2043	159.92	0.14	27.28	1.26	0.02	0.87	0.42	0.00	-86.34	-0.02	-9.37	0.32	-0.01	0.09	0.02	1.70	1.97
2044	82.79	0.13	17.33	1.69	0.02	1.28	1.00	1.56	-9.21	-0.01	0.58	-0.11	-0.01	-0.32	-0.56	0.14	1.04
2045	85.73	0.19	21.86	0.32	0.01	0.47	0.28	0.14	-12.15	-0.07	-3.95	1.26	0.00	0.49	0.16	1.56	1.11
2046	131.64	0.13	21.95	0.00	0.01	0.65	0.22	0.00	-58.06	-0.01	-4.04	1.58	0.00	0.31	0.22	1.70	1.65
2047	73.38	0.11	17.70	0.00	0.00	0.40	0.07	0.00	0.20	0.01	0.21	1.58	0.01	0.56	0.37	1.70	0.97
2048	37.96	0.13	17.04	0.14	0.00	0.26	0.02	0.00	35.62	-0.01	0.87	1.44	0.01	0.70	0.42	1.70	0.63
2051	81.12	0.13	23.63	0.00	0.01	0.46	0.13	0.17	-7.54	-0.01	-5.72	1.58	0.00	0.50	0.31	1.53	1.05
2052	65.63	0.11	23.83	0.00	0.01	0.48	0.08	0.08	7.95	0.01	-5.92	1.58	0.00	0.48	0.36	1.62	0.94
3064	94.89	0.12	22.03	0.00	0.01	0.46	0.89	0.00	-21.31	0.00	-4.12	1.58	0.00	0.50	-0.45	1.70	1.27
3065	61.54	0.13	30.23	0.14	0.01	0.42	0.08	0.00	12.04	-0.01	-12.32	1.44	0.00	0.54	0.36	1.70	1.05
3066	101.74	0.27	23.45	0.00	0.01	0.49	0.20	0.00	-28.16	-0.15	-5.54	1.58	0.00	0.47	0.24	1.70	1.32
3067	30.63	0.18	24.69	0.27	0.00	0.31	0.05	0.00	42.95	-0.06	-6.78	1.31	0.01	0.65	0.39	1.70	0.66
3068	74.82	0.12	40.05	0.00	0.01	0.78	0.07	0.00	-1.24	0.00	-22.14	1.58	0.00	0.18	0.37	1.70	1.39
3069	98.34	0.11	12.29	0.00	0.01	0.41	0.09	0.00	-24.76	0.01	5.62	1.58	0.00	0.55	0.35	1.70	1.16
3070	58.53	0.11	15.82	2.87	0.01	0.37	0.07	0.00	15.05	0.01	2.09	-1.29	0.00	0.59	0.37	1.70	0.81
3071	58.92	0.12	13.11	2.60	0.01	0.59	0.16	2.39	14.66	0.00	4.80	-1.02	0.00	0.37	0.28	-0.69	0.82
2006	70.08	0.12	22.20	0.00	0.00	0.36	0.05	0.00	3.50	0.00	-4.29	1.58	0.01	0.60	0.39	1.70	0.98
2009	40.74	0.11	14.67	2.30	0.02	0.46	0.07	0.52	32.84	0.01	3.24	-0.72	-0.01	0.50	0.37	1.18	0.61

Table 5 Molarity of major oxides components in ore specimens. Gains and losses are calculated based on 1 liter of specimens.

Sample	Mol/L SiO2	Mol/L TiO2	Mol/L Al2O3	Mol/L Fe2O3	Mol/L MnO	Mol/L MgO	Mol/L CaO	Mol/L Na2O	Mol/L K2O	Mol/L P2O5	G/L SiO2	G/L TiO2	G/L Al2O3	G/L Fe2O3	G/L MnO	G/L MgO	G/L CaO	G/L Na2O	G/L K2O	G/L P2O5
1000	27.32	0.03	5.25	0.01	0.00	0.00	0.20	0.01	0.00	0.00	-7.13	0.00	-2.74	0.22	0.00	0.00	0.13	0.16	0.42	0.00
1001	27.03	0.03	5.25	0.00	0.00	0.00	0.25	0.01	0.00	0.00	-6.32	0.00	-2.66	0.22	0.00	0.00	0.07	0.16	0.42	0.00
1005	25.96	0.04	5.06	0.03	0.00	0.00	0.13	0.00	0.00	0.00	4.06	0.00	-0.59	0.19	0.00	0.00	0.26	0.16	0.40	0.00
2007	25.89	0.04	4.09	0.03	0.01	0.00	0.21	0.07	0.00	0.00	-1.13	-0.01	-0.55	0.18	0.00	0.00	0.15	0.08	0.38	0.00
2008	28.74	0.03	3.25	0.21	0.00	0.00	0.35	0.13	0.39	0.00	-7.02	0.00	0.02	-0.03	0.00	0.00	-0.04	0.00	-0.06	0.00
2010	25.24	0.06	5.36	0.19	0.00	0.00	0.37	0.09	0.05	0.00	9.21	-0.01	0.01	0.09	0.00	0.00	0.11	0.09	0.38	0.00
2011	26.22	0.05	5.70	0.11	0.00	0.00	0.17	0.06	0.00	0.00	11.64	0.00	0.45	0.16	0.00	0.00	0.29	0.12	0.42	0.00
2026	27.51	0.04	5.79	0.06	0.00	0.00	0.18	0.02	0.00	0.00	0.61	-0.01	-1.83	0.17	0.00	0.00	0.22	0.15	0.43	0.00
2027	28.07	0.03	3.48	0.21	0.00	0.00	0.50	0.73	0.54	0.00	2.53	0.00	0.83	0.03	0.00	0.00	-0.05	-0.48	-0.07	0.00
2028	28.09	0.04	4.63	0.01	0.00	0.00	0.17	0.02	0.00	0.00	0.38	0.00	-0.59	0.21	0.00	0.00	0.23	0.14	0.41	0.00
2291	25.45	0.04	3.40	0.24	0.02	0.38	0.46	0.64	0.71	0.00	-29.02	-0.05	-3.64	-0.31	-0.03	-0.18	-0.63	-1.22	-1.15	0.00
2292	25.82	0.04	4.49	0.01	0.00	0.00	0.15	0.02	0.00	0.00	2.29	0.00	-0.38	0.19	0.00	0.00	0.22	0.13	0.38	0.00
2030	26.08	0.04	3.99	0.06	0.00	0.00	0.20	0.06	0.07	0.00	0.84	-0.01	-0.12	0.15	0.00	0.00	0.17	0.09	0.31	0.00
2031	23.02	0.06	5.21	0.17	0.00	0.00	0.39	0.11	0.24	0.00	12.92	0.00	0.79	0.11	0.00	0.00	0.14	0.09	0.25	0.00
2035	24.64	0.03	6.48	0.00	0.00	0.00	0.20	0.02	0.00	0.00	-0.21	0.00	-3.43	0.23	0.00	0.00	0.17	0.14	0.42	0.00
3085	26.50	0.03	3.80	0.21	0.00	0.00	0.37	0.15	0.39	0.00	0.00	0.00	0.00	0.00	0.00	0.00	0.00	0.00	0.00	0.00
3086	24.69	0.04	4.15	0.38	0.01	0.00	0.39	0.12	0.88	0.00	8.98	0.01	0.85	-0.06	0.00	0.00	0.09	0.07	-0.23	0.00
3087	27.28	0.03	3.99	0.29	0.00	0.00	0.17	0.02	0.00	0.00	-3.05	0.00	-0.52	-0.10	0.00	0.00	0.19	0.13	0.39	0.00
2041	26.21	0.04	4.88	0.00	0.00	0.00	0.38	0.03	0.00	0.00	4.69	0.00	-0.28	0.22	0.00	0.00	0.06	0.13	0.40	0.00
2042	28.29	0.04	4.19	0.29	0.01	0.00	0.48	0.43	0.51	0.00	4.15	0.00	0.48	-0.02	0.00	0.00	-0.01	-0.20	-0.01	0.00
2043	31.49	0.02	3.17	0.09	0.00	0.00	0.18	0.08	0.00	0.00	-33.05	-0.01	-2.11	0.05	0.00	0.00	0.04	0.01	0.42	0.00
2044	29.56	0.03	3.65	0.23	0.00	0.00	0.49	0.35	0.36	0.00	-3.53	0.00	0.13	-0.02	0.00	0.00	-0.13	-0.21	0.04	0.00
2045	29.19	0.05	4.39	0.04	0.00	0.00	0.17	0.09	0.03	0.00	-4.65	-0.02	-0.89	0.18	0.00	0.00	0.20	0.06	0.38	0.00
2046	33.44	0.02	3.29	0.00	0.00	0.00	0.18	0.06	0.00	0.00	-23.24	0.00	-0.95	0.24	0.00	0.00	0.13	0.08	0.44	0.00
2047	31.43	0.03	4.47	0.00	0.00	0.00	0.18	0.03	0.00	0.00	0.08	0.00	0.05	0.24	0.00	0.00	0.24	0.14	0.44	0.00
2048	25.05	0.06	6.63	0.04	0.00	0.00	0.18	0.01	0.00	0.00	13.93	0.00	0.20	0.21	0.00	0.00	0.29	0.16	0.43	0.00
2051	28.86	0.04	4.95	0.00	0.00	0.00	0.17	0.05	0.04	0.00	-2.94	0.00	-1.31	0.23	0.00	0.00	0.21	0.12	0.38	0.00
2052	26.78	0.03	5.73	0.00	0.00	0.00	0.21	0.03	0.02	0.00	3.11	0.00	-1.37	0.23	0.00	0.00	0.20	0.14	0.41	0.00
3064	30.56	0.03	4.18	0.00	0.00	0.00	0.16	0.28	0.00	0.00	-8.30	0.00	-0.95	0.23	0.00	0.00	0.21	-0.17	0.42	0.00
3065	23.56	0.04	6.82	0.02	0.00	0.00	0.17	0.03	0.00	0.00	4.61	0.00	-2.78	0.21	0.00	0.00	0.22	0.13	0.42	0.00
3066	29.96	0.06	4.07	0.00	0.00	0.00	0.15	0.06	0.00	0.00	-10.78	-0.04	-1.25	0.23	0.00	0.00	0.19	0.09	0.42	0.00
3067	18.15	0.08	8.62	0.06	0.00	0.00	0.20	0.03	0.00	0.00	16.44	-0.02	-1.53	0.19	0.00	0.00	0.27	0.14	0.42	0.00
3068	23.28	0.03	7.34	0.00	0.00	0.00	0.26	0.02	0.00	0.00	-0.50	0.00	-5.21	0.24	0.00	0.00	0.08	0.14	0.44	0.00
3069	33.85	0.03	2.49	0.00	0.00	0.00	0.15	0.03	0.00	0.00	-9.48	0.00	1.27	0.23	0.00	0.00	0.22	0.13	0.42	0.00
3070	28.21	0.04	4.49	0.52	0.00	0.00	0.19	0.03	0.00	0.00	6.01	0.00	0.49	-0.19	0.00	0.00	0.25	0.14	0.44	0.00
3071	28.52	0.04	3.74	0.47	0.00	0.00	0.31	0.08	0.74	0.00	5.61	0.00	1.08	-0.15	0.00	0.00	0.15	0.10	-0.17	0.00
2006	26.65	0.03	4.97	0.00	0.00	0.00	0.15	0.02	0.00	0.00	1.28	0.00	-0.93	0.22	0.00	0.00	0.24	0.14	0.40	0.00
2009	24.10	0.05	5.11	0.51	0.01	0.00	0.29	0.04	0.20	0.00	12.03	0.00	0.70	-0.10	0.00	0.00	0.19	0.13	0.28	0.00

quartz-rich bodies, locally precipitated from silica supersaturated fluids at any favorable sites, can cause local variation of silica gains and losses to a great extent. Although silica changes widely in mass, SiO_2/Al_2O_3 ratio does not change much between the precursor and the ore zone. Since only SiO_2 and Al_2O_3 are contained as major components in the system, and assuming Al_2O_3 as immobile, mass changes in SiO_2 would have a major effect on the modal abundance of quartz and kaolinite. Within the bonanza, SiO_2 concentration of ore specimens has a negative correlation to Al_2O_3 content, without any systematic relation with other major components. So, gains and losses plots between SiO_2 and other major oxides display scattered points in the graph, suggesting that the mass changes of SiO_2 was independent of the others, except Al_2O_3. Interrelation in mass gains and losses of components within the ore deposit is present diagramatically in Fig. 10.

Graphical presentations of gains and losses of other major elements reveal no systematic relation between Fe_2O_3 and alkalies. Consequently, it can be deduced that these components left the system with different ratio or they didn't do together. But opposite is true for alkalis. Strong interdependency between Na_2O and CaO displayed in Fig. 11, leads to the conclusion that these components simultaneously went into and out of the system during the alteration. K_2O show no relation to Na_2O and CaO.

K_2O and Rb element pair (Fig. 12) shows high correlation coefficient (R = 0.973) as Nb-Zr pair. Major difference between two element-pairs is that the Nb and Zr have positive concentration values (4 and 72 ppm) in the least-concentrated specimen, i. e. they explicitly remained in the system after alteration. Therefore, their high correlation coefficient is an evidence of their immobility. Meanwhile K_2O and Rb show 0.00wt% in many specimens and this fact characterizes total removal or mobility of these elements during alteration process. Thus, K_2O-Rb relation can be interpreted as both were contained in a certain mineral (possibly K-feldspar) and went into and out of the system with constant interelement ratio due to precipitation or dissolution of that mineral.

Among possible candidates for immobile elements, TiO_2 and Al_2O_3 do not show high correlation coefficients as expected. TiO_2 reveals R values of 0.667, 0.688, and 0.506 in correlation with Nb, Zr, and Al_2O_3, respectively. Al_2O_3, in particular, shows lowest correlation coefficient of 0.506, 0.401, and 0.471 in correlation with TiO_2, Nb, and Zr, respectively. This result is quite contrary to theoretical and empirical consideration of metasomatic process in which Al_2O_3 is

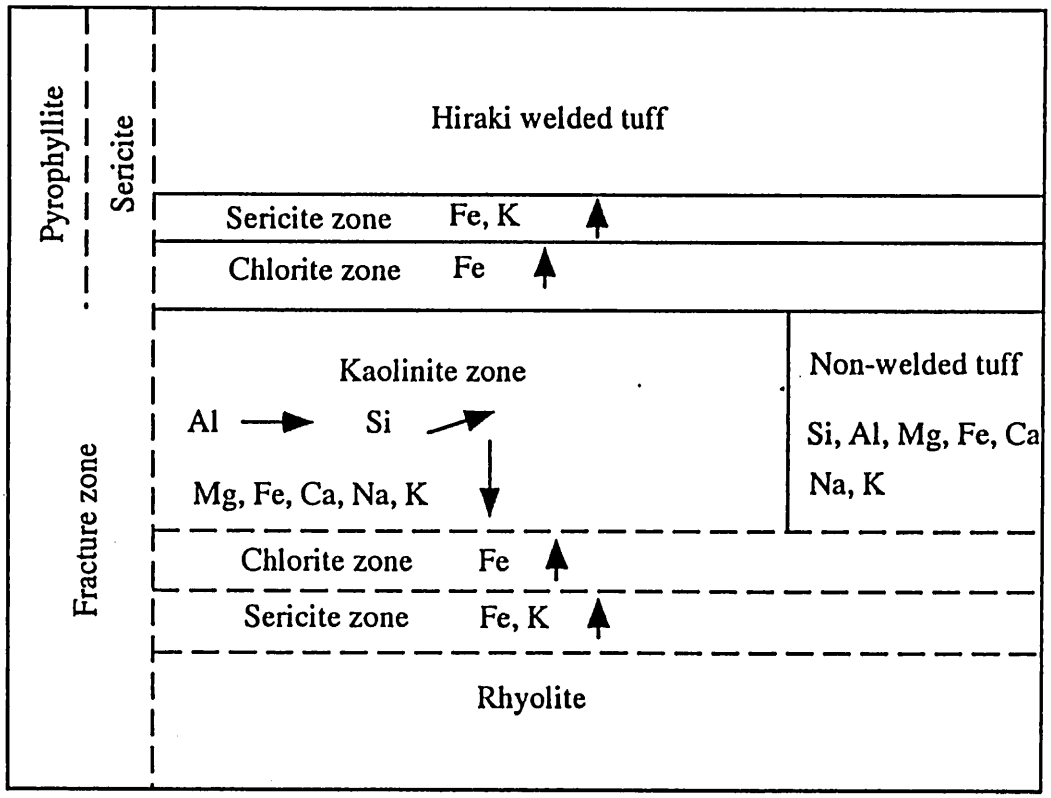

Fig. 10 Graphical presentation of the nature of gains and losses in mass of chemical components between protolith and alteration "zones" in the Hiraki mine.

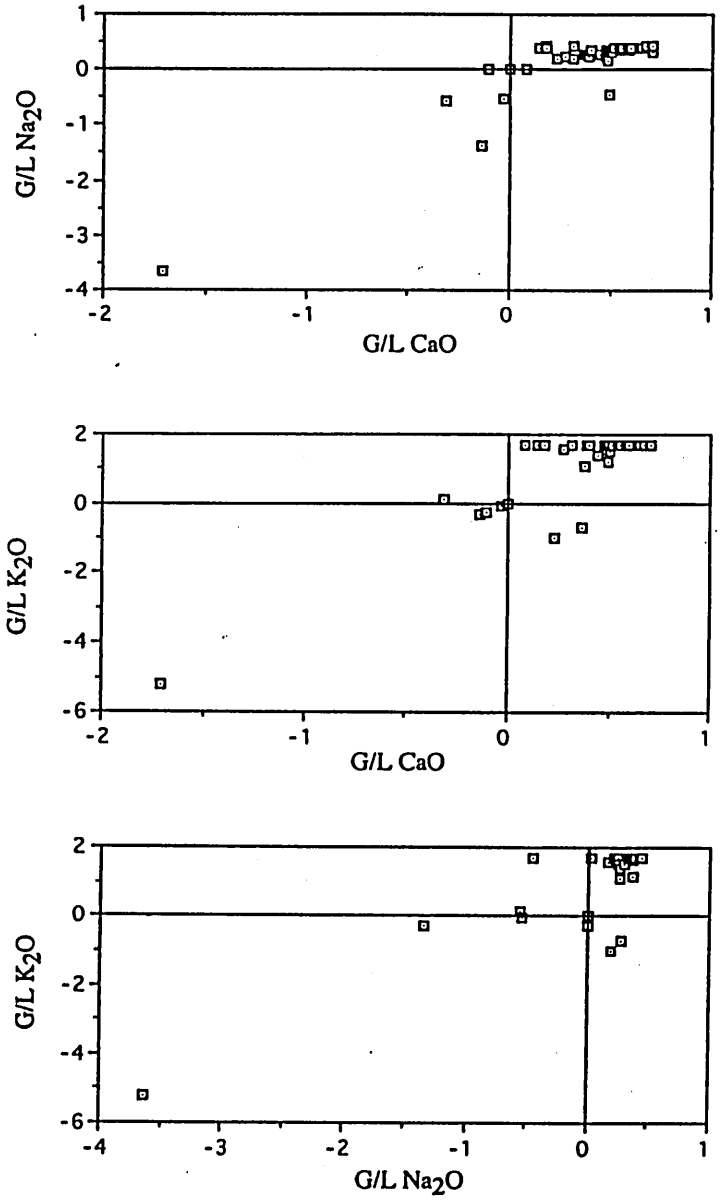

Fig. 11 Interrelations of gains and losses among alkalis and alkali earth elements. Almost all plots in CaO - Na_2O fall in lower left quadrant (-ve vs. -ve, i. e. both added in constant ratio) and upper right quadrant (+ve vs. +ve, i. e. both depleted in constant ratio).

assumed as truly immobile component in the hydrothermal alteration because of its very low solubility (Gressens, 1967; Korzhinskii, 1970; Grant, 1986). In most geochemical systems involving aqueous solutions the activity of aluminum species in the aqueous phase are so low that even large changes in their activities do not appreciably affect the mass transfer among the solids in the system. For this reason such a process can be viewed as one in which aluminum is essentially conserved among the solid phases.

Hydrolysis constants of aluminum species are at least 6.0 ~ 10.0 log unit lower than other major dissolved species at a given pressure, temperature, and pH conditions (Bower et al., 1984; Bourcier et al., 1993, and references therein). Hence, Al_2O_3 is apparently immobile in alteration process of aluminosilicate minerals. Experimental results of Hemley et al., 1980, reveal isobaric stability relation among minerals in the system Al_2O_3 - SiO_2 - H_2O as a function of temperature and the concentration of dissolved silica. Mineral solubility calculations show that at quartz saturation, aluminum is essentially inert component compared to the alkali earths (Mg^{2+}, Ca^{2+}, etc.) and alkali metals (Na^+, K^+, etc.) and it therefore can be considered to be conserved among solid in metasomatic environments, particularly under acid condition.

In concern with metasomatic mechanism (kaolinization) in which clay minerals are formed as precipitates after dissolution of feldspars, aluminum

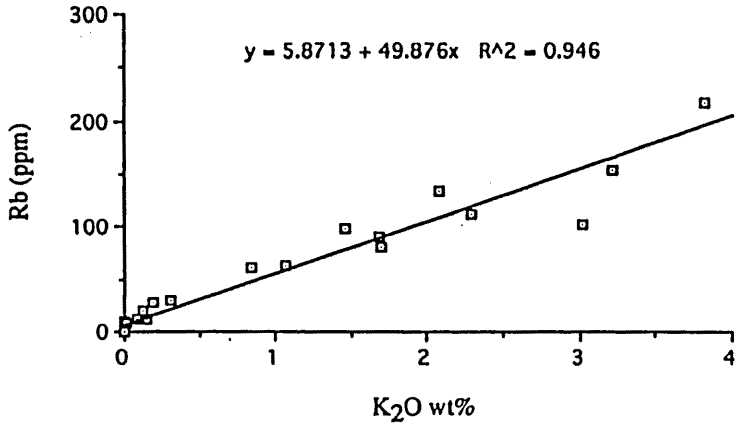

Fig. 12 Correlation between K_2O and Rb. Many samples with 0.00 wt% and undetected values do not appear in the figure. High correlation coefficient is because of their chemical affinity, not because of immobility as indicated in Fig. 9.

constant assumption has much more advantage than other concepts. In fact kaolinization is H^+ metasomatism (Meyer and Hemley, 1967) which is characterized by exchange of hydrogen ion for other cation, typically Na^+, K^+, and Ca^{+2}, of feldspars. H_2O, CO_2, and S are commonly added whereas aluminum species are conserved, in this process (Helgeson, 1979, and references therein; Hemley, et al., 1980, and references therein).

Thus, the present finding of the low correlation coefficient for Al_2O_3 might be due to some reasons other than its mobility in alteration process. In this connection, the low R value for Al_2O_3 might be caused by; (1) inhomogeneous composition in pyroclastics which naturally is not as homogeneous as magma derived volcanic rocks, and (2) the accuracy of calibration line used in chemical analyses which initially installed up to 20 wt% Al_2O_3. Both factors seem to affect in combination. If the former point is a principal cause, the limit of compositional variation of the non-welded tuff regarding Al_2O_3 can be estimated by the method described in the followings. Volcanic fractionation line can be drawn for the non-welded tuff on the binary plot of igneous compatible (Al_2O_3)-incompatible (Zr) element pair. If that compatible component can be assumed as immobile during alteration, the alteration trend which radiates from the origin will pass precursor composition on the fractionation line. Detailed explanation for fractionation line and alteration line is given in MacLean (1990).

As shown in Fig. 13, volcanic fractionation line was drawn based on precursor composition. If the non-welded tuff has variation in its Al_2O_3 concentration, their composition will be somewhere on the fractionation line. Two alteration lines were drawn to cover all possible compositions. Variation limit on the fractionation line can be fixed at the points *A* and *B* which were marked by crossing of alteration line and fractionation line. Numerical values of points *A* and *B* were read from their projection on y-axis and, these turn out to 24.0 and 15.0 respectively. Thus, it can be concluded from Fig. 7 that Al_2O_3 wt% of the non-welded might vary from 15.0 to 24.0.

Decrease in R value for Nb-Zr element pair (from 0.958 in bonanza to 0.911 for whole deposit) supports the existence of compositional variation within the non-welded tuff. This fact also points out that the concentration of Zr in precursor might vary to some extent. That is why some ore samples plot very far from precursor value (defined here at 208 ppm.) on the regression line and leading to unreasonable conclusion of 50% loss in total mass. If the Zr concentration in precursor could be up to 300 ppm., then total mass loss would decrease to ~25% and such change would be an expectable amount in natural alteration processes. Moreover, localized huge anomalies in SiO_2 content in the deposit might also satisfy the total mass gain / loss problem. Anyhow, plots of most of specimens represent the resultant loss in total mass, general phenomenon of alteration process, in the Hiraki deposit. Hence, present calculation frame of Zr as immobile monitor is valid for mass gain and loss estimation in the Hiraki mine.

VI. STABLE ISOTOPE SYSTEMATICS

Inasmuch as H_2O is the dominant constituent in fluid-rock interaction, a knowledge of its origin is fundamental to any theory of hydrothermal alteration process. At present the application of D/H and $^{18}O/^{16}O$ analyses as indicators of the origin and history of H_2O in the hydrothermal fluids has been practised for various geothermal fields and sea floor alteration around the world. Present paper will describe and discuss the nature and role of fluid, conceivably H_2O, in ore formation process at the Hiraki clay deposit.

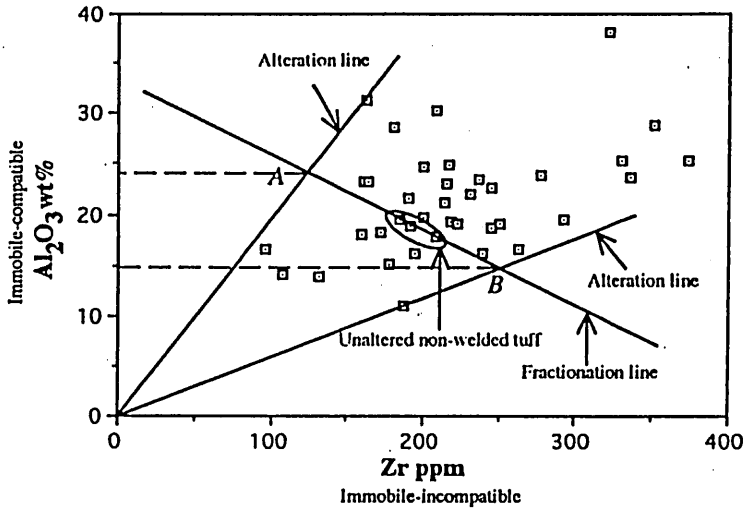

Fig. 13 Graphical method used to calculate the variation of Al_2O_3 content in precursor. Fractionation line is defined by igneous compatible-incompatible element-pair. Alteration lines were drawn to cover the maxima of lowest and highest depleted altered specimens.

1. Samples and analytical methods

Oxygen and hydrogen isotopic ratios were measured on whole-rock (not including veins), kaolinite-quartz samples and quartz. $\delta^{18}O$ measurements were done for three different types of quartz; (1) primary veined quartz in the Hiraki welded tuff (QV), (2) quartz from the extremely quartz-rich body formed in the orebody, and (3) quartz extracted from the kaolinite-quartz samples (ores). All these quartz are of hydrothermal origin based on their field occurrences and microscopic characteristics (Ko Ko Myint and Watanabe, 1995). Whole-rock powders were prepared by selecting a representative portion of the hand specimen. Quartz separates from ore samples (kaolinite+quartz) were hand-picked under the microscope from a coarse fraction (>45 mesh) to a fairly high purity and then altriated in water cylinder of 30 cm height for 2~3 hr.. After the precipitates were washed by dilute HCl, ultrasonic washing was applied for 30 minutes and three times for each specimen to remove any residual kaolinite and other fine-grained fractions. Quartz grains after ultrasonic washing were dried at room temperature and then checked their purity under binocular microscope, and X-ray diffractometer for fine-grained fractions. Later their isotopic values were used to calculate those for associated kaolinite by comparing whole-rock's values with the aid of mass balance calculation.

Firstly samples were pre-heated at 200°C for 12 hr. and placed into nickel reaction tubes. After introducing the nitrogen gas into the reaction tubes, those were heated at 250°C for 2.5 hr and then vacuumed all assembly line. Oxygen was extracted from samples by reaction with BrF_5 (550° C) for 12 hr (Taylor and Epstein, 1962). The oxygen was then converted to CO_2 by reaction with hot graphite at 800° C and this gas was analyzed for its $^{18}O/^{16}O$ on a dual-collector mass spectrometer. Isotopic data are reported as $\delta^{18}O$ values in ‰ relative to SMOW. The mean $\delta^{18}O$ value for NBS-28 quartz standard is +9.6‰. Analytical error associated with the $\delta^{18}O$ values is generally less than ± 0.2‰.

After removal of absorbed water at 200° C for 2 hr, hydrogen was extracted from hydrous minerals by dehydration under vacuum at ca. 1500°C. The gas (H_2 or H_2O) obtained, after passing through CuO reaction box at 400°C, was reduced to H_2 by reaction with uranium at 700°C (Bigeleisen et al.., 1952; Godfrey, 1962). The results are expressed as δD values in ‰ , relative to SMOW. The overall reproducibility of δD values has averaged ± 0.2‰. The H_2 yield, which is measured manometrically, is recalculated as the H_2O^+ content in wt%.

2. Analytical results

Oxygen isotopic composition

The measured $\delta^{18}O$ values for volcanics, pyroclastics and ore samples are given in Table 6 and Fig. 14 together with δ D values and brief lithologic descriptions. The results show a remarkably narrow range of values within and very close to magmatic water composition. The highest values obtained here are for those of the Hiraki welded tuff with 10.0 ‰ and the lowest values of 5.5 ‰ for ore samples. The rhyolite and the overlying non-welded tuff have fairly constant $\delta^{18}O$ values at about 8 ‰, which fall in the range of those of common rhyolites and granites ($\delta^{18}O \approx 6$ to 13 ‰, Field and Fifarek, 1985). Ore samples from the fracture zone which cut across all the volcanic sequences including the Hiraki welded tuff have $\delta^{18}O$ values of 6.6 ‰ and 6.9

Table 6 Hydrogen and oxygen isotopic values of volcanics, pyroclastics, and ores from the Hiraki mine.

Sample	Mineral/rock	H_2Owt%	δD_{SMOW} ‰	$\delta^{18}O_{SMOW}$ ‰
WT-2	Hiraki welded tuff	0.50	-63.7	10.0
4000	Hiraki welded tuff	0.69	-66.4	10.0
Q.V	Veined quartz			7.2
1013	Fracture zone	2.11	-67.5	6.6
1015	Fracture zone	0.65	-73.92	6.9
Q.R.B	Quartz-rich body			8.6
2042	Chlorite	2.60	-137.6	
1008	Ore	4.63	-93.76	5.5
1008-A	Quartz from 1008			8.3
1008-B	Kaolinite*	4.63	-93.76	0.932
2007	Ore	4.38	-95.31	7.4
2007-A	Quartz from 2007			8.3
2007-B	Kaolinite*	4.38	-95.31	0.9467
2008	Non-welded tuff	1.59	-79.54	7.9
2027	Non-welded tuff	1.85	-75.54	7.8
2034	Rhyolite	0.72	-82.77	8.0
R-1	Rhyolite	0.90	-84.46	7.3

Precision for $\delta^{18}O_{SMOW}$ ‰ measurements are 0.004 to 0.03. * = calculated value.

‰. $\delta^{18}O$ values of hydrothermal quartzes collected from three different places can be divided into two groups: (1) group with higher values for quartz separates from ore samples and quartz-rich body in the ore horizon, characterized by nearly constant values of 8.3 ‰ to 8.6 ‰; and (2) group with lower value for quartz from the vein, cutting across the Hiraki welded tuff, having 7.2 ‰. However, *in sensu lato*, $\delta^{18}O$ values of quartzes are fairly consistent around 8.0‰.

When a rock undergoes isotopic re-equilibration with fluid, the resulting isotope redistribution among constituent minerals (isotopic fractionation) is dependent of the respective mole fraction (or mass) of these minerals and temperature concerned. It can simply be stated as mass balance for any stable isotope between the rock and its minerals, since temperature can be assumed constant in a single reaction. Mathematical solution for this process is expressed by: -

$$\delta I_r = \sum_{m=1}^{m} X_i \delta I_m. \qquad \text{VI- 1,}$$

where $\delta I_r = \delta$ value of stable isotope species i of whole-rock in ‰

X_i = mole fraction of isotope species i in the mineral m

$\delta I_m = \delta$ value of isotope species i of mineral m in ‰, and summation is done for all constituent minerals.

Inasmuch as it simply states the mass-balance relation among the co-existing components (minerals) concerned, the Eq. (VI- 1) is independent of temperature-

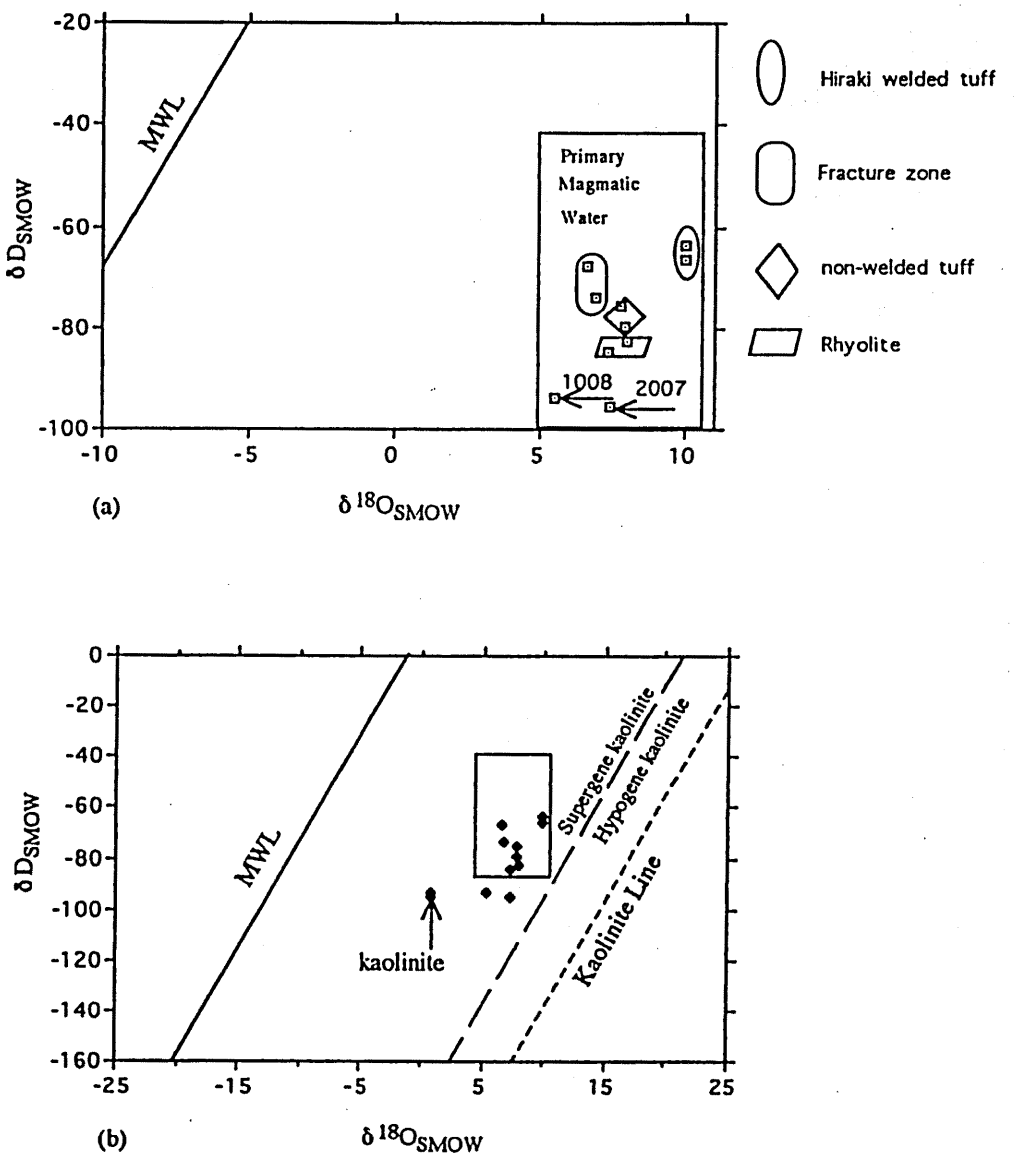

Fig. 14 Distribution of δD and $\delta^{18}O$ of volcanic rocks and ores in the Hiraki mine.

$\delta\ ^{18}O_{smow}$ values for Kaolinite in (b) are of results calculated by mass-balance method.

Magmatic water box and kaolinite lines are from Field and Fifarek (1985).

controlled. In other words, it uses the isotope values of minerals which underwent isotopic exchanges at same temperature.

Consequently, δ value of a constituent mineral can be determined, if mole fraction of all minerals, δ values of other minerals, and δ value for the whole-rock are known. Mole fraction of constituent minerals can be estimated either by petrographic (modal) or chemical (normative) analysis. Equation (VI- 1) is useful especially for rock of simple mineralogy such as ores of the Hiraki deposit.

In the present study $\delta^{18}O$ values for kaolinite are calculated from Eq. (VI- 1). Normative compositions of ore samples are computed based on the assumption that all of Al_2O_3 is conserved for kaolinite. This is because both ore samples, no. 2007 and no. 1008, are composed of single aluminum phase (kaolinite) and quartz. From the chemical formula of kaolinite ($Al_2Si_2O_5(OH)_4$), it can be defined that one mole of Al_2O_3 and two mole of SiO_2 are needed to form one mole of kaolinite, neglecting the replacement of $(OH)^{-1}$ to O^{-2} in lattice. Thus, molar concentration of Al_2O_3 in each ore sample represents number of mole of kaolinite in respective sample. Silica concentration after kaolinite formation (= mol. SiO_2 - 2*mol. Al_2O_3) was counted as quartz content of the specimen concerned. Calculations based on Al_2O_3 conserved frame give 0.2239 mol. kaolinite and 0.781 mol. of quartz for 100 gm of the sp. 2007 and, 0.2195 mol. of kaolinite and 0.7599 mol. of quartz for 100 gm of the sp. 1008 (n.b. chemical compositions were taken from Ko Ko Myint and Watanabe, 1995). So their respective

mole fractions of kaolinite and quartz turn out to be: 0.2228 and 0.7772 for the sp. 2007 and, 0.2241 and 0.7759 for the sp. 1008. Then, respective mineral mole fraction was multiplied by 4.5, to obtain O_2 mole fraction in kaolinite, and by 1.0, to obtain O_2 mole fraction in quartz. Substituting these figures together with $\delta^{18}O_{whole\ rock}$ data (Table 6) into Eq. (**VI-** 1), the results yield:

for sp. 2007, $\delta^{18}O_{kaol.} = (7.4 - 8.3*0.7772)/0.2228*4.5 = 0.9467$; and

for sp. 1008, $\delta^{18}O_{kaol.} = (5.5 - 8.3*0.7759)/0.2241*4.5 = 0.9320$.

These results disclosed that the calculated $\delta^{18}O_{kaol.}$ for each specimen are essentially the same and that the difference in values of $\delta^{18}O_{whole\text{-}rock}$ depends much on the mole fraction of quartz involved in the rock. This is probably because of the sluggish or no isotopic exchange of silica with water even at high temperature (500° ~ 600°C) can cause the quartz to retain its igneous isotopic nature (Taylor, 1974; Field and Fifarek, 1985). Therefore, $\delta^{18}O_{quartz}$ needs a particular treatment in the consideration of stable isotope systematics in hydrothermal alterations.

Hydrogen isotopic composition

δD composition of whole rock was measured for all volcanostratigraphic units exposed in the Hiraki mine, and ore samples. Similar to those of $\delta^{18}O$ values, the Hiraki welded tuff has heaviest composition with δD values of -64 ‰ and -66 ‰, and also samples from fracture cutting across the Hiraki welded tuff reveal high values, -68 ‰ and -74 ‰. Most deuterium depletion was detected in the ore samples from bonanza with δD of -94 ‰ and -95 ‰. Since the ore samples analyzed are composed purely of kaolinite and quartz, their δD values are applicable for kaolinite, only hydrous mineral in these samples . These isotope values of kaolinite (both δD and $\delta^{18}O$) plot far away from the supergene kaolinite and hence, suggests hydrothermal origin. The non-welded tuff shows moderate values of -76 ‰ and -80 ‰, while rhyolite reveals slightly depleted values of -83‰ and -84 ‰. From the results shown in the Table, it can be stated that there is only negligible deviation in δD values within each volcanostratigraphic unit and within ore samples from the same mineral zone.

It is noteworthy that chlorite has most depleted in D (deuterium) with δD value of -138‰. Suzuoki and Epstein (1976) demonstrated that the fractionation of D between micas and water is not only a function of temperature, but also related to the molar fraction of cations (Al, Mg, and Fe) by a general relation:

$$1000 \ln \alpha = -22.4 (10^6/T^2) + 28.2 + (2X_{Al} - 4X_{Mg} - 68X_{Fe})$$

where X is the molar fraction of each cation. From this mica-water fractionation, it may be inferred that values of 1000 ln α at constant temperature become progressively more depleted (negative) in D with the compositional succession from Al-rich through Mg-rich to Fe-rich micas. Experimental study by Marumo et al., 1980, also reveals that the α chlorite-water is related closer to chlorite's Fe/(Fe+Mg) ratio than equilibrium temperature. Its low δD value, interpreted by using the α chlorite-water - Fe/(Fe+Mg) relation diagram of Marumo et al., 1980, suggests that the chlorite from the Hiraki mine may have high Fe/(Fe+Mg) ratio. Criss and Taylor (1986) also noted low δD value (-149) of Fe-rich stilplomelane in a fossil meteoric-hydrothermal system associated with a gabbro body of the 55 Ma Skaergaard intrusion, Greenland.

VII. DISCUSSION

1. Physicochemical condition of alteration

Temperature and pressure estimations for the formation of the Hiraki kaolin deposit were done mainly based on well-established isotope method, since no measurable fluid inclusions were observed in hydrothermal quartz and other minerals.

Since the temperature dependency serves as the rationale for isotopic fractionation, $\Delta_{mineral\text{-}water}$ or $\Delta_{mineral\text{-}mineral}$ are used successfully for geothermometry in many active geothermal fields. In the Hiraki deposit, like other fossil hydrothermal system, isotope composition of equilibrium water cannot be detected by direct methods and thus, geothermometry of mineral-water fractionation is inapplicable. However, by use of two mineral-water fractionation equations, the unknown (δ_{fw}) can be neglected from calculation. This is based on the assumption that if two minerals in a system attain isotopic equilibrium with a fluid under the same temperature, the algebraic difference of their fractionation equations reveals the relation:

$$1000 \ln \alpha_{A-H2O} - 1000 \ln \alpha_{B-H2O} = 1000 \ln \alpha_{A-B} \qquad \textbf{VII-}\ 1,$$

where A and B represent minerals.

Nowadays, experimentally determined isotopic fractionation equations for common minerals in the geothermal fields are available from many sources. In the case of Hiraki mine, most prominent alteration mineral pair, quartz—kaolinite is used to estimate the formation temperature of the kaolin deposit. By use of the fractionation equations for kaolinite—H_2O pair (1000 $\ln\alpha_{kaolinite-H2O} = 2.05(10^6/T^2) - 3.85$, Kulla and Anderson, 1978) and for quratz—H_2O pair (1000 $\ln\alpha_{quartz-H2O} = 3.34\ (106/T2) -3.31$, Matsushita et al., 1979), Eq. (**VII-** 1) gives the following relation:

$$1000 \ln \alpha_{quartz-H2O} - 1000 \ln \alpha_{kaol-H2O} = 1000 \ln \alpha_{quartz-kaol}$$

$$\approx \Delta_{qtz-kaol} = \delta^{18}O_{qtz} - \delta^{18}O_{kaol} = 1.29(10^6/T^2) + 0.54$$

$$T^\circ K = 1.13 (10^3) / (\Delta_{qtz-kaol} - 0.54)^{1/2} \qquad \textbf{VII-}2.$$

Replacing the $\delta\ ^{18}O_{qtz}$ and $\delta\ ^{18}O_{kaol}$ values from Table 6 into Eq.(**VII**- 2) yields the isotopic equilibrium temperature as 159° C and 151°C. Since isotopic exchange process is independent of pressure, isotope thermometer is more reliable than other methods.

Based on experimental and geological evidences, Rising (1973) concluded that all the pure marcasite, formed above 157° C, are metastable. Thus, the common occurrence of marcasite in the Hiraki mine indicates that the formation temperature of kaolin deposit at the mine may be lower than 157° C. Above obtained relatively lower temperature is consistent with the extremely fine-grained nature of quartz and kaolinite in ores of the Hiraki mine.

Apart from kaolinite, a small amount of pyrophyllite is detected together with quartz and sericite in some fractures in the Hiraki deposit. Hence, the formation temperature can be estimated alternatively from the mineral stability relation in the system Al_2O_3 - SiO_2 - H_2O. There are two different configurations (topology) of stability fields depended upon source of data extracted, experimental data from Hemley et al., 1980, in the one hand and computational data of Bowers et al., 1984, on the other. The defined temperature for the pyrophyllite-kaolinite-quartz invariant points are falling at two different points of 259° and 293° C, respectively. Experimental results of Tsuzuki and Mizutani (1969, 1971) reported that kaolinite changes to pyrophyllite at

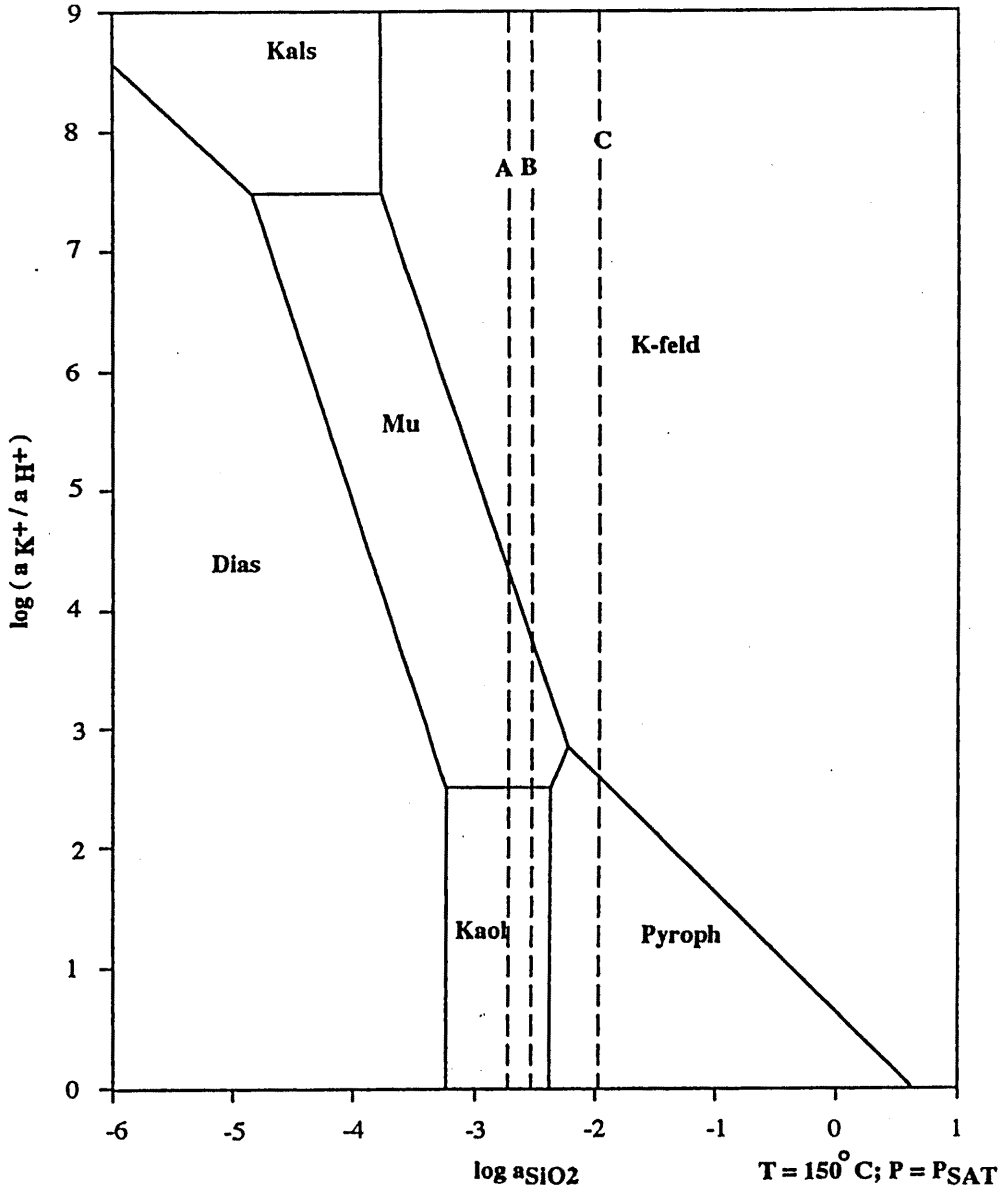

Kals = Kalsilite; **Mus** = Muscovite; **K-feld** = K-feldspar (microcline);
Dias = Diaspore; **Kaol** = Kaolinic; **Pyroph** = Pyrophyllite
Saturation limits : (A) quartz; (B) chalcedony; (C) amorphous silica.

Fig. 15 Activity diagram depicting the phase relation in the system HCl - H_2O - (Al_2O_3)- K_2O - SiO_2.

270°C. These results do not mean that pyrophyllite cannot occur at low temperature, instead it simply states that if physico-chemical parameters other than temperature are kept to be constant, kaolinite is more stable than pyrophyllite at low temperature.

It is conceivable from the activity diagrams (Fig. 15, 16 & 17) that pyrophyllite is stable at 150°C and vapour pressure, if the activity of SiO_2 is sufficiently high. This fact is in agreement with occurrence of extremely quartz-rich bodies in the Hiraki mine.

Many of the hydrothermally altered "Roseki" (= clayey rocks showing wax-like appearance, Fujii et. al., 1976) deposits in Japan made up of pyrophyllite or sericite as major clay minerals are supposed to be formed at temperature around 250° C (from fluid inclusion study) along vapor-pressure curve (Domen, 1988; Watanabe et al., 1994; Miyazaki, 1995; Katsura, 1995). In contrast to those deposits, major constituent mineral in the Hiraki deposit is kaolinite for which stability temperature is lower than that of pyrophyllite (Hemley et. al., 1980). Moreover, the stability field of kaolinite, major clay mineral in the Hiraki mine, becomes narrow in this type of diagram at temperature around 300°C. Based on these reasonings, the formation temperature of the Hiraki kaolin deposit was estimated to 150°C.

The aforementioned K - Ar age data, as well as volcanostratigraphy, indicate that at the time of alteration there was only the uppermost part of the Hiraki welded tuff, about 200 m thick (e. g., Ozaki and Matsuura, 1988), overlying the non-welded tuff. Therefore, pressure exerted would be lithostatic, corresponding to about 70 bars (assuming average rock's density as 2.7 g/cc), not far from the pressure reading on the vapor-pressure curve for pure water at 150° C. Even if the thickness of the overburden can be estimated accurately, it cannot be concluded that the underlying rocks were under pressure that produced by the overlying rocks. If there was not enough fluid to fill the available pore spaces, the overburden pressure could have been reduced to some extent. Hence formation pressure of the kaolin deposit at the Hiraki mine would be lower than 70 bars, more probably along the water vapor-pressure curve.

Chemical changes calculation described above testifies mass gains and losses during alteration process, a solid evidence for open-system metasomatism. In open-system alteration process, usually, huge mass of water is needed to flow through the system. This requirement is also fulfilled in formation of kaolin deposit at the Hiraki mine (matter pertaining to water/rock ratio will be discussed later). Such amount of fluids can infiltrate the

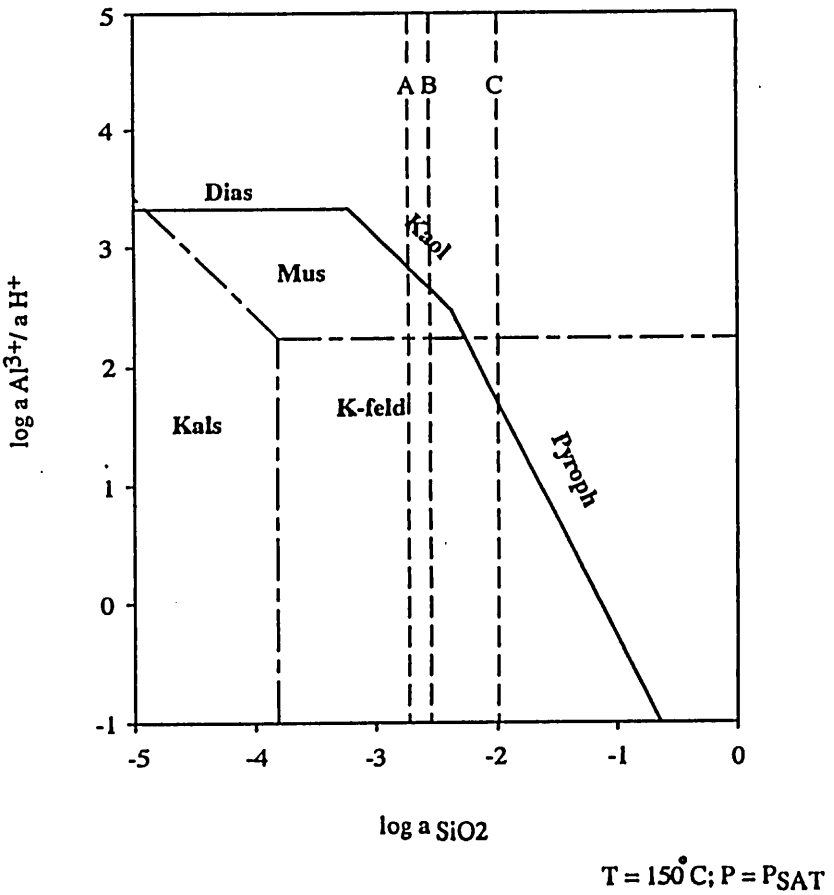

Fig. 16 Activity diagram depicting the phase relation in the system HCl - H_2O - Al_2O_3 - (K_2O) - SiO_2.

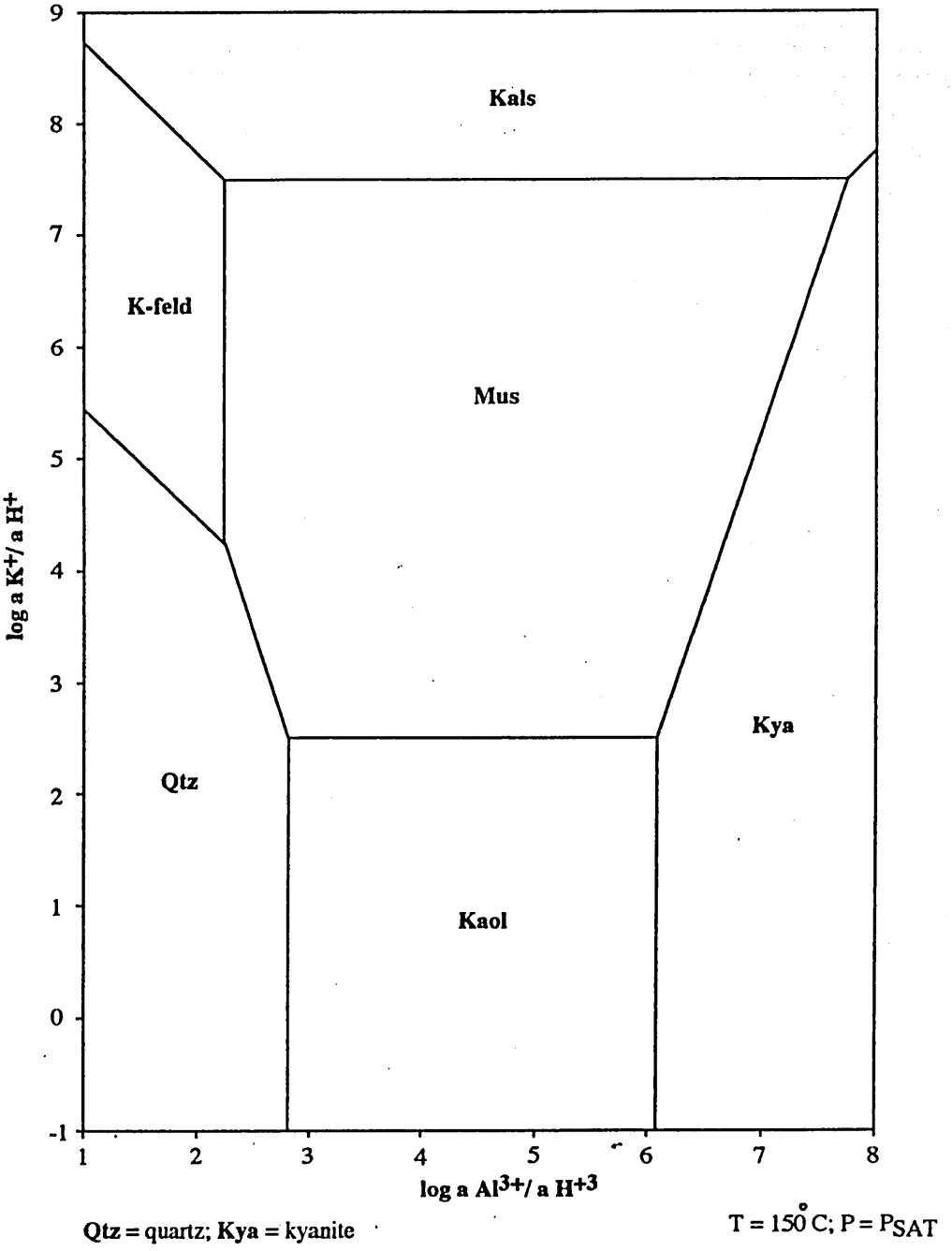

Fig. 17 Activity diagram depicting the phase relation in the system HCl - H_2O - Al_2O_3 - K_2O - (SiO_2).

rocks only when the system is dominated solely by vapor-pressure. This fact points out that pressure prevailing during alteration process may be vapor-pressure.

Therefore, to show the mineral stabilities, chemical activity diagrams of the Al_2O_3-K_2O-SiO_2-H_2O system are drawn for temperature 150° C and pressure along the vapour-liquid equilibrium curve for H_2O (Fig. 15, 16 & 17). Stability boundaries in the activity diagrams are defined by reactions shown in the Table 7, where activities of H_2O and mineral phases are assumed to be unity, being true for many geothermal systems in which inflowing fluids are generally weak electrolytes and common ion effect is extremely low.

2. Chemical stability of clay minerals

A wide variety of parameters, including pressure, temperature, mole fraction, molality, Eh, pH, fugacity, activity, and chemical potential are used by different scholars in expressive diagrams of mineral equilibria. Among them activity diagrams have an advantage for its

simplicity and usefulness in interpretation of fluid chemistry in metasomatism. Assuming local equilibrium between aqueous solutions and coexisting mineral assemblages in hydrothermal environments, logarithmic activity diagrams have been used extensively to interpret the chemical stability of these minerals.

Activity diagrams are very sensitive to the accuracy of thermodynamic data used to construct them. For instance, Al_H-s diagrams of Giggenbach (1984) in comparison with those of Giggenbach (1981) provided a general shift in the coexistence boundaries to higher Al_H values by about one log-unit without changes in their relative positions due to the different source of thermodynamic data. Most of thermodynamic data for high temperature mineral assemblages were, in fact, extended from empirical low temperature mineral dissolution constants by using computer routines. Therefore, sometimes those are needed to modify, in some geothermal fields, to match natural occurrence of clay minerals, which do not appear in activity diagrams applying computer derived data, e. g. Hendenquist and Browne, 1989.

Since the Hiraki clays are almost pure of kaolinite and quartz with a few mixed-layer clays, illite, montmorillonite, phengite, sericite and pyrophyllite, the Al_2O_3 - K_2O - SiO_2 - H_2O system is used to describe their chemical stability in activity diagrams. Ca and Na clays are not detected for the whole deposit and the reason will appear in following discussion. Activity diagrams are constructed for constant Al_2O_3 and constant SiO_2, and later those are combined to present in three-dimensional view. Equilibrium constants used to construct these diagrams were taken from Bower et al., 1984. Mineral coexistence boundaries were delineated by the mineral hydrolysis reactions (Table 7) where activities of H_2O and other stoichiometric mineral phases are assumed to be unity. This is true for many geothermal systems in which inlet fluids are generally weak electrolytes and common ion effect is extremely low.

However, nonstoichiometric minerals such as illite and montmorillonite are commonly represented in such type of diagram by either hypothetical end-member or pseudostoichiometric analogs of natural solid solution with specified composition and discrete, standard molal Gibbs free energy of formation. Although the idealized stoichiometric minerals may define the intercepts and slopes of their stability field boundaries on stability diagrams, the compositions of these minerals rarely coincide with those of natural counterparts. Some researcher, (e. g., Kittrick, 1971; Routson and Kittrick, 1971) measured the standard molal Gibb's free energy of formation experimentally from the elements for nonstoichiometric minerals with specified compositions and others, (e. g., Helgeson, 1969; Tardy and Garrels, 1974; Nriagu, 1975; Mattigod and Sposito, 1978; Merino and Ransom, 1982) estimated from cation-exchange data, water compositions and corresponding states algorithms, but they hardly represent the wide spectrum of composition observed in natural minerals, and in many respects their reliability is open to serious question.

At the Hiraki mine illite, montmorillonite and other mixed layer clay minerals often occur sporadically in the main orebody, and it is impossible to present their chemical stability in the conventional activity diagrams, which are prepared based on the stoichiometric minerals. However, attempts of Aagaard and Helgeson (1983),

Table 7 Reactions governing the mineral stability boundaries in the activity diagrams.

REACTIONS	log K (150 C; P_{SAT})
$AlO(OH) + K^+ + SiO_2 \rightleftharpoons KAlSiO_4 + H^+$	2.59
$KAlSiO_4 + 2SiO_2 \rightleftharpoons KAlSi_3O_8$	-4.23
$3\ AlO(OH) + K^+ + 3\ SiO_2 \rightleftharpoons KAl_2(AlSi_3O_{10})(OH)_2 + H^+$	-7.21
$3\ KAlSiO_4 + 2\ H^+ \rightleftharpoons KAl_2(AlSi_3O_{10})(OH)_2 + 2\ K^+$	-14.98
$3\ KAlSi_3O_8 + 2H^+ \rightleftharpoons KAl_2(AlSi_3O_{10})(OH)_2 + 2\ K^+ + 6\ SiO_2$	7.85
$Al_2Si_2O_5(OH)_4 \rightleftharpoons 2\ AlO(OH) + 2\ SiO_2 + H_2O$	6.47
$3\ Al_2Si_2O_5(OH)_4 + 2\ K^+ \rightleftharpoons 2\ KAl_2(AlSi_3O_{10})(OH)_2 + 2\ H^+ + 3\ H_2O$	7.79
$Al_2Si_4O_{10}(OH)_2 + H_2O \rightleftharpoons Al_2Si_2O_5(OH)_4 + 2\ SiO_2$	4.76
$Al_2Si_4O_{10}(OH)_2 + 2\ K^+ + 2\ SiO_2 \rightleftharpoons 2\ KAlSi_3O_8$	1.19
$3\ Al_2Si_4O_{10}(OH)_2 + 2\ K^+ \rightleftharpoons 2\ KAl_2(AlSi_3O_{10})(OH)_2 + H^+ + 6\ SiO_2$	19.27

Helgeson and Aagaard (1985) and Giggenbach (1985) in recent years rendered a new approach to depict non-stoichiometric clay minerals' stability fields in the activity diagrams.

Truesdell and Christ (1968) and Stoessell (1979, 1981) adopted regular solution models to calculate the thermodynamic consequences of compositional variation in montmorillonites and illites, respectively. In contrast, Helgeson and MacKenzie (1970) and Tardy and Fritz (1981) regarded clay minerals as ideal solutions of thermodynamic components. On the other hand, some authors, e. g. Garrel, 1984, regard mixed-layer minerals as a common aggregates of two end-members in varying ratios by pointing out the lack of some intermediate composition minerals. In the present study, mixed-layer minerals are assumed as solid-solution products of end-member components.

By assuming properties of clay minerals as ideal mixing of atoms on homological sites in the crystal lattices, the activity of the jth thermodynamic component of a solid solution can be computed from (Helgeson and Aagaard, 1985),

$$a_i=k_i\prod_s\prod_j a_{j,s}^{\nu_{s,j,i}}=k_i\prod_s\prod_j (X_{j,s}\lambda_{j,s})^{\nu_{s,j,i}} \quad \text{VII-3,}$$

where k_i represents a constant relating the inter- and intracrystalline states for the i th component (which may be temperature and/or pressure dependent), $a_{j,s}$, $\lambda_{j,s}$, and $X_{j,s}$ stand for the activity, activity coefficient, and mole fraction of the j th atom on the s th homological sites in the solid solution, and $\nu_{s,i,j}$ refers to the stoichiometric number of these sites occupied by the j th atom in the one mole of the i th component. As the mole fraction of the i th component of the solid solution approaches unity at any pressure and temperature, $\prod_s\prod_j a_{j,s}^{\nu_{s,j,i}}\rightarrow\prod_s\prod_j X_{j,s,i}^{\nu_{s,j,i}}$ for an intracrystalline state. Hence, an intercrystalline standard state calling for unit activity of the pure thermodynamic component in any specified state of substitutional order/disorder at a given pressure and temperature, k_i can be express as (Helgeson and Aagaard, 1985)

$$k_i=\prod_s\prod_j X_{j,s,i}^{-\nu_{s,j,i}} \quad \text{VII-4,}$$

where $X_{j,s,i}$represents the mole fraction of the j th atom on the s th sites in one mole of the i th thermodynamic component. If, in addition, all of the atoms mix ideally on the respective sites represented by s so that $\prod_s\prod_j \lambda_{j,s}^{\nu_{s,j,i}}=1$, Eq. (VII-3) reduces to

$$a_i= k_i\prod_s\prod_j X_{j,s}^{\nu_{s,j,i}} \quad \text{VII-5.}$$

Note that perfectly ordered component does $k_i = 1$.

To determine the thermodynamic stability fields of illite, montmorillonite and other mixed-layer clays in the activity diagrams, Aagaard and Helgeson (1983) considered thermodynamic components corresponding in stoichiometry to pyrophyllite, margarite, paragonite, and muscovite as end-members and computed their respective activities by use of Eq. (VII- 5) as

$$a_{Al_2Si_4O_{10}(OH)_2}=$$

$$k_1(X_{V,A})(X_{Al,M(2)_7})^2(X_{Si,T})^4 \quad \text{VII-6,}$$

$$a_{CaAl_2(Al_2Si_2O_{10})(OH)_2}=$$

$$k_2(X_{Ca,A})(X_{Al,M(2)})^2(X_{Al,T_1})^2(x_{Si,T_2})^2 \quad \text{VII-7,}$$

$$a_{NaAl_2(AlSi_3O_{10})(OH)_2}=$$

$$k_3(X_{Na,A})(X_{Al,M(2)})^2(X_{Al,T})\,(X_{Si,T})^3 \quad \text{VII-8,}$$

and

$$a_{KAl_2(AlSi_3O_{10})(OH)_2}=$$

$$k_4(X_{K,A})(X_{Al,M(2)})^2(X_{Al,T})\,(X_{Si,T})^3 \quad \text{VII-9,}$$

where k_1, k_2, k_3, and k_4 are the factors normalizing the activity of the pure end-member components to unity, $X_{V,A}$ stand for the mole fraction of vacancies (V) and the A (exchange) sites, $X_{Ca,A}$, $X_{Na,A}$, $X_{K,A}$ refer to the corresponding mole fractions of Ca, Na, and K on the A sites, $X_{Al,T}$, X_{Al,T_1} , $X_{Si,T}$, X_{Si,T_2} , and $X_{Al,M(2)}$ denote the mole fractions of Al and Si on the tetrahedral (T or T_1 and T_2) and M(2) octahedral sites.

An alternative approach to depict stability of dioctahedral clay minerals over a range delineated by three end-members pyrophyllite, alkali mica, and celadonite is given by Giggenbach, 1985. Dioctahedral clays have general composition corresponding to:

$$Y_{m+c}(Al_{2-c}(Mg^{2+},Fe^{2+})_c)O_{10}(Al_mSi_{4-m})_TO_{10}(OH)_2 \quad \text{VII-10}$$

where m and c are the number of Al^{3+} ions and divalent cations on the tetrahedral (T) and octahedral (O) sites, respectively; and Ym+c the sum of cation equivalents (Na+K+2Mg+2Ca) on the exchange sites. If we consider that the proportion of Fe^{3+}, substituting for Al^{3+} in octahedral and possibly tetrahedral sites, is negligibly small under reducing conditions prevailing in geothermal system (Giggenbach, 1984), the values of m correspond to the mole fraction of alkali mica (muscovite, paragonite) and c to the mole fraction of celadonite with an end-member composition:

$$Y^+Al(Mg^{2+},Fe^{2+})Si_4O_{10}(OH)_2$$

By use of the general composition of dioctahedral clays above-mentioned, the mole fractions of atoms on homological sites may be expressed in terms of the two parameters m and c, and Eq. (VII- 6) to (VII- 9), after Giggenbach (1985), becomes:

$$a\ \text{pyrophyllite} =$$

$$(1\text{-}m\text{-}c)[(2\text{-}c)/2]^2\ X\ [(4\text{-}m)/4]^4 \quad \text{VII-11,}$$

and

$$a\ \text{alkali mica} =$$

$$x_j(m+c)[(2\text{-}c)/2]^2\ X\ m[(4\text{-}m)/3]^3 \quad \text{VII-12,}$$

where x_j is the cation j contributing to the sum (m+c) of exchange sites occupied by alkali or alkali-earth elements. Relation (VII- 12) explains that with decreasing end-

member activities the stability ranges of clay minerals can be expected to invade deeply those of neighbouring phases.

Clay minerals' composition defined by in terms of end-members (muscovite and pyrophyllite) composition are diagramatically presented in the Fig. 18, in which possible tetrahedral replacement is neglected because of undevelopment of trioctahedral phases in the Hiraki deposit. However, in general case Fe^{3+} may enter into tetrahedral coordination in montmorillonite, however (Ericsson et al., 1977).

Thus, the stability boundaries for illite, phengite, celadonite, mixed layer, beidellite, and montmorillonite in $K_H = \log aK^+/aH^+$ vs. $s = \log aSiO2$ diagrams can be fixed by relations :

$$K_H = K_{20} + 1.5A_{microcline} - 0.5A_{muscovite} - 3s \quad \text{VII-13}$$

and,

$$K_H = K_{21} + A_{microcline} - 0.5A_{pyrophyllite} - s \quad \text{VII-14}$$

where $A_{microcline} = \log a_{microcline}$, $A_{muscovite} = \log a_{muscovite}$, $A_{pyrophyllite} = \log a_{pyrophyllite}$, K_{13} and K_{14} are the logarithms of the equilibrium constants describing the $K^+ - H^+$ exchanging reaction among microcline and the two clay mineral end-members, muscovite and pyrophyllite according to:

$$1.5\ \text{microcline} + H^+ \rightleftharpoons 0.5\ \text{muscovite} + 3\ \text{silica} + K^+ \quad \text{VII-15}$$

and,

$$\text{microcline} + H^+ \rightleftharpoons 0.5\ \text{pyrophyllite} + \text{silica} + K^+ \quad \text{VII-16}$$

The general tie lines between two base limits (microcline-muscovite and microcline-pyrophyllite) correspond to the general equation:

$$K_H = K_{muscovite} - 1.5K_{pyrophyllite} + 3s + D_K \quad \text{VII-17},$$

where K_i is the logarithm of the hydrolysis constant of the corresponding phases; and $D_K = A_{muscovite} - 1.5A_{pyrophyllite}$, a parameter describing the deviation of data points from the line describing the theoretical coexistence of the two end-members muscovite and pyrophyllite according to the reaction:

$$1.5\text{pyrophyllite} + K^+ \rightleftharpoons \text{muscovite} + 3\ \text{silica} + H^+ \quad \text{VII-18}$$

A detailed discussion of the procedure for the construction of stability diagrams involving dioctahedral clay minerals by use of Eqns. (VII- 11) and (VII- 12) is given by Giggenbach (1985). Care must be taken that such type of diagrams are as valid as its basic assumption, i. e. solid solution model, since there are some authors (e. g. Garrel, 1984) argue that these are not true solid solution series and are mere mixture of two phases based on the equilibrium concentration of silica in coexisting

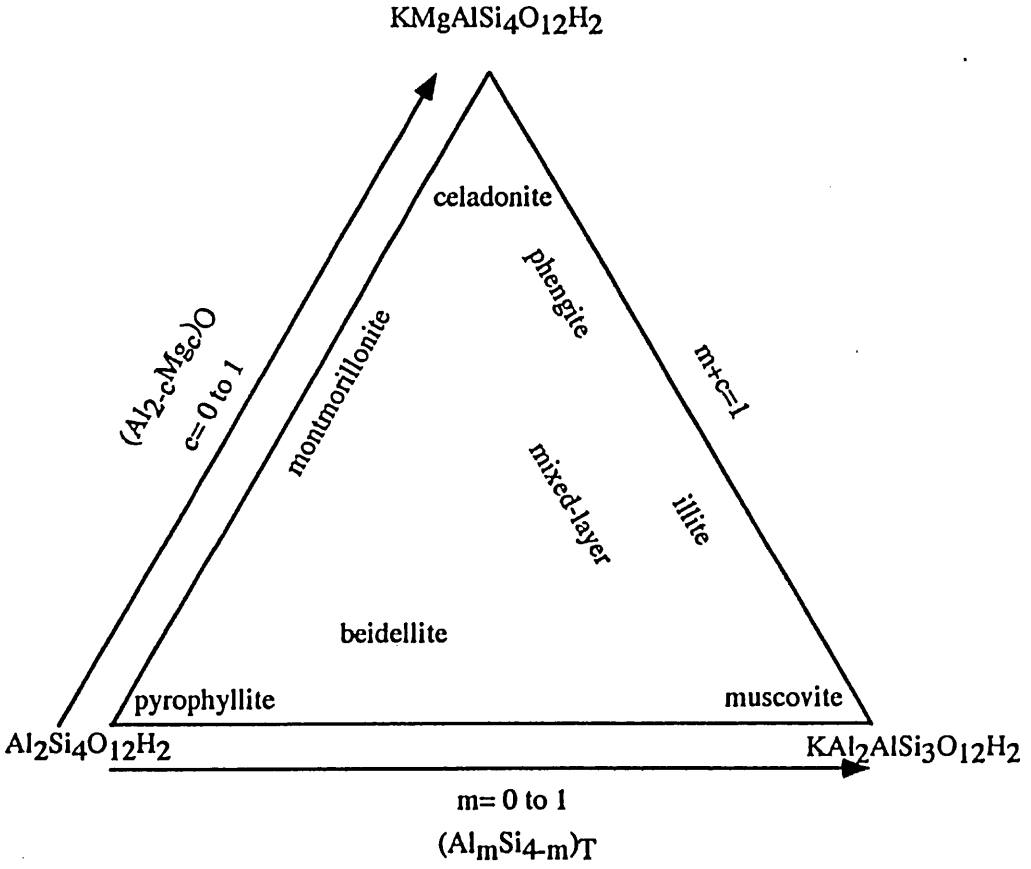

Fig. 18 Potential stability fields of dioctahedral K+ clay minerals in the solid solutions among the three-end-member system, pyrophyllite-muscovite-celadonite (for c,m,t = 0 to 1). (Modified after Giggenbach, 1985).

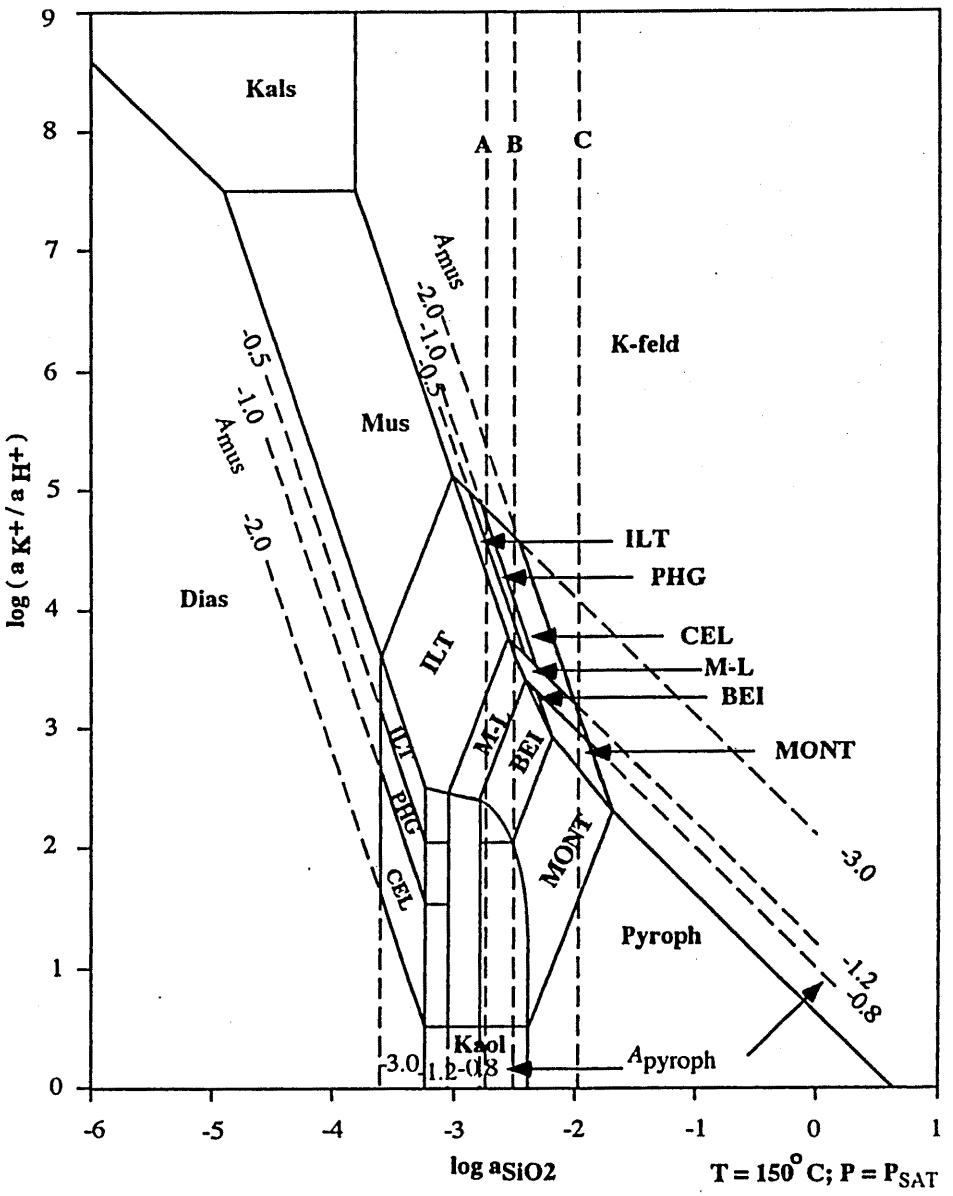

Kals = Kalsilite; **Mus** = Muscovite; **K-feld** = K-feldspar (microcline);
Dias = Diaspore; **Kaol** = Kaolinie; **Pyroph** = Pyrophyllite;
ILT = Illite; **PHG** = Phengite; **CEL** = Celadonite; **M-L** =Mixed-layer;
BEI = Beidellite; **MONT** = Montmorillonite.

Saturation limits : **(A)** quartz; **(B)** chalcedony; **(C)** amorphous silica.

Fig. 19 Stability of non-stoichiometric clays in terms of pyrophyllite and muscovite end-members' activities.

equilibrated aqueous solutions . Temperature effects on these diagrams can be visualized by comparing of same diagrams in differing temperatures (not shown in here). In thermodynamic consideration alone, it is revealed that the stability fields of non-stoichiometric clay minerals shifted to lower K_H values and higher silica activity with increasing temperature without any noticeable changes in its topology.

It is obvious from the activity diagrams, Fig. 19 & 20, that at any temperature, the non-stoichiometric clays are more stable than their end-member alkali-mica at relatively low K_H and high silica activity, and this facts again support the formation condition of phengite when the strong peraluminous (low alkalis) host-rock undergoes hydrothermal alteration in silica saturated system. Also activities of other divalent elements, such as Fe^{2+}, Mg^{2+}, may cooperate in above system by their replacement of Al^{3+} ions at the octahedral site. Giggenbach (1984) pointed out that formation of phengites and celadonites, octahedrally more highly substituted phases, is restricted to water with comparatively high Fe^{2+} and Mg^{2+} activities.

In geothermal systems dissolved silica activities

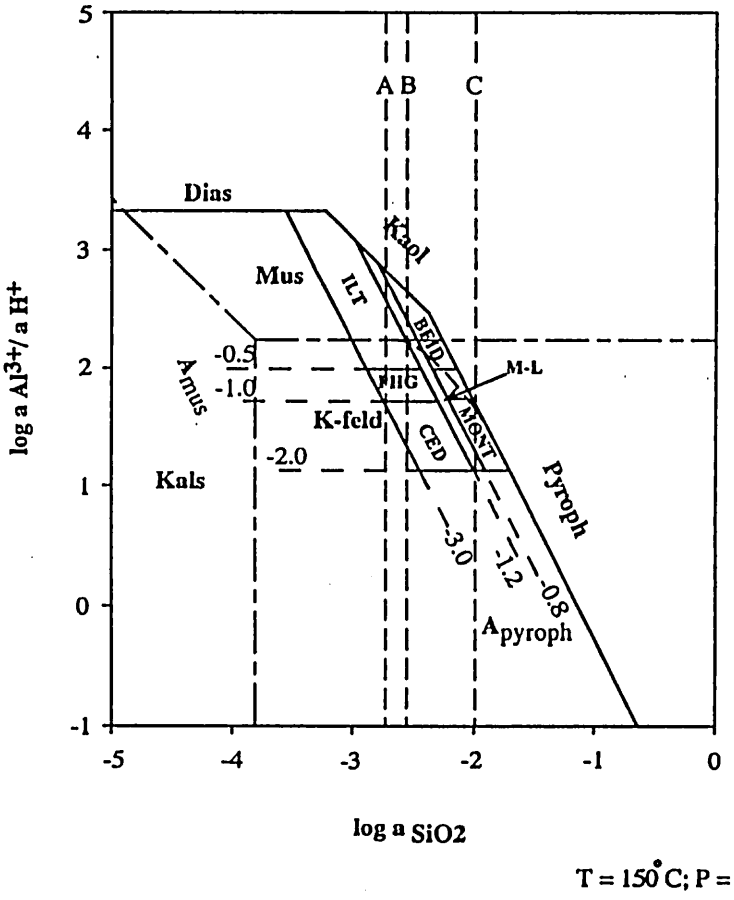

Fig. 20 Stability of non-stoichiometric clays in terms of pyrophyllite and muscovite end-members' activities.

generally range from those corresponding to saturation with quartz to those for equilibrium with chalcedony (Arnorsson, 1975). Occurrence of unaltered chalcedonic quartz spherules in the ores supports this range of silica activity prevailed during hydrothermal alteration at the Hiraki mine. Over this range of silica activity, the most stable dioctahedral clay minerals then are illite and mixed-layers minerals at relatively high, and montmorillonite at lower pH's or alkali ion activity.

Comparison of activity diagrams between K_2O - Al_2O_3 - SiO_2 - H_2O and Na_2O - Al_2O_3 - SiO_2 - H_2O systems (Fig. 21) reveals that K^+ clay minerals occur at lower Y_H (Y_H = Y/H; Y = log a cation ; H = log a H^+) values and extends over wider ranges than Na^+ clays. This may well explain the general predominance of K^+ clay minerals over formation of Na^+ clay phases in the Hiraki deposit, which is well consistent with the absence of Ca^+ and Na^+ clay minerals such as paragonite. This phenomenon is generally true in most geothermal alteration assemblages.

3. fluid-rock interaction

Fluid-rock interaction occurs when a fluid which was initially out of equilibrium with the constituent minerals incur host rocks. Alteration processes are mainly rearrangements of the modes (minerals and volume) of original rock to a new mineral assemblages stable under newly formed P-T condition, resulting in mas change. Thus metasomatism is essentially formed under open-system. Mineral paragenetic sequences and stable mineral phases formed by metasomatism vary widely depending mainly on following controlling factors: whether it occurred (1) at low ambient temperature or relatively high temperature, (2) epithermal or hypothermal; (3) mechanism of mass transport i. e. diffusion or infiltration ;and (4) composition of fluids which interacted with the host rocks. In natural alteration processes, thermal diffusion rate or conductivity is much higher than any kind of diffusion or infiltration of fluids in the same medium and then water-rock interaction take place under homogeneous temperature condition. In general, small fluid pressure gradient in porous rock is needed for fluid to infiltrate, and the gradient prevailing during alteration may be assumed as constant or stable. Thus various parameters described above can be reduced to two principle categories: (1) type of metasomatism — diffusion metasomatism in which solvent is the pore-water and the mass or aqueous species transfer occurs within stationary volume of water, and infiltration metasomatism where chemical species are transported by

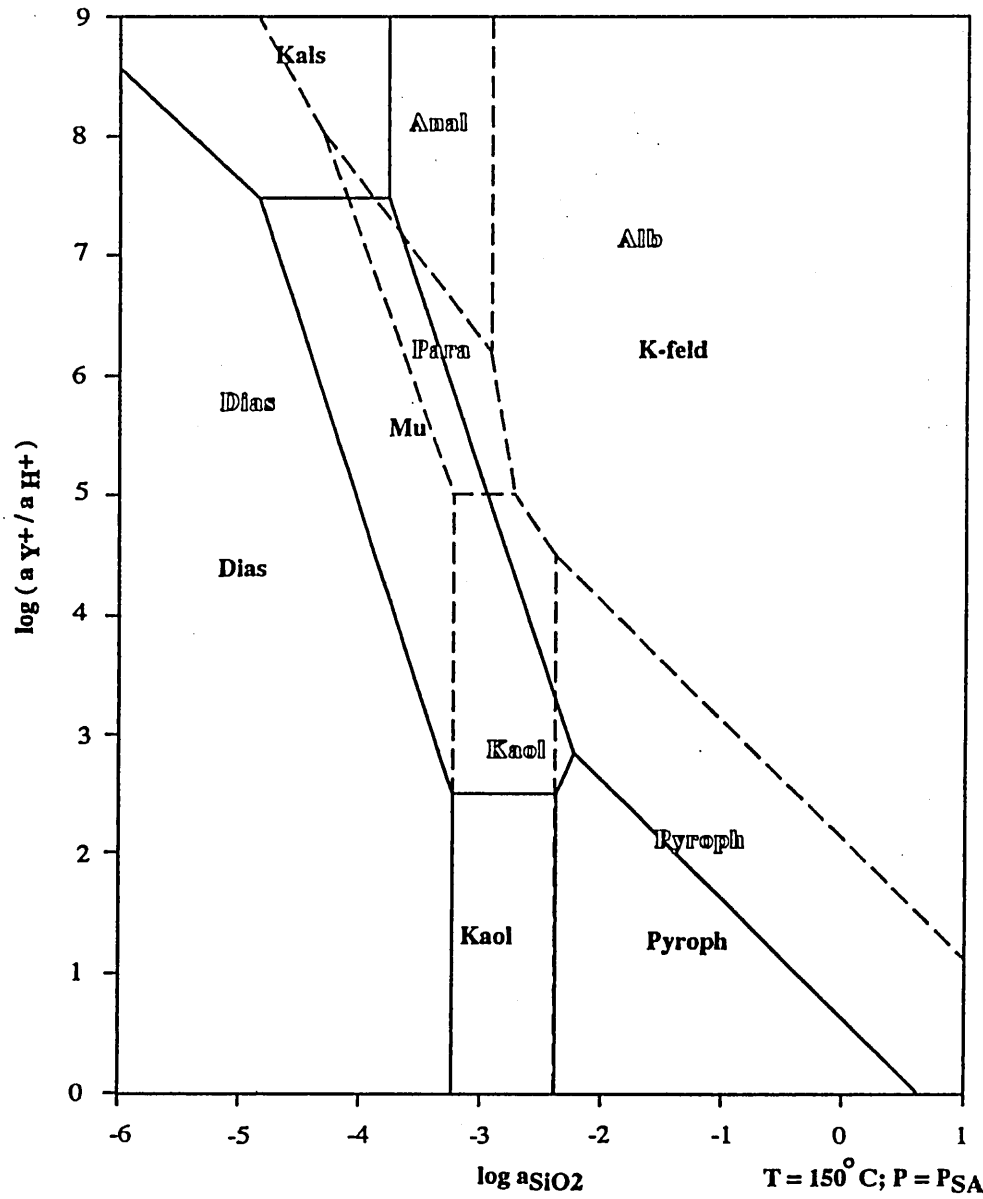

Fig. 21 Activity diagram depicting the comparative phases relation in the system HCl - H_2O - (Al_2O_3)- K_2O - SiO_2 and HCL - H_2O - (Al_2O_3) - Na_2O - SiO_2.

infiltrating fluids; and (2) fluids composition. Generally speaking diffusion is an important process in the high temperature regime, e.g. skarnization, whereas infiltration mechanism seems to be more important at low temperature metasomatism e. g. weathering. However, this discernment has not been clearly established, yet. More likely, both diffusion and infiltration mechanism play coupled-action in water-rock interaction, although leading process could be different from case to case.

In this section possible alteration zone sequence that should occur under previously discussed physical condition is considered within the frame of two concepts; hydrolysis of feldspars (Helgeson, 1979), and infiltration metasomatism (Korzhinskii, 1970). Then the resultant sequence is compared to the actually exposed zone sequence in the Hiraki mine and deviation, if any, from estimated sequence will be explained with the aid of additional hypothesis.

Feldspar hydrolysis

Investigation into the origin of clay minerals produced by fluid-rock interaction, in both weathering and hydrothermal alteration, are usually focused on the hydrolysis of feldspars, both alkali feldspar and plagioclase, because of their chemical and crystallographic similarities. Hemley (1959) was the first to determine comprehensively and systematically the composition of aqueous solutions in equilibrium with feldspar and other minerals in the system K_2O-Al_2O_3-SiO_2-HCl-H_2O at high temperatures and pressures. Since then a number of experimental and theoretical studies of feldspar synthesis and alteration in hydrothermal systems have been carried out in both thermodynamic and kinetic aspects (Helgeson, 1979 and references therein; Lichtner and Balashov, 1993 and references therein). Thus, to understand the paragenesis of hydrothermal clay minerals completely, it is essential to study the process of feldspar hydrolysis reactions, which is an alternate approach that is not restricted to mechanism of mass transfer nor explicit with respect to space and time (Helgeson, 1979). Using this concept, it is possible to calculate the extent to which components are redistributed among minerals and an aqueous solution as the solution reacts irreversibly with its mineralogic environment on the basis of thermodynamic constraints.

At least the feldspar dissolution process can be differentiated into three sequential stages (Helgeson, 1974): (1) initial stage — in this stage, essential process is the exchange reaction of K^+ for H^+ and the formation of H-feldspar (Garrels and Howard, 1959; Wollast, 1967); (2) main stage — in the main stage feldspar dissolve congruently until aqueous solution reaches the saturation limit of a certain mineral to produce; (3) later stage — in the later stage reaction of feldspar with an aqueous solution becomes incongruent and hence, subsequent reaction then leads to the appearance of solid reaction products. Among these stages the most important process is the congruent dissolution in the main stage which is strongly dependent of the initial composition of aqueous solution which reacts with feldspars. Composition of the resultant solution of this dissolution determines the first product mineral, to appear as a reactant in the later incongruent hydrolysis, with which aqueous solution needs to equilibrate.

Initial exchange reaction, which occurs when feldspar is placed in H_2O, appears as exchange of H^+ for K^+ or Na^+ on the surface of feldspar grains to form H-feldspar or protonated feldspar. This process causes the pH of the solution to rise rapidly and lead to further reactions.

After the initial stage, congruent dissolution of alkali feldspar causes the total concentration of silica, aluminum, and potassium or sodium in solution to increase in the relative proportion of 3:1:1, according to the stoichiometry of feldspar. Since the change in pH in the early stage of reaction progress is small, the initial pH of the solution and concentrations of silica and aluminum among aqueous species may remain almost constant. The reaction consuming or producing H^+ is dependent of the initial pH. If the initial pH is low (acidic condition), the bulk of the aluminum in the solution is present as Al^{3+} by the following reaction:

$$KAlSi_3O_8 + 4H_2O + 4H^+ \rightarrow K^+ + Al^{+++} + 3H_4SiO_4$$

In contrast, if the initial pH is high the hydrolysis reaction can be written as

$$KAlSi_3O_8 + 8H_2O \rightarrow K^+ + Al(OH)_4^- + 3H_3SiO_4^- + 3H^+,$$

and solution pH tends to decrease as feldspar dissolves. In any case the contents of total Si, K and Al species all increase proportionally to the number of moles of dissolved K-feldspar $(kg\ H_2O)^{-1}$. As the congruent reaction of K-feldspar continues, the solution composition approaches saturation with respect to one or more of the minerals corresponding to the stability fields shown in the activity diagram.

An aqueous solution with a given aK^+/aH^+ and $aSiO_2$ can be represented by a point ("O") inside the box (block) bounded by saturation surfaces of minerals defined by activity diagram (Fig. 22) if it was undersaturated with respect to these minerals (corresponding to the stability field surrounding the coordinate point), and above the plane of saturation if it was supersaturated. The direction of the congruent reaction path vector is controlled by the concentration of aqueous species in the initial solution and the relative extent to which they change as the reaction proceeds. For example, if the solution initially contains no silica but 10^{-3} m_{K+} and $10^{-3} m_{H+}$, destruction of 10^{-6} moles of feldspar $(kg\ H_2O)^{-1}$ causes a negligible change in log aK^+/aH^+ but change the saturation index of silica to increase rapidly. Hence, the reaction path inclines upward in the plane parallel to the abscissa of the activity diagram (Fig. 15). In contrast, if m_{SiO2} at the outset of the reaction process is 10^{-4} and m_{K+} and/or m_{H+} are much smaller, reaction causes the solution composition to change in a plane parallel to the ordinate of the diagram.

Congruent dissolution of feldspar in different solutions, thus, causes the solution composition to change along different reaction paths which impinge on the plane of the activity diagram at different points (e.g.. points A, B and C in the Fig. 22). Because these points may lie in different mineral stability fields, the identity of the first mineral to appear as a reaction product and the subsequent consequences of the hydrolysis of feldspar depend on the composition and speciation of the aqueous phase at the outset of the reaction process as well as the relative solubility of the minerals in the system.

The change of temperature also affects the identity of the first mineral to precipitate at the end of congruent dissolution. Stability field boundaries in the activity diagram shift toward the origin of the diagrams without change in its slope as temperature increases. For an instance, a fluid with a composition of log $a_{K+}/a_{H+} = 2$ and log $a_{SiO2} = -3$ in the activity diagram is in equilibrium with kaolinite at 150°C (Fig. 15), but is saturated with pyrophyllite at 25°C (not shown here). This behaviour would be a consequences of the increase in the relative stabilities of anhydrous phases compared to their hydrous phases with increasing temperature. As a result, identical reaction paths of congruent dissolution of

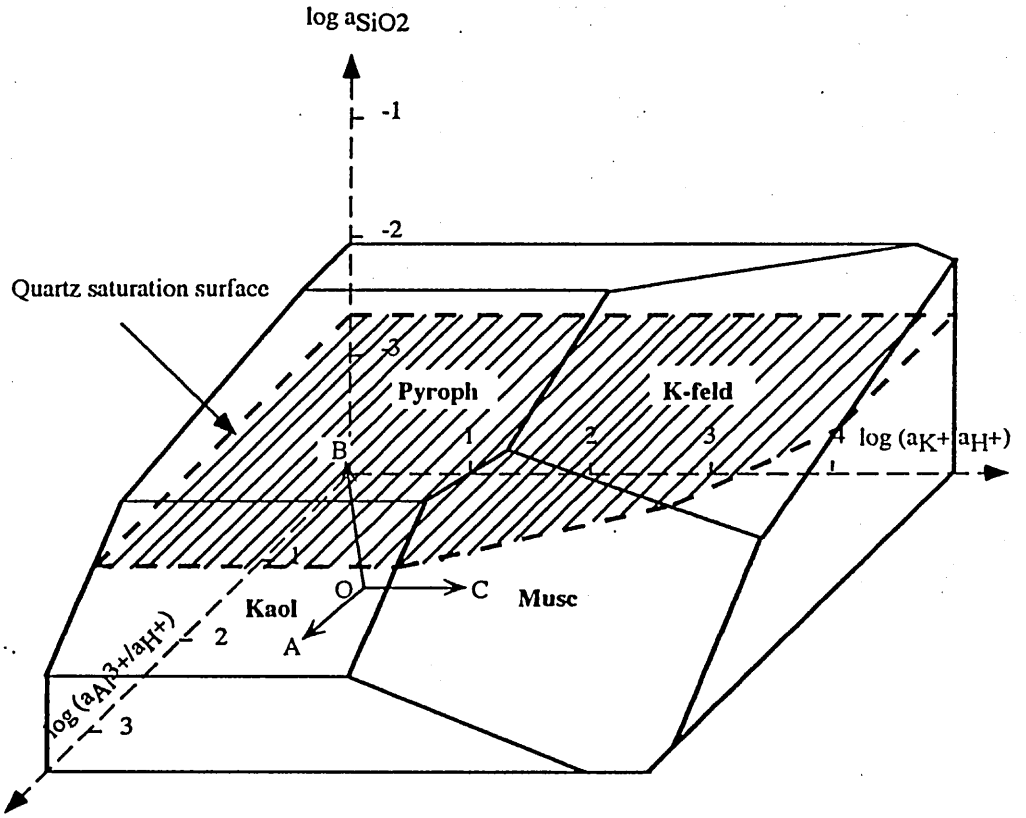

Fig. 22 Three-dimensional view of mineral stabilities in the system HCl - H_2O - Al_2O_3 - K_2O - SiO_2 bounded by saturation surfaces of respective minerals. Point "O" is situated inside the box whereas "A", "B" and "C" lie on the saturated surfaces.

feldspar at successively higher temperatures lead to the first appearance of different reaction products (minerals).

If temperature decrease gradually during metasomatism, the aH^+ (pH) changes to more alkaline condition and the parameter aK^+/aH^+ becomes smaller accordingly, then might lead to the appearance of different stable minerals, e. g. precipitation of kaolinite in place of muscovite. Similarly, increase in temperature may affect the system in reverse way. Thus, the thermal impulse or wave, which generally is expectable in heat source, can be accountable for a probable controlling factor in the metasomatism occurred at the Hiraki mine, at least qualitatively.

Based on the local chemical equilibrium (LCE), when initial reaction path touches the stability field of certain mineral defined in the activity diagram, the reaction of the feldspar with aqueous solution becomes incongruent , and then precipitation of that mineral takes place when aqueous species concentrations in the solution reach saturation limit of the mineral concerned. This kind of reaction is known as dissolution/precipitation reaction.

A reaction path and mineral paragenesis according to K-feldspar hydrolysis model for the closed-system is schematically illustrated in Figs. 23 & 24. In these figures, quartz is not considered as a reaction product. But in the actual process quartz will precipitate when the concentration of aqueous silica species in the solution reaches the solubility limit of quartz. If quartz appears as a reaction product, continuing dissolution of feldspar will lead reaction path to go along quartz saturation line. The path does not proceed beyond the silica line. Proceeding in this direction (passing quartz limit) means a decrease of the dissolved aluminum without precipitating any other Al-bearing mineral and solution oversaturated with dissolved silica species, which is contradictory to the dissolution of feldspar.

Major difference between closed- and open-system is that solvent in the former is stationary fluids while in the latter continuously inflowing volume of fluids are the primary solvent. Once stationary pore fluid's composition attained equilibrium value with final reaction product, phases those are not in equilibrium with fluid could be no longer stable in the system. In contrast to the situation in the closed-system, dissolution of product phases is not allowed even in the "simple" open-system model (without change in the physicochemical condition). According to the infiltration metasomatism every box of fluid flux infiltrating the rock may attain downstream equilibrium condition (Walsh et al., 1984; Lichtner, 1991). Regarding

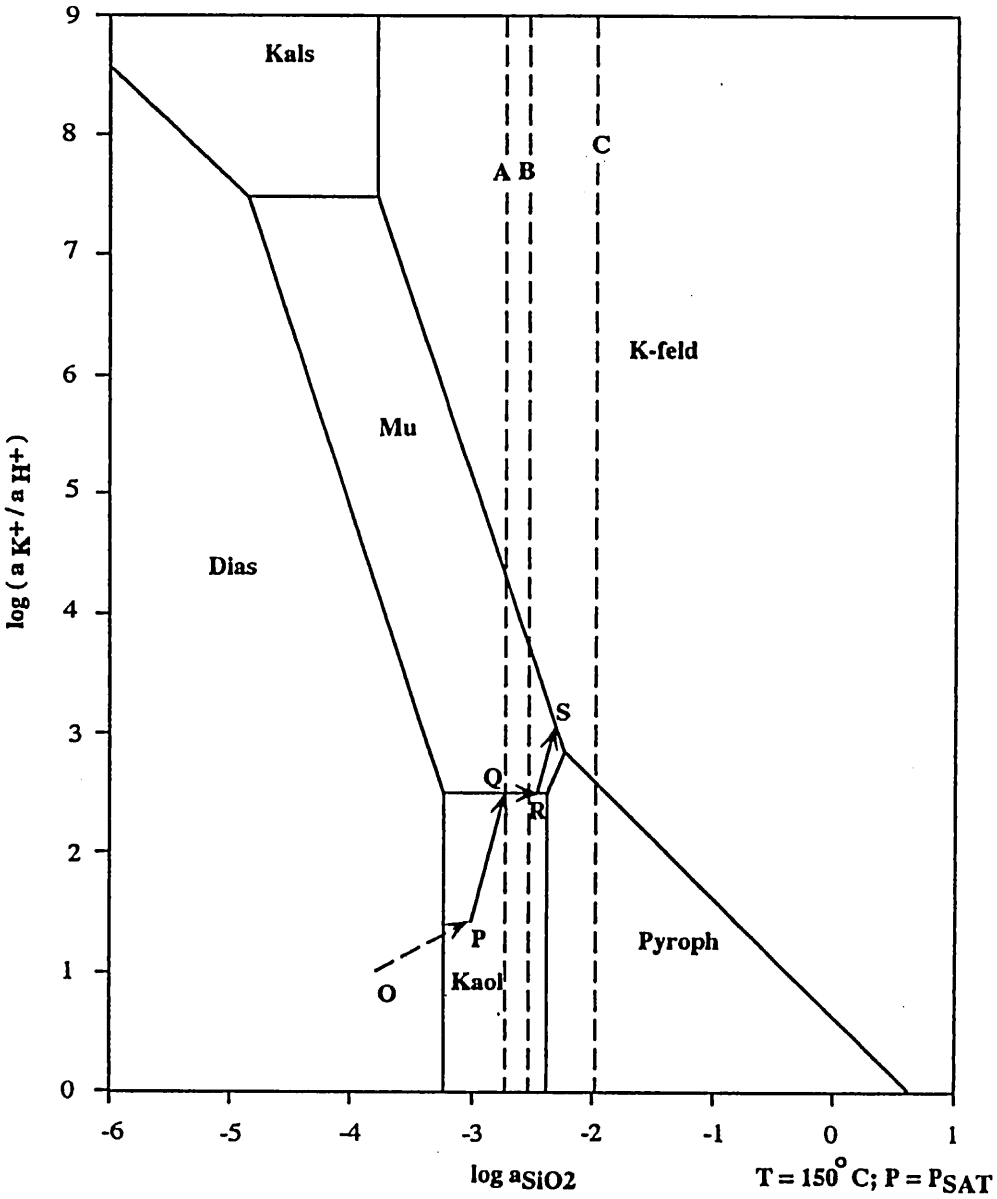

Kals = Kalsilite; **Mus** = Muscovite; **K-feld** = K-feldspar (microcline);
Dias = Diaspore; **Kaol** = Kaolinie; **Pyroph** = Pyrophyllite

Saturation limits : (A) quartz; (B) chalcedony; (C) amorphous silica.

Fig. 23 Reaction path in the feldspar hydrolysis process.

to the study of Lichtner and Balashov (1993), downstream equilibrium condition might be achieved during infiltration metasomatism of geological time-scale. In this case, the alteration products do not interact with the system after they have formed, and they are assumed to be left behind in the hydrothermal conduit.

As previously described, the hydrothermal alteration of the Hiraki non-welded tuff, indicated by mass changes, occurred under isothermal open-system, and hence, the phases produced along the reaction progress may remain as alteration minerals in metasomatic column.

On the basis of above thermodynamic mass transfer constraint, the possible reaction path occurred during the water-rock interaction at the Hiraki mine can be illustrated as shown in the Fig. 25. Since there is no diaspore detected in the Hiraki ores, the solution composition after initial stage and congruent dissolution of feldspars was saturated with kaolinite, major alteration mineral in the Hiraki ore. The presence of quartz grains with dissolved boundary also suggests that the initial fluid has silica concentration slightly below the quartz saturation limit. These relatively large (≈ 1 mm) quartz grains are identified as volcanic origin since they contain

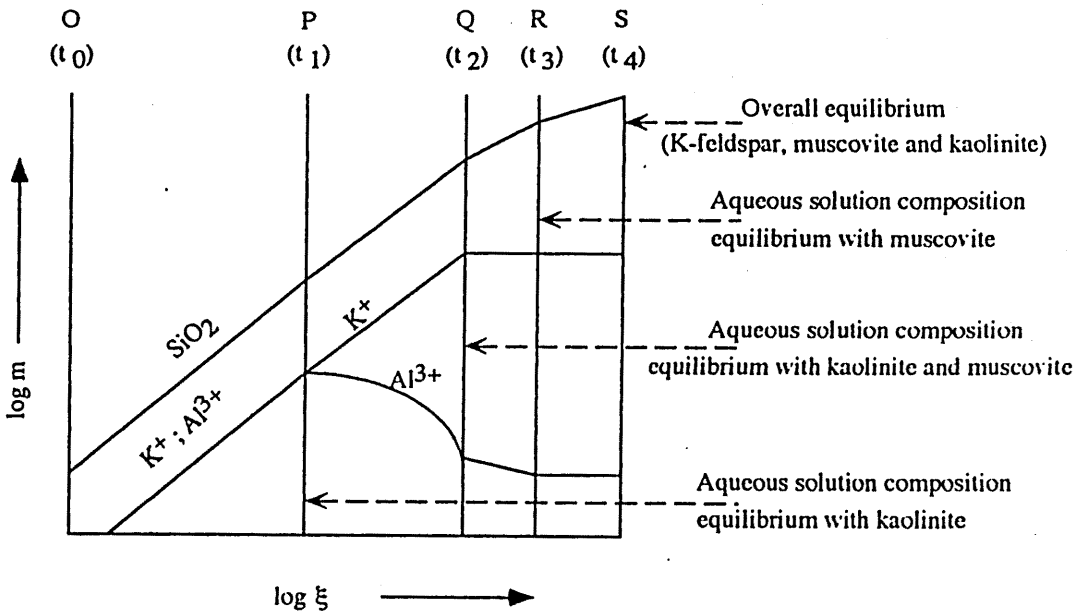

log m = molality of solute species in the aqueous phase
log ξ = reaction progress described by log mol. of K-feldspar dissolved
Total dissolved aluminum species as Al^{3+}
Note: quartz is not considered as a reaction product.

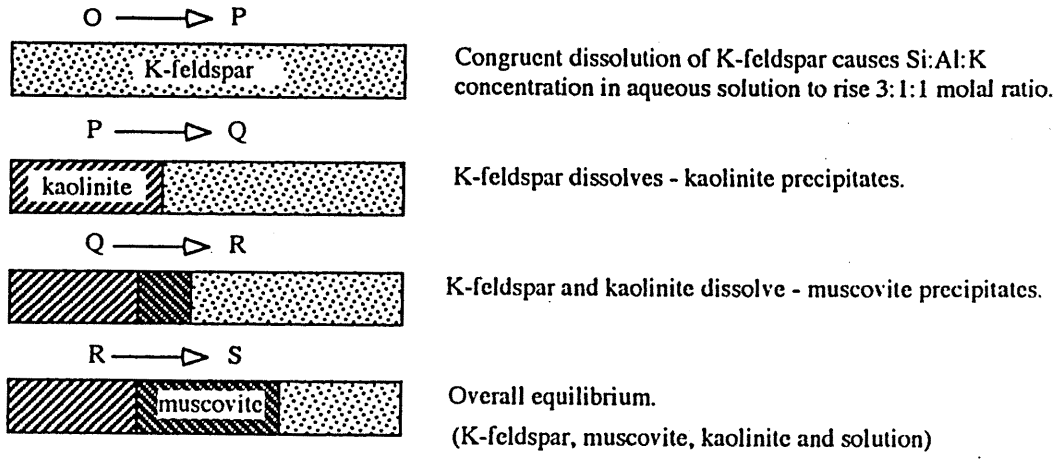

Fig. 24 Mineral paragenesis in the feldspar hydrolysis process. P, Q, R and S are the points notified in the Fig. 23.

two-phase (solid-gas) glass inclusion (Plate VIII). If initial solution has silica concentration well below the quartz limit, all these volcanic quartz will be dissolved and they remain no longer in the altered specimens. Otherwise, these quartz will remain unchanged and no dissolved boundary would be formed, if the initial solution is saturated with quartz. Therefore, aqueous solution's composition at the beginning of the incongruent hydrolysis of feldspar may be plotted somewhere in the kaolinite stability field below quartz saturation limit in the activity diagram. At 150°C, starting point will reach saturation surface between diaspore-kaolinite boundary ($\log a_{SiO2} = -3.23$) and quartz saturation limit ($\log a_{SiO2} = -2.72$). Inasmuch as this range is very short, the initial fluid would have a silica concentration very close to quartz saturation limit. Because of the narrowness of the kaolinite stability field in terms of the activity of SiO_2 at 150°C, the starting point ("E" in Fig. 25) would lie very close to the saturation limit of quartz and thus the solution could reach its composition to quartz limit soon after the incongruent hydrolysis of feldspar begins.

Occurrence of quartz as a major alteration phase in the Hiraki ore indicates the precipitation of quartz during reaction progress. So when bulk solution reaches its silica concentration saturated with quartz (point "F"), reaction path would proceed along the quartz saturation line defined by temperature concerned.

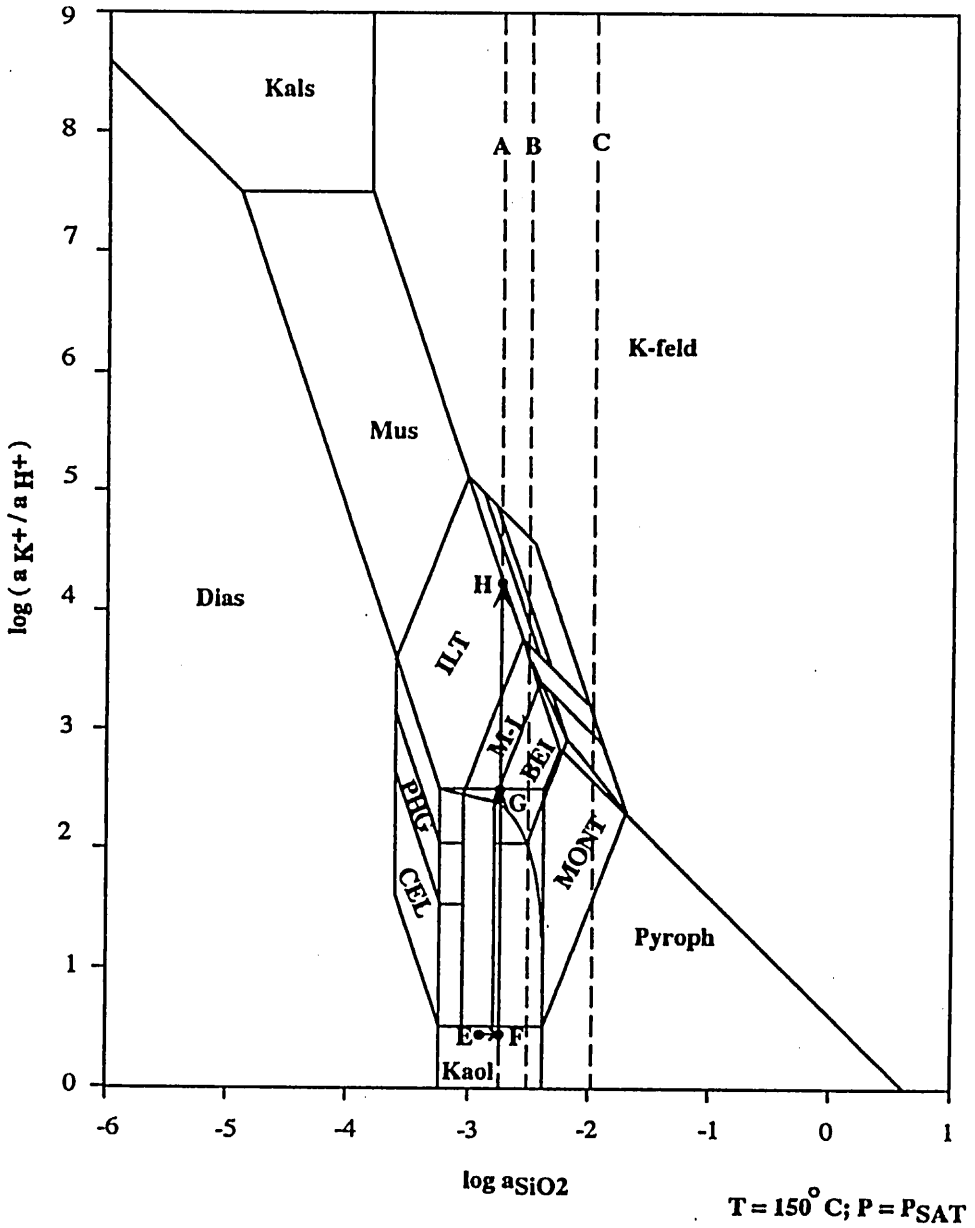

Kals = Kalsilite; **Mus** = Muscovite; **K-feld** = K-feldspar (microcline);
Dias = Diaspore; **Kaol** = Kaolinic; **Pyroph** = Pyrophyllite
Saturation limits : (A) quartz; (B) chalcedony; (C) amorphous silica.

Fig. 25 Depicting the possible path of changes in fluids composition during fluid - rock interaction process at the Hiraki deposit.

Material balance at point "F" is governed by the reaction:

$$2KAlSi_3O_8 + H_2O + 2H^+ = 4SiO_2 + Al_2Si_2O_5(OH)_4 + 2K^+$$

As it can be predictable from the Fig. 25 that if the activity of muscovite in the system is less than unity, the solid solution clay minerals, viz. montmorillonite, mixed-layer minerals, phengite, and illite will be formed instead of muscovite. Sporadic occurrence of montmorillonite and other mixed-layer minerals indicates that the activity of muscovite in the Hiraki solution might be lower than unity. Therefore, the reaction path would advance on the quartz saturation surface and below the muscovite saturation surface as shown in the Fig. 26.

Occurrence of phengite at the upper most part of the rhyolite suggests that the incongruent hydrolysis reaction ceased when concentrations of all dissolved species in the bulk solution reached equilibrium value between muscovite (phengite) and K-feldspar at 150°C.

Reaction occurs at this point can be expressed by:

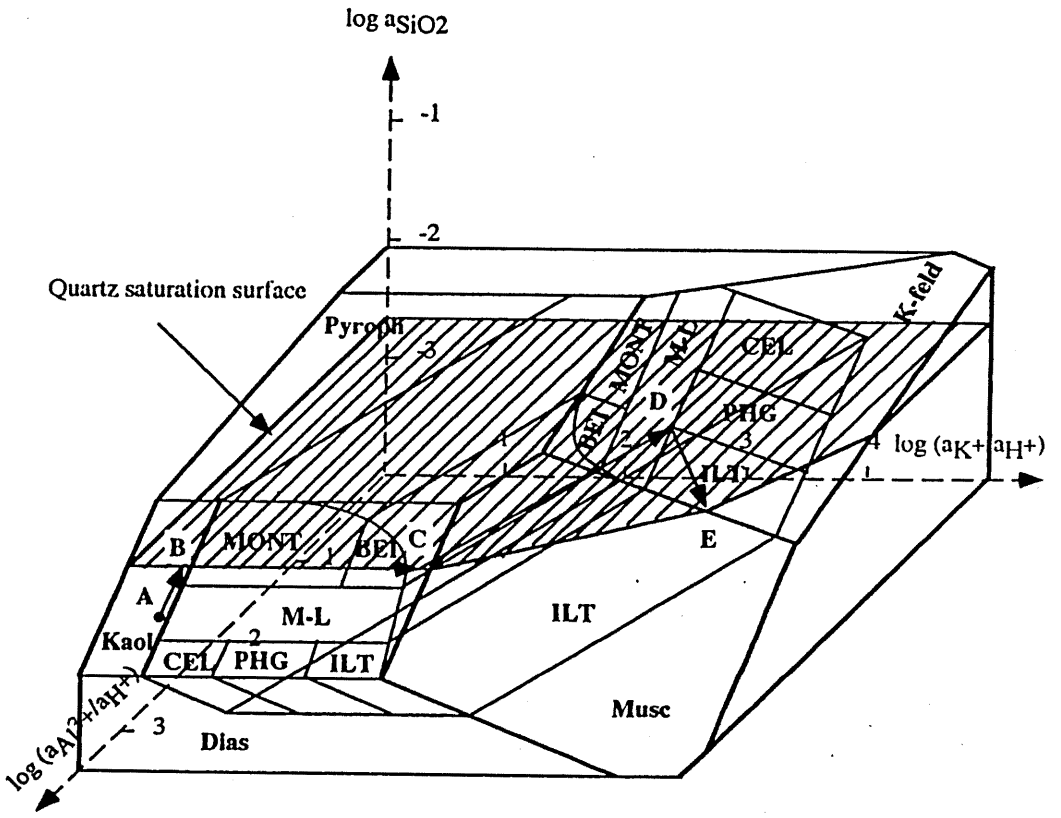

Fig. 26 Possible course of solution composition change in the formation of hydrothermal kaolin deposit at the Hiraki mine. A represents the starting point or inlet solution composition at the beginning. Path **BCDE** is on the quartz saturation surface and inside the solid solution prism.

$$3KAlSi_3O_8 + 2H^+ = KAl_2(AlSi_3O_{10})(OH)_2 + 2K^+ + 6SiO_2$$

This phenomenon is explained in the Fig. 25. However, reliable data of hydrolysis constants of mixed-layer minerals and phengite are still needed and thus reactions governing the formation of these mineral could not have been discussed further.

Kaolin deposit at the Hiraki mine is characterized by sharpness in its mineral zone boundaries, a prominent symptom of infiltration metasomatism (Korzhinskii, 1970; Hoffman, 1972). Since the abrupt changes in concentration of components occur at zone boundary, the mineral composition within individual zones should be constant. Let us consider a possible mineral assemblages and zone formed when a hypothetical rock composed only of K-feldspar and quartz undergoes infiltration metasomatism. Because of its low solubility aluminum species are assumed to be inert component, i. e., a small aluminum concentration in the fluid is needed to maintain equilibrium with the rock and thus no dissolution occur. If infiltrating fluids have SiO_2 concentration not far from saturation limit of quartz at given temperature, then SiO_2 also is immobile and no dissolution of quartz through metasomatic column. pH also is determined if temperature is given. Therefore, the composition of product minerals after replacement of K-feldspar depend on concentration of highly mobile component, here K^+, in solution and rock, and can be represented by the ratio of K^+/Al^{3+}. It is shown in the Fig. 27, that the resultant zone sequence, fluid / kaolinite + quartz / muscovite + quartz / K-feldspar + quartz, is the same as that formed in feldspar hydrolysis model if we neglect sequential order of mineral formation. Thus, this zonal sequence is a naturally expectable in hydrolysis or infiltration metasomatism of K-feldspar.

All metasomatic reactions seem to be net transfer reactions and H^+ metasomatism as a primary type, where no other exchange reactions, such as Mg^{2+}, K^+, Ca^{2+}, Na^+ metasomatisms, were evident. However formation of phengite in the uppermost part of the rhyolite may be the result of complex exchange reaction, where gains or loses of components or elements might occur, between alkali feldspar, (plagioclase?), and biotite by the following reaction:

K-feld + pgl. + biot. + H^+ <—> phengite + K^+ + Ca^{++}(Na^+)

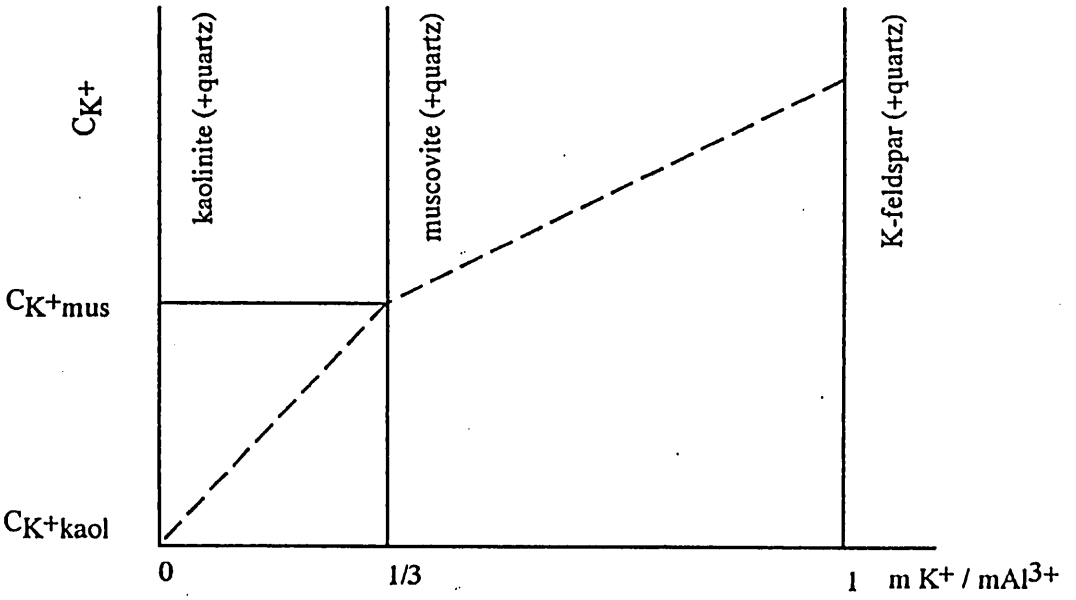

C_{K^+} = concentration of K^+ in fluid

C_{K^+mus} = concentration of K^+ in fluid equilibrium with muscovite

C_{K^+kaol} = concentration of K^+ in fluid equilibrium with kaolinite

a_{SiO2} = saturated with quartz

Fig. 27 Possible mineral zone sequence in the infiltration metasomatism of K-feldspar.

Inlet fluids composition

As it has been pointed out that inlet fluids composition is a major controlling factor in aspect of which minerals to be formed in metasomatic column. Although inlet fluids themselves cannot be available for analytical purposes in fossil hydrothermal system, its composition is evaluated mathematically from relative thickness and sequence of mineral zones in alteration column (e.g.. Lichtner and Balashov, 1993). In the present study, composition of the inlet fluids which are responsible for hydrothermal kaolinization at the Hiraki mine is considered on the basis of hydrothermal mass transfer model.

If we can estimate the rate of all reactions (kinetics) as a constant or same, the ratios of EF : FG : GH in Fig. 25 may represent the thickness (width) of alteration mineral zones in an infiltration column, in here kaolinite zone : kaolinite + quartz zone : muscovite + quartz zone, respectively. In the Hiraki mine, the width of kaolinite + quartz zone dominate extremely over others and hence, the length of FG in the Fig. 25 should be much greater than others. Alteration zone composed exclusively of kaolinite is believed to be very narrow because there are very few ore samples with kaolinite + volcanic quartz observed in the mine. Therefore, the point E (starting point) would be very close to quartz saturation limit, and again supports the fact that the inlet fluid was slightly undersaturated with quartz.

It was already explained in the previous section that fluid composition at starting point of reaction path was very likely to be lied in stability field of kaolinite and having log m_{SiO2} = -2.8 (slightly undersaturated with quartz at 150° C). For a fluid equilibrium with kaolinite at T = 150° C, P = along vapour-pressure curve, and pH = 5.792 (neutral water at 150° C), concentration of Al^{3+} is defined by following hydrolysis reaction:

$$\log a_{Al2Si2O5(OH)4} + 6 \log a_{H+} \rightarrow 2 \log a_{Al^{3+}} + 2 \log a_{SiO2} + 5 \log a_{H2O}$$

log K = 0.19 for the above reaction (Bower et al., 1984), and then $\log a_{Al^{3+}} = -14.48$.

Since the activity coefficient for electrolyte species in weak acids is unity, then m_{Al3+} is equal to $10^{-14.48}$. From the Fig. 25, it can be speculated that point "E" must has a log aK^+ / aH^+ less than 0.5 (below solid-solution prism) at least. For the pH of 5.79, log m_{K+} in the solution should be of $10^{-5.29}$ in maximum. Thus, inlet solution at starting point ("E" in the Fig. 25, $m_{SiO2(aqueous)} = 10^{-2.8}$) of alteration process would have concentration of $m_{Al^{3+}} = 10^{-14.48}$ and $m_{K+} = 10^{-5.29}$ at pH of 5.79.

Here, pH = 5.79 is the value for neutral water at 150° C (Glover, 1982).

It is also noted that "$\delta^{18}O$"-shift trend of the non-welded tuff in the Hiraki mine represents a slope (≈3°) similar to those of sulfate-predominant acid geothermal waters (Ellis and Mahon, 1964; White et. al., 1973). Co-existence of marcasite and pyrite in the ore deposit and above similarity of isotope-shift trend to the sulfate-dominated acid geothermal water point out that inlet fluids were acidic at 150° C. According to the experimental study of Murowchick and Barnes (1988) and Murowchick (1992), marcasite is stably formed under the condition of pH < 5. Therefore, pH would be less than 5.79. If pH drops by one unit (i. e., 4.79), respective fluids composition becomes $m_{Al3+} = 10^{-11.38}$ and $m_{K+} = 10^{-4.29}$ at $m_{SiO2} = 10^{-2.8}$.

It is apparent from the above calculation that the solute concentrations will change in accordance with changes in the pH of fluids and, also the formation temperature. Temperature corrections for equilibrium constants of minerals are readily available from many sources (e. g. Bower et al., 1984; Helgeson et al., 1978). pH of fluid should be determined by unrelated method because change of one unit in pH fluid could result in one log unit change in W/R ratio estimated by material balance of K^+.

Removal of gases (CO_2, H_2S, etc.) from solution caused by boiling or precipitation of minerals such as calcite, pyrite, etc., can be expectable from the equilibrium relation $HCO_3^- + H^+ \rightarrow CO_2, g + H_2O$. This loss of gas is accompanied by a decrease in aH^+. Therefore, precipitation of pyrite in the upper member and calcite in the lower member of non-welded tuff could disturb the pH of the system during hydrothermal alteration.

In actual process, number of moles of K-feldspar congruently dissolved is very small compared to later incongruent hydrolysis stage and huge mass of fluids. And hence, the inlet fluid composition does not change effectively. Therefore, solution concentrations at point "E" can be regarded as the same as that of fluids at inlet of the metasomatic column.

4. Water/rock ratio

Water/rock ratio or amounts of water that should physically flow through the system and thus might actually interact with the rock can be estimated by the material-balance method. That is based on the assumption that if a fluid with defined concentration of certain chemical species interacts with a rock consisting of mineral "X" and then leaves the system in equilibrium with mineral "Y", the fluid flux is the amount needed to redistribute the common chemical species to equilibrium concentration among the fluid, "X" and "Y". If we can know the concentration of common chemical species for initial fluids, minerals "X" and "Y" by use of independent method, amount of fluids flux can be estimated. The material-balance W/R ratio needed to change the felsic volcanic rock to essentially kaolin deposit may be tens of thousands times greater than that revealed by isotopic method.

As discussed in the previous section, the initial fluids in the hydrothermal alteration process at the Hiraki mine would have a composition of $m_{K+} = 10^{-4.29}$, $m_{Al3+} = 10^{-11.38}$ and $m_{SiO2} = 10^{-2.8}$ at pH = 4.79. Alteration mineral assemblages in the Hiraki deposit show the final fluid would have a solute concentration in equilibrium with K-feldspar and quartz. Concentration of Al^{3+} is very low ($10^{-17.14}$ at log m_{SiO2} = saturated with quartz) and thus negligible in calculation. Log of equilibrium constant for K-feldspar hydrolysis reaction at 150° C is -1.69 (Bower et al., 1984). If a fluid of that composition enter at an inlet and interacts with the non-welded tuff which has an average concentration of $m_{K+} = 10^{-0.11}$ (from Table 5), and then leave the system by a fluid composition equilibrium with K-feldspar, the W/R ratio which satisfies the material-balance would be $10^{4.18}$ (≈ 15000) : 1 by volume.

As pointed out by Criss and Taylor (1986), these gigantic W/R ratios along the fluid path are not only real, but also are perfectly compatible with the overall material balance W/R ratio of about 0.5 to 1.0 required by the energy-balance and by the mass balance of oxygen isotopes.

5. Origin of ore fluid

In the hydrothermal system host-rocks inevitably interact with one or mixtures of the some types of natural waters, such as those of sea water, meteoric water and magmatic water. The δ values may decrease if a rock reacts with water which has lighter isotopic values than the rock, and increase if a rock does with water of isotopically heavier than it. Then the resultant isotopic composition of re-equilibrated species can be represented by a value somewhere on the isotopic tie-line connecting between host-rock's and fluid's compositions. Exact location of the point on the tie-line would depends on the fractionation equation of a rock or mineral concerned, reaction temperature and water/rock ratio. Applying these characteristics as fundamental rule, a graphical method to evaluate the isotope composition of the initial fluids in the hydrothermal system is presented in Fig. 28.

If a rock having a δ value of "O" interacts with sea water "A", meteoric water "MWL" and magmatic water, the δ value of altered specimen would lie at "P", "Q" and "S", respectively. Let us consider the case when the resultant value is at "R", the fluid composition might be represented by "F" if a reacting fluid is believed to be meteoric water. On the other hand, if the rock was altered by a mixture of meteoric and magmatic waters (here "Z"), two-water tie-line would be one between ZD and ZE, not ZC and others, and the respective δ values will range within "X" to "Y". Then, ZX : DX or similar relations would express the mass ratio of magmatic water to meteoric water. In hydrothermal field, only the δ values of the altered rock and pristine-rock could be known by analytical methods. Therefore, this graphical solution may be useful for estimation of the δ values of hydrothermal fluids. In the case of unknown precursor,

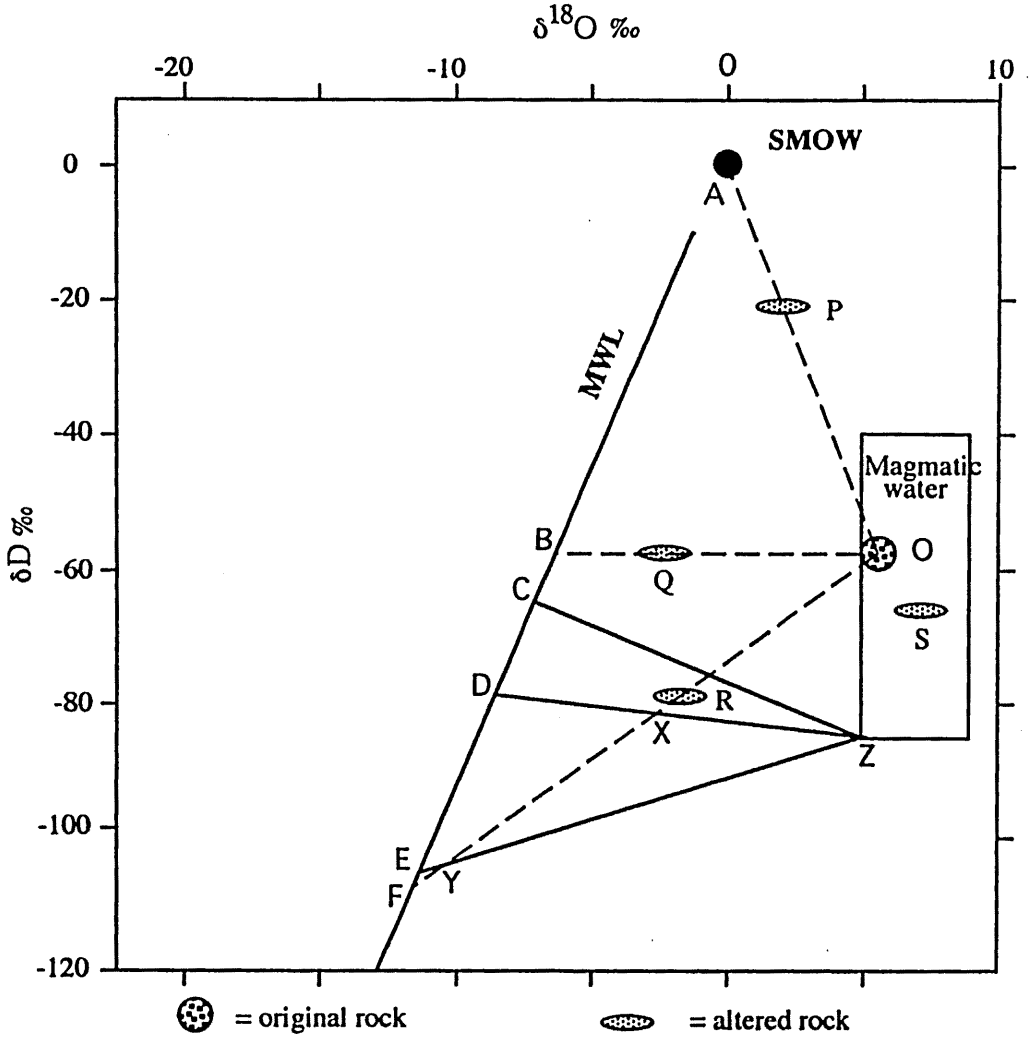

Fig. 28 Schematic diagram explaining the graphical method used to determine the isotope values of initial fluids from the isotope values of original and altered rocks.

isotope tie-line could be similar to a common regression line of altered rock's values.

Light stable isotopic studies on active geothermal fields and wall-rock alteration associated with mineralization reveal that almost all host rocks experienced isotopic exchange with meteoric water of nearby area, resulting in depletion in both δD and $\delta^{18}O$ values of altered rocks (e. g., Taylor, 1979). Also in the Hiraki mine, the non-welded tuff has higher δD and $\delta^{18}O$ values than its altered counterparts, ore samples. As shown in Fig. 29, $\delta^{18}O$-shift is smaller compared to the change in δD value. $\delta^{18}O$ value changes from 7.9 to 5.5 and 7.4 ‰, whereas δD change from -80 and -76 to -95 and -94 ‰. This is an evidence of isotopic exchange between the non-welded tuff, enriched in heavier isotope, and some kinds of fluid depleted in heavier isotope than the non-welded tuff.

By use of the δD and $\delta^{18}O$ values of the non-welded tuff and ores, the isotopic composition of the ore fluid (δ i.f) in the hydrothermal alteration at the Hiraki mine was estimated. A "tie-line" (OM) is drawn between δ plots of the non-welded tuff and ore. If the ore fluid is determined as of meteoric origin by other method, then its isotopic composition may be represented by the point ("L") where extrapolation of isotope-shift meets the meteoric water line (MWL). In the case of mixing, the isotopic composition of ore fluid would be represented by a point (e. g., "N") between kaolinite value ("M") and "L", not between "M" and "O". This is because the exchange reaction between fluids and rocks of isotopically heavier compositions cannot result in final product of lighter isotope composition.

An alternative method to define the isotope values of initial water is that the δ value of the present-day meteoric water of nearby area in the geothermal field is

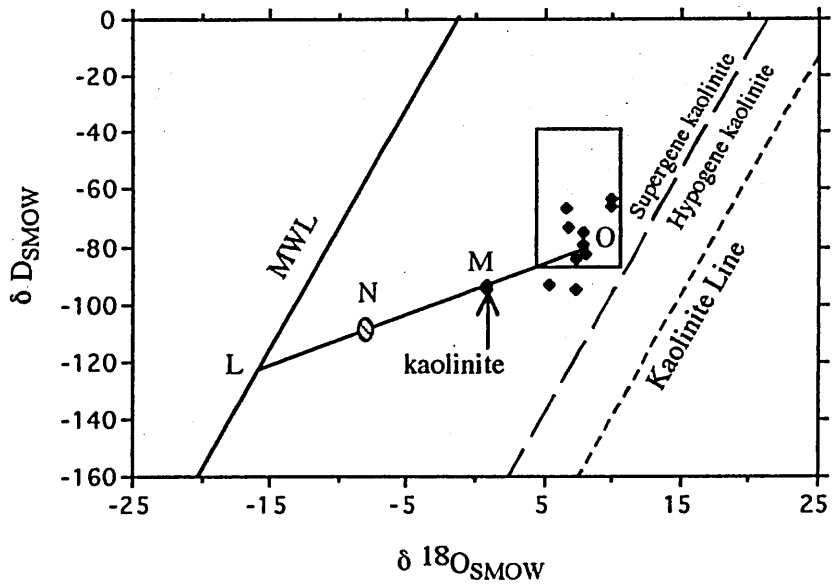

Fig. 29 Figure explaining the isotopic relationship among the non-welded tuff, ores and hydrothermal fluids in the formation of kaolin deposit at the Hiraki mine. Magmatic water box and kaolinite lines are from Field and Fifarek (1985).

assumed as that for initial fluid. This method is widely practised in estimation of origin and isotope values of reacting fluids in most of the present-day geothermal areas where no host-rock remain unchanged (e. g., Sheppard et al., 1969; Taylor, 1974).

In the present study, the above methods were tested for their compatibility. Since the δD and $\delta^{18}O$ values for the present-day meteoric water at the Hiraki mine themselves are not available, those of the area adjacent to the Hiraki mine were considered. According to Mizota and Kusakabe (1994), the present-day meteoric water of the area around the Hiraki mine has isotope values of δD = -50 ‰ ~ -60 ‰ and $\delta^{18}O$ = -8 ‰ ~ -9 ‰. If this water represents its isotope values for meteoric water of the Hiraki mine area during the latest Cretaceous and exchanged its isotope species with the non-welded tuff, the resultant kaolinite would have heavier δD value than the precursor. However, results of isotope analyses (Table 6) of ore specimens strongly against the above estimation. Rather ore specimens (δD ≈ -95 ‰) show their deuterium depleted nature than the precursor (δD = -78 ‰). This fact implicitly indicates that the volcanic rocks of the Hiraki mine area inevitably exchanged their deuterium with water of δD value lower than theirs (≈ -78 ‰). Therefore, the isotopic values of the present-day meteoric water at the Hiraki mine area can not stand for that of the ore fluid being responsible for the formation of kaolin deposit during the earliest Tertiary time. It is noteworthy to point out that the assumption of the present meteoric water of nearby area as an ore fluid for fossil-hydrothermal system might lead to serious errors in estimation of origin of ore fluids.

Graphical solution ("L" in Fig. 29) gives isotope values of δD= -120 ‰ and $\delta^{18}O$= -16 ‰. If the origin of initial fluid can be assumed or defined as meteoric water, above isotope values would be taken as that for ore fluid. However, as will be discussed below, this water could not represent the ore fluid in the case of Hiraki deposit. Meteoric water with such an extremely low δ values is represented by present-day river water at Changbaishan (42° 00' N, 120° 01' E with elevation of 1500 ~ 2000 m), China, having δ D and $\delta^{18}O$ of -104 ‰ and -15‰ (Mizota and Kusakabe, 1994). In this connection, if the Hiraki mine area was located in the present-day Southern Hokkaido region during the latest Cretaceous, meteoric water would have such extremely low isotopic compositions at high-elevation area. Therefore it is suggested that paleographic position of Southwest Japan including the Hiraki mine area would lie at much further north of the present position during the latest Cretaceous to earliest Tertiary. The above suggestion agrees well with paleomagnetic interpretations that the Japanese Island Arcs was separated from Asian Continent (northerly position) in the earliest Tertiary (e. g., Kawai et al., 1961; Otofuji et al., 1986).

Isotope composition of the final equilibrium fluid is calculated for quartz and kaolinite of the Hiraki mine at 150°C by use of fractionation equation given by Matsushita et al. (1979) and Kulla and Anderson (1978). Resulted $\delta^{18}O$ values of water are -7.3‰ for quartz and -6.7 ‰ for kaolinite, with the average value of about -7 ‰.

As described above, a huge mass of fluids infiltrated the non-welded tuff during the alteration. In the open-system fluids may exchange its isotope species with host rock until the final equilibrium is attained between fluids and altered rocks. As long as the W/R is large, the isotope composition of the initial fluids would affect greatly on the final fluids' composition and probably initial fluid's composition would not change significantly. In other words, fluid and host rocks may interact until the isotopic composition of final fluid attains the same values with those of the initial fluids. Therefore, it can be assumed that the isotopic composition of the initial fluid would be the same as that of final equilibrium fluid, i. e., .$\delta^{18}O$ = -7 ‰ and δD = -108 ‰ ("N" in Fig. 29).

The initial fluids of this value falls neither in the magmatic water box nor meteoric water line, rather it should lie on the isotope-shift line ("N" in Fig. 29). This fact suggests that the initial fluids would be of mixed origin between magmatic water ("O", $\delta^{18}O$ = 8‰) and meteoric water ("L", $\delta^{18}O$ = -16‰). If it is a case, the mixing ratio (in mass) of magmatic water to meteoric water is calculated to be 0.37 : 0.63.

VIII. SUMMARY AND CONCLUSIONS

The hydrothermal kaolin deposit at the Hiraki mine occurs in low alkali and strongly peraluminous (ASI = 2.6 ~ 6) rhyolitic non-welded tuff of the Late Cretaceous Kamogawa formation. As disclosed by volcanostratigraphy, gently dipping (*ca.* 20° SE), wedge-shaped non-welded tuff overlies conformably the vitritic rhyolite (ASI = 1.5 ~ 3.0) and underlies unconformably the vitritic rhyolitic welded tuff (ASI = 1.4 ~ 3.2). Based on the field observation, lithochemical studies and K-Ar datings, the magmatic events and related kaolin mineralization at the Hiraki mine can be established in chronological sequences as follow:

(1) Emplacement of the Kamogawa rhyolite and non-welded tuff in the Inner Zone of The Median Tectonic Line (*ca.* 69 ~ 70 Ma);

(2) Hiatus of volcanic activity (*ca.* 69 ~ 67 Ma);

(3) Emplacement of the Hiraki welded tuff (67 Ma);

(4) Cessation of all volcanic activities and deformation of all lithologic sequences prior to the sedimentation of younger units (67 ~ 63 Ma); and

(5) Infiltration dominated hydrothermal alteration mineralization (*ca.* 63 Ma).

Hydrothermal alteration has largely converted the sequence of the non-welded tuff to mainly kaolinite-quartz zone with local development of kaolinite-chlorite-quartz, sericite (phengite)-kaolinite-quartz and sericite-pyrophyllite quartz zones of negligible thickness. However, some portions of the non-welded tuff remain unaltered in open-pit and thus, petrochemistry of precursor has been defined with high accuracy.

Immobility of elements in hydrothermal alteration was determined by the degree of standard deviation from common regression lines of each element-pair. The results reveal that Zr and Nb are the most immobile among trace elements, probably because of their extremely low solubility. Chemical changes during alteration were calculated by use of Zr as an immobile element monitor and the results indicated the following conclusions.

(1) An addition of 20 ~ 30 wt% SiO_2 and dissolution of Na_2O, K_2O, Fe_2O_3, CaO and MnO occurred in the kaolinite zone.

(2) Local enrichment of Fe_2O_3 and K_2O in the sericite "zone" and Fe_2O_3 in the chlorite "zone" is detected.

(3) CaO and Na_2O were depleted or enriched together in the alteration system and their gains and losses in mass had no relation to other components.

(4) K_2O and Rb correlate strongly in altered samples (R =0.973) probably because of their chemical affinity.

(5) Although proportional abundance between quartz and kaolinite varies widely within the ore zone, their normative abundance is about 2.5:1 in the final alteration product.

(6) Unlike volcanic rocks, pyroclastic precursor shows low correlation coefficient for Al_2O_3 , reflecting somewhat inhomogeneous lithochemistry.

(7) Al_2O_3 content of the non-welded tuff might vary within the range of 15.0 ~ 24.0 wt%.

Although the alteration minerals of the Hiraki mine have simple mineralogy, widely varied relative abundance of minerals, especially between kaolinite and others, and uneven spatial distribution hamper to delineate individual mineral zones. These facts in combination with the slight inhomogeneity of the non-welded tuff (protolith) and difference in density between after and before the alteration may lead to a result of enormous mass changes for some chemical components, such as SiO_2, locally.

δD and $\delta^{18}O$ analyses of the volcanic host rocks and ores from the Hiraki deposit reveal that all volcanic sequences show their magmatic $\delta^{18}O$values, with deuterium depleted nature except for the Hiraki welded tuff, while ores are much depleted in both deuterium and ^{18}O compared to the protolith, the rhyolitic non-welded tuff. $\delta^{18}O$ values of quartz (≈ 8‰) from the ores change very negligibly from those of the protolith and suggest that a little silica exchanged its oxygens with fluids at relatively low temperature (*ca.* 150°C). Kaolinite has nearly constant isotope values at $\delta D \approx$ -95 ‰ and $\delta^{18}O \approx$ 0.94 ‰. Chlorite, amongst the alteration minerals, shows most D-depleted values (δD = -137), probably because of its high Fe/(Fe+Mg) ratio.

Oxygen isotope thermometer, based on $\Delta_{quartz-kaolinite}$, indicates the formation temperature of the kaolin deposit to be about 150°C. Pressure dominating during the alteration process is estimated to be fluid pressure rather than lithostatic. Kaolin mineralization at the Hiraki mine is assumed to occur under almost isothermal and isobaric conditions. Occurrence of marcasite in the orebody and the similar isotope-shift to sulfate dominated acid geothermal water suggest that the

kaolin mineralization occurred under acidic condition (pH < 5) at about 150° C and vapor-pressure.

Thermodynamic stabilities of illite, montmorillonite, illite-montmorillonite mixed-layer clays and phengite are depicted in activity diagram on the basis of solid-solution model. Resultant stability fields indicate that these non-stoichiometric dioctahedral clays are more stable than their end-members, muscovite and pyrophyllite, at relatively low activity of K^+ and high activity of silica.

The Hiraki clays are composed almost of kaolinite and quartz. The reason(s) for the development of such a monomineralic alteration product is a combined effect of composition of protolith, invading fluids composition and physicochemical condition of alteration. However, our present knowledge about water-rock interaction from laboratories and computer simulations is not enough to predict which factor(s) plays a decisive role in the formation of a monomineralic deposit. Since the hydrothermal alteration is generally considered to have occurred under isothermal and isobaric conditions, precursor's and inlet fluid's compositions might be more effective controlling factors in the hydrothermal alteration.. On the fact that feldspars are of principal reactant minerals, strongly peraluminous (alkali deficient) protolith might be one of possible controlling factors for the poor development of pure sericite as a reaction product, at least qualitatively.

Sharpness of the mineral zone boundaries at the Hiraki mine indicates that the kaolinization was formed by infiltration metasomatism. Regardless of type of alteration mechanism, it is revealed that the inlet fluid composition was in equilibrium with the kaolinite at the beginning and changed along the course through equilibrium with non-stoichiometric clays to K-feldspar at the final stage. Occurrence of non-stoichiometric clays in place of muscovite points out that the aqueous solution composition was slightly undersaturated with muscovite in most of time of the alteration process. Aqueous solution composition change path is presented in Fig. 26.

Chemical composition (at assumed $m_{SiO2} = 10^{-2.8}$) of the inlet fluids responsible for the appearance of alteration zone sequences in the mine is calculated to be $m_{Al3+} = 10^{-11.38}$ and $m_{K^+} = 10^{-4.29}$ at pH = 4.79 for the formation temperature of 150°C on the vapour-pressure curve.

The W/R calculated by material-balance of K^+ between the fluids and rocks gives 15000:1 at 150°C and vapour pressure condition. The W/R ratio depends on the pH of the initial fluid.

δD- and $\delta^{18}O$-shift phenomenon between the precursor and ores in the Hiraki mine indicates that the fluids reacted with the non-welded tuff may be of mixed origin of acidic meteoric water ($\delta D_{SMOW} = -120‰$ and $\delta^{18}O_{SMOW} = -16‰$) and magmatic water. The mixing ratio (in mass) of magmatic to meteoric water is calculated to be 0.37 : 0.63. Calculated isotope values of final equilibrated fluid are $\delta^{18}O_{SMOW} = -7‰$ and $\delta D_{SMOW} = -108$.

The so-called high temperature mineral, pyrophyllite, can be stable in low ambient temperature if favorable chemical conditions are fulfilled. This fact suggests that the chemical environments is more important controlling factor than physical environment in alteration process. It is also noted that chemical conditions in turn are mainly controlled by pH of fluids. Another noteworthy point is the influence of fluids' pH on W/R ratio.

Moreover, the possibility of formation of same alteration mineral zone sequence under different alteration mechanism has been elucidated. Thus, if we do not consider the thickness and boundary characteristics of mineral zones and matter relating to reaction kinetics, possible alteration mineral sequences are determined, once the physico-chemical conditions are fixed.

All facts and results observed in the present work collectively lead to a final conclusion that the fluid-rock interaction process is mainly controlled by the composition, especially pH, of inlet fluids.

Although there were some efforts (e.g., Shibata and Fujii, 1971; Kitagawa et al., 1988) to establish the temporal relationship between the "Roseki" deposits and associated igneous activities in Japan, only a few (e. g. Shibata and Kamitani, 1974) have been achieved with satisfaction.

K-Ar dating on the ore from the Hiraki mine elucidates that the deposit was formed at ≈63 Ma (the latest Cretaceous to earliest Paleocene). Most of granite intrusion in the region around the Hyogo Prefecture are pertaining to "Phase II intrusion" (Yamada, 1977) or the latest Cretaceous to earliest Paleocene igneous activities (Nozawa, 1975). If there was a relation between the emplacement of these intrusions and the formation of hydrothermal clay deposits of the same region, kaolin deposit at the Hiraki mine would be formed by infiltration metasomatism related to these igneous intrusions. These intrusion served as a heat-engine and boiled the meteoric water circulating above it. Mixing of two waters, i. e. meteoric and magmatic, could take place at a zone above the intrusion, where circulating meteoric water met an uprising hot magmatic water. Temperature in this zone might be higher than 150° C, and decrease gradually while water was on the way to the ore horizon (the non-welded tuff). The overlying Hiraki welded tuff would served as a cap-rock and hindered the upwelling hot mixed-water to go further upward. Thus these fluids would flow laterally into the pervious non-welded tuff and would lead to infiltration metasomatism. Mixing ratio of two waters suggests that either intrusion would take place at relatively shallow depth or aquifer existed to a great depth. In connection with these conclusions, schematic model for the formation of hydrothermal kaolin deposit at the Hiraki mine is proposed in the Fig. 30.

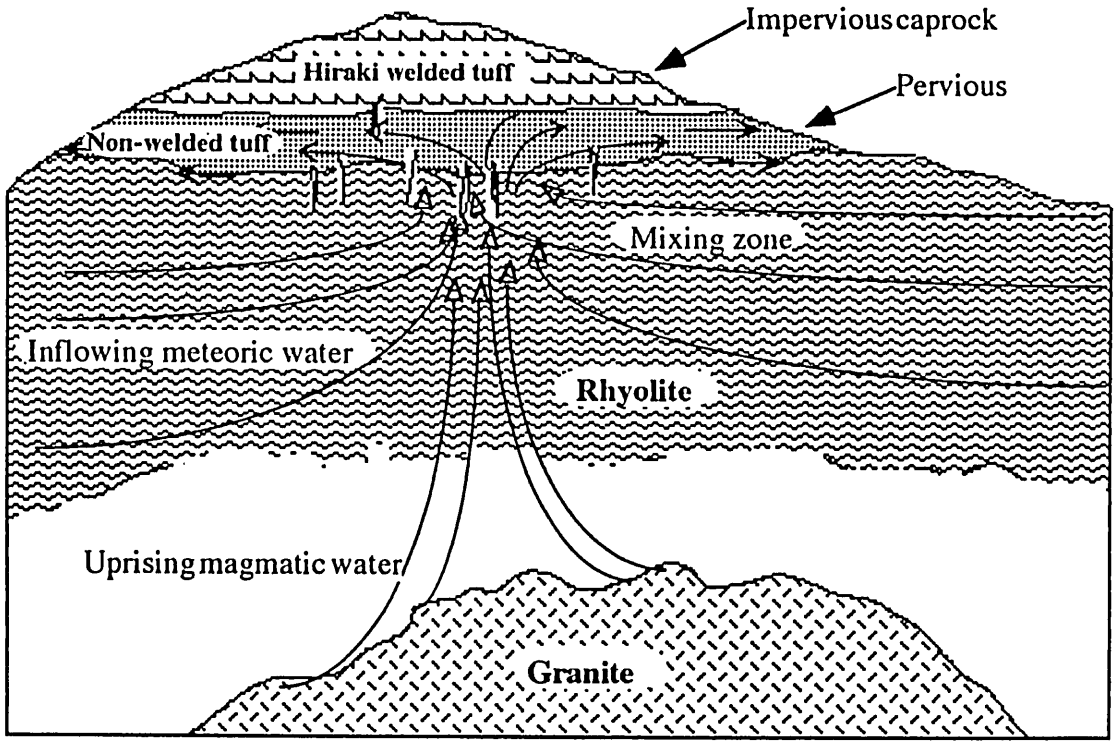

Fig. 30 A schematic model illustrating the possible mode of formation of kaolin mineralization at the Hiraki mine. Granite intrusions are at unknown depth. Magmatic water from intrusion rises upward and mixes with meteoric water inflowing above the intrusions, and then invades into the non-welded tuff through fractures. Only some parts of the system can be seen now.

ACKNOWLEDGMENTS

The author wishes to express his sincerest gratitude and appreciation to Dr. Makoto Watanabe and Dr. Kenichi Hoshino of the Hiroshima University for their enthusiastic guidance, encouragement, valuable criticisms and advice throughout the progress of the present work and during his stay in Japan. He is also greatly indebted to Profs. Yuji Sano, Yuji Okimura, Ikuo Hara, Setsuo Takeno and Satoru Honda of the Hiroshima University for their critical reading on the manuscripts. Dr. Ryuji Kitagawa and Mr. Asao Minami, who helped in mineral identification, are thankfully acknowledged. Prof. Minoru Kusakabe of the Institute for Study of the Earth's Interior, Okayama University, Dr. Hirotsugu Nishido of the Research Institute of Natural Sciences, Okayama University of Science, and Dr. Harue Masuda of the Department of Geosciences, Osaka City University, kindly provided laboratory facilities for isotope analyses.

Sincere thanks are extended to Mr. Shozo Taninami, chairman of HATTORI Co., for his permission to study the Hiraki mine, and personnels of the Hiraki mine for their kind guidance during field works. Special thanks are due to Japanese Government's Ministry of Education who granted a monthly scholarship for four years.

Finally, the author would like to express heart-deep appreciation to Mrs. Than Than Myint, his wife, and Yar Zar Myint, his son, for their understanding in the present work and struggles in daily life while he was away from them for a long time.

REFERENCES

Aagaard, P. and Helgeson, H. C. (1983): Activity composition relations among silicates and aqueous solutions: II. Chemical and thermodynamic consequences of ideal mixing of atoms on homological sites in montmorillonites, illites, and mixed-layer clays. Clay Miner., **31**, 207 ~ 217.

Arnorsson, S. (1975): Application of silica geothermometer in low temperature hydrothermal areas in Iceland. Amer. J. Sci., **275**, 763 ~ 784.

Barth, T. W. F. (1948): Oxygen in rocks: a basis for petrographic calculations. J. Geol., **56**, 50 ~ 60.

Barton, M. D. (1987): Lithophile-element mineralization associated with Late Cretaceous two-mica granite in the Great Basin. Geology, **15**, 337 ~ 380.

Bernier, L. R. and MacLean, W. H. (1989): Auriferous chert, banded iron formation and related volcanogenic hydrothermal alteration, Atik Lake, Manitoba: Canadian Jour. Earth Sci., **26**, 2676-2690.

Bigeleisen, J., Perlman, M. L. and Prosser, H. C. (1952): Conversion of hydrogenic materials to hydrogen for isotopic analysis. Anal. Chem., **24**, 13 ~ 56.

Bourcier, W. L., Knauss, K. G. and Jackson, K. J. (1993): Aluminum hydrolysis constants to 250°C from boehmite solubility measurements. Geochim. Cosmochim. Acta, **57**, 747 ~ 762.

Bowers, T. S., Jackson, K. J. and Helgeson, H. C. (1984): *Equilibrium activity diagrams*. Springer-Verlag, pp. 397.

Brady, J. B. (1975): Reference frames and diffusion coefficients. Am. J. Sci., **275**, 954 ~ 983.

Brimhall, G. H., Jr. and Dietrich, W. E. (1987): Constitutive relationships between chemical composition, volume, density, porosity, and strain in metasomatic hydrothermal systems. Geochim. Cosmochim. Acta, **51**. 567 ~ 587.

Cattalani, S., Barret, T. J., MacLean, W. H., Hoy, L. and Hubert, C. (1989): Metallogeny of base-metal sulfide deposits in the Abitibi belt, Quebec: 2. The Ansil, Mobrun and Aldermac mines, Noranda area. Ministere de l'Energie et des Resources du Quebec. Mineral Explor. Research Inst., Proj. 89-2, 65 p.

Choquette, P. W. and Pray, L. C. (1970): Geologic nomenclature and classification of porosity in sedimentary carbonates. Am. Assoc. Petrol. Geol. Bull., **54**, 207 ~250.

Criss, R. E. and Taylor, H. P. Jr. (1986): Meteoric-hydrothermal systems. In "Stable Isotopes in High Temperature Geological Processes", J. W. Valley, H. P. Taylor, Jr. and J. R. O'Neil, Eds., Rev. Mineral., **16**, 373 ~ 424.

Deer, W. A., Howie, R. A. and Zussman, J. (1970): *An Introduction to the Rock Forming Minerals*. Longman Group Ltd., London. pp. 528.

Ellis, A. J. and Mahon, W. A. J (1964): Natural hydrothermal systems and experimental hot water/rock interactions (Part II). Geochim. Cosmochim. Acta, **31**, 519 ~ 538.

Ericsson, T., Wappling, R. and Punakivi, K. (1977): Mössbauer spectroscopy applied to clay and related minerals. Geol. For. Forhandlingar, **99**, 229 ~ 244.

Field, C. W. and Fifarek, R. H. (1985): Light stable-isotope systematics in the epithermal environment. In "Geology and geochemistry of epithermal systems", B. R. Berger and P. M. Bethke, Eds., Rev. Econ. Geol., **2**, 99 ~ 128.

Finlow-Bates, T. and Stumpfl, E. F. (1981): The behaviour of so-called immobile elements in hydrothermally altered rocks associated with volcanogenic submarine-exhalative ore deposits. Mineral. Deposita , **16**, 319 ~ 328.

Fisher, J. R., and Zen, E-an (1971): Thermochemical calculations from hydrothermal phases equilibrium data and the free energy of H_2O. Amer. J. Sci., **276**, 1254 ~ 1285.

Fujii, N., Togashi, Y. and Igarashi, T. (1976): An outline of kaolin, pyrophyllite and sericite clay deposits in Japan. Geol. Surv. Japan.

Garrels, R. M. and Howard, P. F. (1959): Reactions of feldspar and mica with water at low temperature and pressure. Proceedings of the Sixth National Conference on Clays and Clay Minerals, Pergamon, New York, 68 ~ 88.

Garrel, R. M. (1984): Montmorillonite/illites stability diagrams. Clay Miner., **32**, 161 ~166.

Giggenbach, W. F. (1981): Geothermal mineral equilibria. Geochim. Cosmochim. Acta, **45**, 393 ~ 410.

Giggenbach, W. F. (1984): Mass transfer in hydrothermal alteration system. Geochim. Cosmochim. Acta, **48**, 2693 ~ 2711.

Giggenbach, W. F. (1985): Construction of thermodynamic stability diagrams involving dioctahedral potassium clay minerals. Chem. Geol., **49**, 231 ~ 242.

Giere, R. (1990): Hydrothermal mobility of Ti, Zr, and REE., examples from the Bergell and Adamello contact aureoles (Italy). Terra Nova, **2**, 60 ~ 67.

Glover, R. B. (1982): Calculation of the chemistry of some geothermal environments. New Zealand D. S. I. R. Chemistry Division Report CD 2323.

Godfrey, D. (1962): The deuterium content of hydrous minerals from the East-Central Sierra Nevada and Yosemite National Park. Geochim. Cosmochim. Acta, **26**, 1215 ~ 1245.

Gordon, T. M. (1973): Determination of internally consistent thermodynamic data from phase equilibrium experiment. J. Geol., **81**, 199 ~ 208.

Grant, J. A. (1986): The isocon diagram — a simple solution to Gressens' equation for metasomatism. Econ. Geol. , **81**. 1976 ~ 1982.

Gresscns, R. L. (1967): Composition-volume relationships of metasomatism. Chem. Geol., **2**. 47 ~ 65.

Helgeson, H. C. (1968): Evaluation of irreversible reactions in geochemical processes involving minerals and aqueous solutions — I. Thermodynamic relations. Geochim. Cosmochim. Acta., **32**, 853 ~ 877.

Helgeson, H. C. (1969): Thermodynamics of hydrothermal systems at elevated temperatures and pressures. Amer. J. Sci., **267**, 729 ~ 804.

Helgeson, H. C., Nigrini, A., and Jones, T. A. (1970): Calculation of mass transfer in geochemical processes involving aqueous solutions. Geochim. Cosmochim. Acta, **34**, 569 ~ 592.

Helgeson, H. C. and MacKenzie, F. T. (1970): Silica-sea water equilibria in the ocean system. Deep-sea Res., **17**, 877 ~ 892.

Helgeson, H. C. (1974): Chemical interaction of feldspars and aqueous solutions. In: "The Feldspars", W. S. MacKenzie and J. Zussman, Eds., Manchester University Press, 184 ~ 217.

Helgeson, H. C., Nesbitt, H. W. and Delany, J. (1975): Summary and critique of the thermodynamic properties of rock-forming minerals. Geol. Soc. Am. Abstr. Programs, **7**, 1108 ~ 1109.

Helgeson, H. C., Delany, J. M., Nesbitt, H. W. and Bird, D. K. (1978): Summary and critique of the thermodynamic properties of rock-forming minerals. Amer. J. Sci., **278**-A, 1 ~ 229.

Helgeson, H. C. (1979): Mass transfer among minerals and hydrothermal solutions: In: "Geochemistry of Hydrothermal Ore Deposits", 2nd ed., H. L. Barnes, Ed., New York, John Wiley and Sons, 568 ~ 610.

Helgeson and Aagaard (1985): Activity/composition relations among silicates and aqueous solutions: I. Thermodynamics of intrasite mixing and substitutional order/disorder in minerals. Amer. J. Sci., **285**, 769 ~ 844.

Hemley, J. J. (1959): Some mineralogical equilibria in the system $K_2O—Al_2O_3—SiO_2—H_2O$. Amer. J. Sci., **257**, 241 ~ 270.

Hemley, J. J., and Jones, W. R. (1964): Chemical aspects of hydrothermal alteration with emphasis on hydrogen metasomatism. Econ. Geol., **59**, 538 ~ 569.

Hemley, J. J., Montaya, J. W., Nigrini, A., and Vincent, H. A. (1971): Some alteration reactions in the system CaO-Al2O3-SiO2-H2O. Soc. Mining Geol. Japan, Spec. Issue, **2**, 58 ~ 63.

Hemley, J. J., Montaya, J. W., Marinenko, J. W., and Luce, R. W. (1980): General equilibria in the system Al2O3-SiO2-H2O and some implications for alteration/mineralization process. Eco. Geol., **75**, 210 ~ 228.

Hendesquist, J. W. and Browne, P. R. L.(1989): The evolution of the Waiotapu geothermal system, New Zealand, based on the isotopic composition of its fluids, minerals and rocks. Geochim. Cosmochim. Acta, **53**, 2235 ~ 2257

Hofmann, A. (1972): Chromatographic theory of infiltration metasomatism and its application to feldspars. Amer. J. Sci., **272**, 69 ~ 90.

Humphris, S. E. and Thompson, G. (1978, a): Hydrothermal alteration of oceanic basalts by seawater. Geochim. Cosmochim. Acta , **42**, 107 ~ 125.

Humphris, S. E. and Thompson, G. (1987, b): Trace element mobility during hydrothermal alteration of oceanic basalts. Geochim. Cosmochim. Acta, **42**, 127 ~ 136.

Itaya, T., Nagao, K., Nishido, H. and Ogata, K. (1966): K-Ar age determination of Late Pleistocene volcanic rocks. Chishitsugaku Zasshi, **90**, 899~909.

Kamitani, M. (1974): Genesis of the andalusite-bearing Roseki ore deposits in the Abu District, Yamaguchi Prefecture, Japan. Bull. Geol. Surv. Japan, **28**, 1~64.

Kanaoka, S. (1980): A mica/smectite interstratified mineral from the Hiraki mine, Hyogo prefecture, Japan. Nendo Kagaku (Journal of Clay Science Society of Japan)., **20**, 60 ~ 63 .*

Kawai, N., Ito, H. and Kume, S. (1961): Deformation of the Japanese Islands as inferred from rock magnetism. Geophys. J. R. Astrom. Soc., **13**, 150 ~ 153.

Kitagawa, R., Nishido, H. and Takeno, S. (1988): K-Ar age of pyrophyllite ("Roseki") deposits in the Chugoku District, Southwest Japan. Mining Geol., **38**, 357~366.

Kittrick, J. A. (1971): Stability of montmorillonites: I. Belle Fourche and Clay Spur montmorillonites. Soil Sci. Soc. Amer. Proc., **35**, 140 ~ 145.

Ko Ko Myint and Watanabe, M. (1995): Geology and geochemical mass-transfer of hydrothermal kaolin deposit at the Hiraki mine, Southwest Japan. Jour. Min. Pet. Econ. Geol., **90**, 310 ~ 326.

Ko Ko Myint, Watanabe, M. and Nishido, H. (1995): K-Ar ages of the felsic volcanism and its significance on volcanostratigraphy and kaolin mineralization at the Hiraki mine, Hyogo prefecture, SW Japan. Res. Geol., **45**, 341 ~ 345.

Korzhinskii, D. S. (1970): *Theory of Metasomatic Zoning*. (trans. J. Agrell). Clarendon Press, pp. 162.

Kulla, J. B. and Anderson, T. F. (1978): Experimental oxygen isotope fractionation between kaolinite and water. In: "Short Papers of the Fourth International Conference, Geochronology, Cosmochronology, Isotope Geology 1978", R. E. Zartman, Ed., U. S. Geol. Surv. Open-File Report 78-701, 234 ~ 235.

Lichtner, P. C. (1991): The quasi-stationary state approximation to fluid-rock reaction: Local equilibrium revisited. Advances in Phys. Geochem., **8**, 454 ~ 562.

Lichtner, P. C. and Balashov, V. N. (1993): Metasomatic zoning: Appearance of ghost zone in the limit of pure advective mass transport. Geochim. Cosmochim. Acta, **57**, 369 ~ 387.

Lindgren, W. (1925): Metasomatism. Geol. Soc. Am. Bull., **36**, 247 ~ 261.

MacLean, W. H. (1984): Geology and ore deposits of the Matagami district. Can. Inst. Min. Met. Sp. Vol., **34**, 483 ~ 495.

MacLean, W. H. (1990): Mass change calculations in altered rock series. Mineral. Deposita, **25**, 44 ~ 49.

MacLean, W. H. and Kranidiotis, P. (1987): Immobile elements as monitor of mass transfer in hydrothermal alteration: Phelps Dodge massive sulfide deposit, Matagami, Quebec. Econ. Geol., **82**, 951 ~ 962.

MacLean, W. H. and Hoy, L. (1991): Geochemistry of hydrothermally altered rocks at the Horna mine, Noranda, Quebec. Econ. Geol., **86**, 506 ~ 528.

Marumo, K., Nagasawa, K and Kuroda, Y. (1980): Mineralogy and hydrogen isotope geochemistry of clay minerals in the Ohnuma geothermal area, northeastern Japan. Earth Planet. Sci. Lett., **47**, 255 ~ 262.

Matsushita, Y., Goldsmith, J. R., and Clayton, R. N. (1979): Oxygen isotopic fractionation in the system quartz - albite - anorthite - water. Geochim. Cosmochim. Acta, **43**, 1131 ~ 1140.

Mattigod, S. V. and Sposito, G. (1978): Improved method for estimating standard free energies of formation ($\delta G_{f,298.15}$) of smectites. Geochim. Cosmochim. Acta, **42**, 1753 ~ 1762.

Merino, E. and Ransom, B. (1982): Free energies of formation of illite solid solutions and their compositional dependence. Clay Miner., **30**, 29 ~ 39.

Meyer, C., and Hemley, J. J. (1967): Wall rock alteration. In: "Geochemistry of Hydrothermal Ore Deposits", H. L. Barnes, Ed., Holt, Rinehart and Winston, New York, 166 ~ 235.

Mizota, C. and Kusakabe, M. (1994): Spatial distribution of δD-$\delta^{18}O$ values of surface and shallow groundwaters from Japan, south Korea and east China. Geochem. Jour., **28**, 387 ~ 410.

Montaya, J. W., and Hemley, J. J. (1975): Activity relations and stabilities in alkali feldspar and mica alteration reactions. Econ. Geol., **70**, 577 ~ 583.

Murowchick, J. B. (1992): Marcasite inversion and the petrographic determination of pyrite ancestry. Econ. Geol., **87**, 1141 ~ 1152.

Murowchick, J. B. and Barnes, H. L. (1988): Marcasite precipitation from hydrothermal solutions. Geochim. Cosmochim. Acta, **50**, 2615 ~ 2629.

Nagao, K., Nishido, H., Itaya, T. and Ogata, K. (1984): An age determination by K-Ar method. Bull. Hiruzen Res. Inst., Okayama Univ. Sci., **8**, 19~38 *

Nriagu, J. O. (1975): Thermochemical approximations for clay minerals. Amer. Mineral., **60**, 834 ~ 839.

Nozawa, T. (1975): Radiometric age map of Japan - Granitic rocks (1:2,000,000). Geol. Surv. Japan.

Okudaira, T., Hayazaka, Y., Hoshino, K. and Ikeda, K. (1993): Quantitative analysis of the trace elements in silicate rocks by X-ray fluorescence method. Earth Science, **47**, 439 ~ 444 .*

Otofuji, Y., Matsuda, T. and Nohda, S. (1986): Brief review of Miocene opening of the Japan sea: Paleomagnetic evidence. In: "Opening of the Japan Sea", K. Hiraoka and M. Torii, Eds., T. Geomag. Geoelec., **38**, 287 ~ 294.

Ozaki, M and Matsuura, H. (1987): Geology of the Sanda district: Quadrangle series, scale 1: 50,00, Tokyo (11) No. 37. Geol. Surv. Japan.*

Pascal, M. L. and Anderson, G. M. (1989): Speciation of Al, Si, and K in supercritical solution: Experimental study and interpretation. Geochim. Cosmochim. Acta, **53**, 1843 ~ 1855.

Pearce, J. A. and Cann, J. R. (1971): Ophiolite origin investigated by discriminant analysis using Ti, Zr and Y. Earth Planet. Sci. Lett., **12**, 339 ~ 349.

Rising, B. A. (1973): Phase relation among pyrites, marcasites and pyrrhotite below 300° C. Unpublished, Ph. D. Thesis, The Pennsylvania State University, 192 p.

Robie, R. A., Hemingway, B. S., and Fisher, J. R. (1978): Thermodynamic properties of minerals and related substances at 298.15 K and 1 bar and at higher temperatures. U. S. Geol. Surv. Bull., **1452**, 456 p.

Routson, R. C. and Kittrick, J. A. (1971): Illite stability. Soil sci. Soc. Amer. Proc., **35**, 714 ~ 718.

Savin, S. M. and Epstein, S. (1970): The oxygen and hydrogen isotope geochemistry of clay minerals. Geochim. Cosmochim. Acta, **34**, 25 ~ 42.

Savin, S. M. and Epstein, S. (1970): The oxygen and hydrogen isotope geochemistry of ocean sediments and shales. Geochim. Cosmochim. Acta, **34**, 43 ~ 63.

Sheppard, S. M. F., Nielsen, R. L. and Taylor, H. P. Jr. (1969): Oxygen and hydrogen isotope ratios of clay minerals from porphyry copper deposits. Econ. Geol., **64**, 755 ~ 777.

Shibata, K. and Kamitani, M. (1974): K-Ar age of the Roseki deposits in the Abu District, Yamaguchi Prefecture. Bull. Geol. Surv. Japan, **25**, 323~330.*

Shibata, K., Uchiumi, S., Uto, K. and Nakagawa, T. (1984): K-Ar age results - 2- new data from the geological survey of Japan. Bull. Geol. Surv. Japan, **35**, 331 ~ 340.*

Steiger, R. H. and Jäger, E. (1977): Subcomission on geochronology: Convention on the use of decay constants in geo- and cosmo-chronology. Earth Planet. Sci. Lett., **36**, 359 ~ 362.

Steiner, A. (1968): Clay minerals in hydrothermally altered rocks at Wairakei, New Zealand. Clay Miner., **16**, 193 ~ 213.

Stoessel, R. K. (1981): Refinements in a site-mixing model for illites: local electrostatic balance and quasi-chemical approximation. Geochim. Cosmochim. Acta, **45**, 1733 ~ 1741.

Stull, D. R. and Prophet, H. (1971): *JANAF Thermochemical Tables* (2nd ed.), Washington, D. C.: National Bureau of Standards.

Suzuoki, T. and Epstein, S. (1976): Hydrogen isotope fractionation between OH-bearing minerals and waters. Geochim. Cosmochim. Acta, **40**, 1229 ~ 1240.

Tanaka, K. (1977): Geologic history. In "Geology and Mineral Resource of Japan", 3rd ed., Geol. Surv. Japan.

Tanaka, M., Taninami, S. and Oya, I. (1963): Fundamental studies on the Hiraki kaolin (I) on the geology ore deposit and mineral constitution. J. Ceram. Assoc. Japan, **71**, 187 ~ 195.*

Taninami, S. (1991): Exploration and development of the Hiraki mine, Hyogo prefecture, Japan. Mining Geol., **41**, 269-278.*

Tardy, Y. and Garrel, R. M. (1974): A method of estimating the Gibbs energies for formation of layer silicates. Geochim. Cosmochim. Acta, **38**, 1101 ~ 1116.

Tardy, Y. and Fritz, B. (1981): An ideal solution model for calculating solubility of clay minerals. Clay Miner., **16**, 361 ~ 373.

Taylor, H. P., Jr. and Epstein, S. (1962): Relationship between $^{18}O/^{16}O$ ratios in coexisting minerals of igneous and metamorphic rocks. Part 1: principles and experimental results. Geol. Soc. Am. Bull., **73**, 461 ~ 480.

Taylor, H. P. Jr. (1974): The application of oxygen and hydrogen isotopes studies to problems of hydrothermal alteration and ore deposition. Econ. Geol., **69**, 843 ~ 883.

Taylor, H. P. Jr. (1977): Water/rock interaction and the origin of H2O in granitic batholiths. J. Geol. Soc. Lond., **133**, 509 ~ 558.

Taylor, H. P. Jr. (1979): Oxygen and hydrogen isotope relationships in hydrothermal ore deposits. In "Geochemistry of Hydrothermal Ore Deposits", H. L. Barnes Ed., Second Edition, John Wiley and Sons, New York, 236 ~ 277.

Truesdell, A. H. and Christ, C. L. (1968): Cation exchange in clays interpreted by regular solution theory. Amer. J. Sci., **266**, 402 ~ 412.

Tsuzuki, Y. and Mizutani, S. (1969): Kinetics of hydrothermal alteration of sericite and its application to the study of alteration zoning. Proc. Intern. Clay Conf. 1969., **1**, 513 ~ 522.

Tsuzuki, Y. and Mizutani, S. (1971): A study of rock alteration process based on kinetics of hydrothermal experiment. Contr. Mineral. Petrol., **30**, 15 ~ 33.

Valsami, E., Cann, J. R. and Rassios, A. (1994): The mineralogy and geochemistry of a hydrothermal alteration pipe in the Orthis ophiolite, Greece. Chemical Geol., **114**, 235 ~ 266.

Walsh, M. P., Bryant, S. T., Schechter, R. S. and Lake, L. W. (1984): Precipitation and dissolution of solids attending flow through porous media. Amer. Inst. Chem. Eng. J., **30**, 317 ~ 327.

Watanabe, T., Ishiyama, D., Mizuta, T., Matsubaya, O. and Ishikawa, Y. (1994): Formation mechanism for Yano-Shokozan Nishiyama-higashi pyrophyllite deposit, Hiroshima Prefecture: Implication for the genesis of the deposit from mineralogic, fluid inclusion and stable isotope data. Resource Geol., **44**, 111 ~ 123.*

White, D. E., Barnes, I. and O'Neil, J. R. (1973): Thermal and mineral waters of nonmeteoric origin, California Coast Ranges. Bull. Geol. Soc. America, **84**, 547 ~ 560.

Winchester, J. A. and Floyd, P. A. (1976): Geochemical magma type discrimination: application to altered and metamorphosed basic igneous rocks. Earth Planet. Sci. Lett., **28**, 459 ~ 469.

Winchester, J. A. and Floyd, P. A. (1977): Geochemical discrimination of different magma series and their differentiation products using immobile elements. Chem. Geol., **56**, 325 ~ 343.

Wollast, R. (1967): Kinetics of the alteration of K-feldspar in buffered solution at low temperature. Geochim. Cosmochim. Acta., **31**, 635 ~ 648.

Yamada, N. (1977): Late Mesozoic and Paleogene. In "Geology and Mineral Resource of Japan", 3rd ed., Geol. Surv. of Japan.

* in Japanese with English abstracts.

KO KO MYINT

Department of Geology, University of Mandalay, University P. O., Mandalay, Union of Myanmar.

Present address — **Department of Earth and Planetary Systems Science, Faculty of Science, Hiroshima University, Higashihiroshima 739, Japan.**

EXPLANATION OF PLATES

Plate I. (A) Chalcedonic quartz and feldspar spherulites in the uppermost part of rhyolite. (PPL)
(B) The same view under crossed Nicol.

Plate II. (A) Partially altered axiolites in the uppermost part of rhyolite. Needles are made up of quartz and feldspar. (PPL)
(B) The same view under crossed Nicol.

Plate III. (A) A feldspar phenocryst in the uppermost part of rhyolite, altered to sericite, showing dirty appearance under plane polarized light.
(B) The same view under crossed Nicol.

Plate IV. (A) Nature of alteration in the non-welded tuff. Although groundmass quartz and feldspar grains altered greater or lesser degree to kaolinite and quartz aggregates, most of chalcedonic quartz spherulites remain unchanged. (PPL)
(B) The same view under crossed Nicol.

Plate V. (A) Subhedral pyrite in the orebody. (Reflected light)
(B) Anhedral pyrite in the orebody. (Reflected light)

Plate VI. (A) Anhedral marcasite in the orebody. (Reflected light)
(B) The same view under crossed Nicol.

Plate VII. (A) Welding structure in the Hiraki welded tuff. (PPL)
(B) The same view under crossed Nicol.

Plate VIII. (A) Volcanic quartz showing dissolved boundary and inclusions. Note the overgrowth of hydrothermal quartz. (PPL)
(B) Two-phase (glass and gas) inclusions in the same volcanic quartz grain. (PPL)

Plate I

(A)

0 2 mm

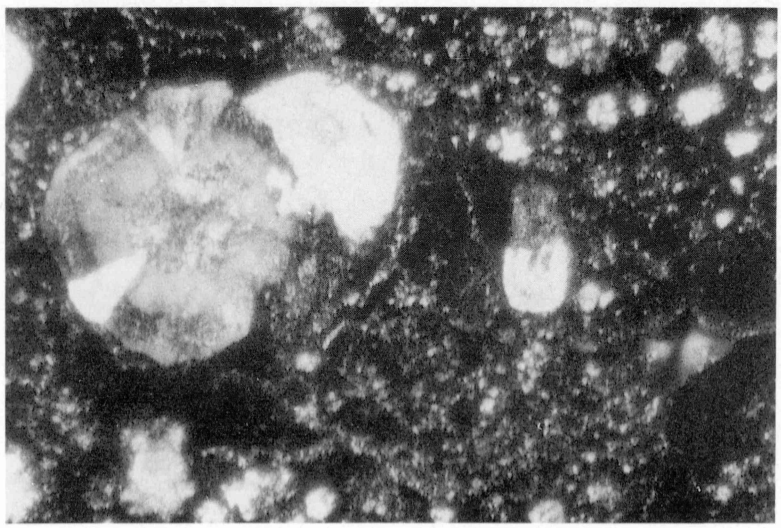

(B)

Plate II

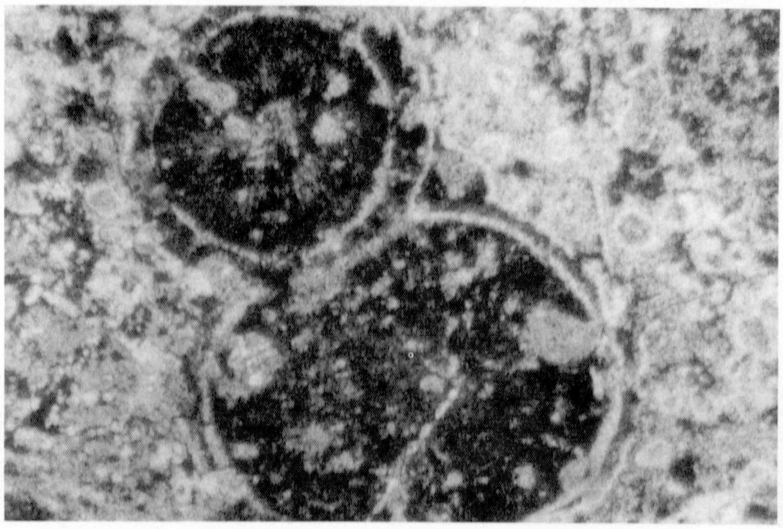

(A)

0 2 mm

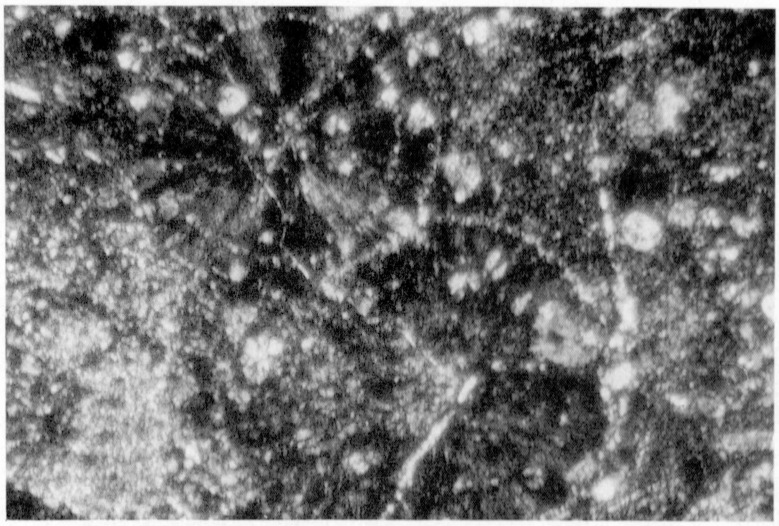

(B)

Plate III

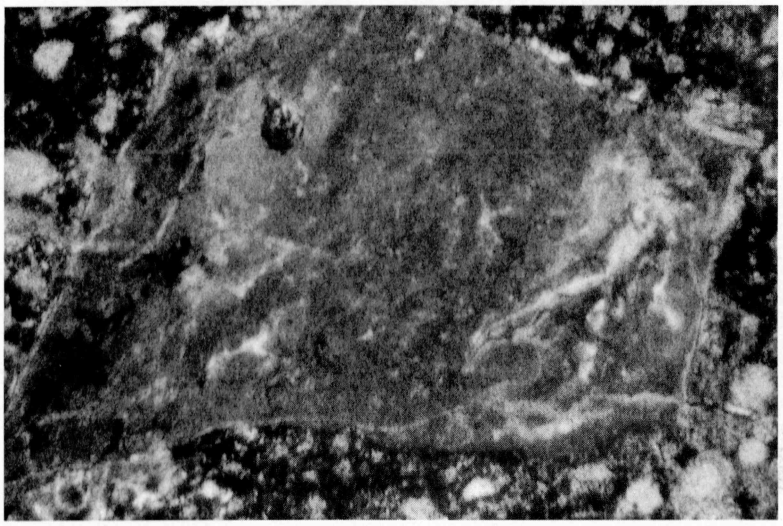

(A)

0 2 mm

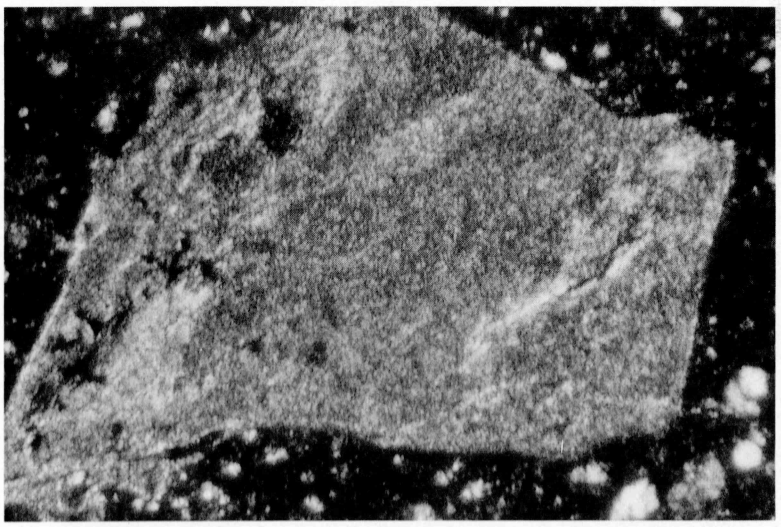

(B)

Plate IV

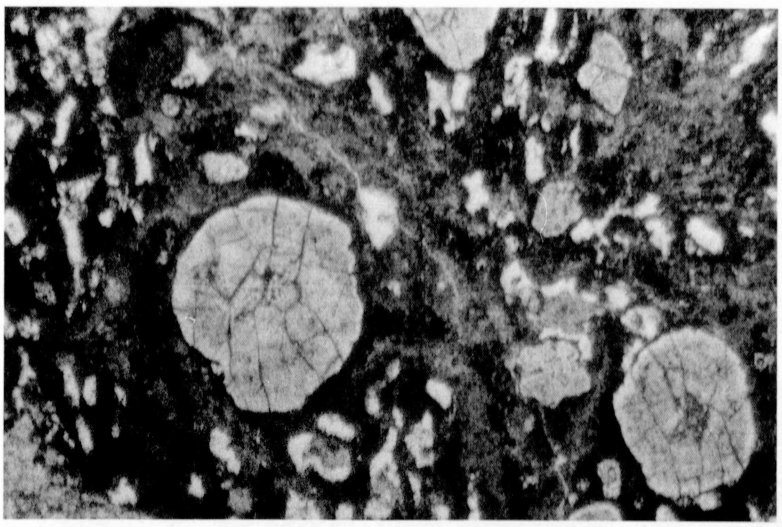

(A)

0 2 mm

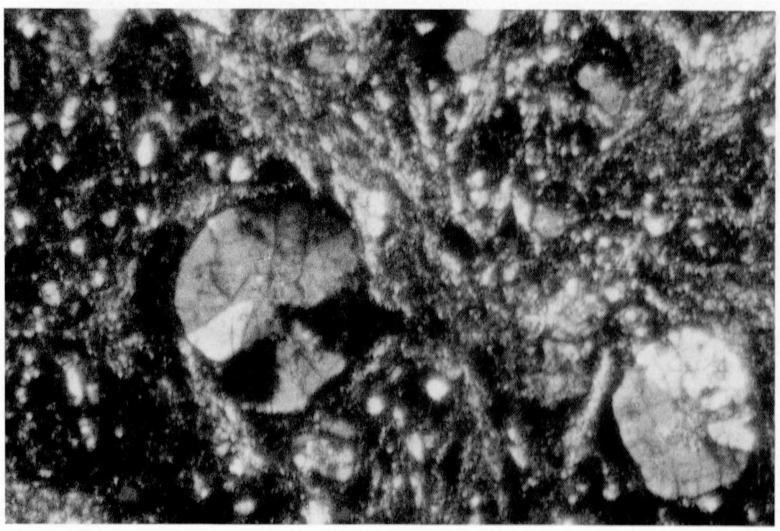

(B)

Plate V

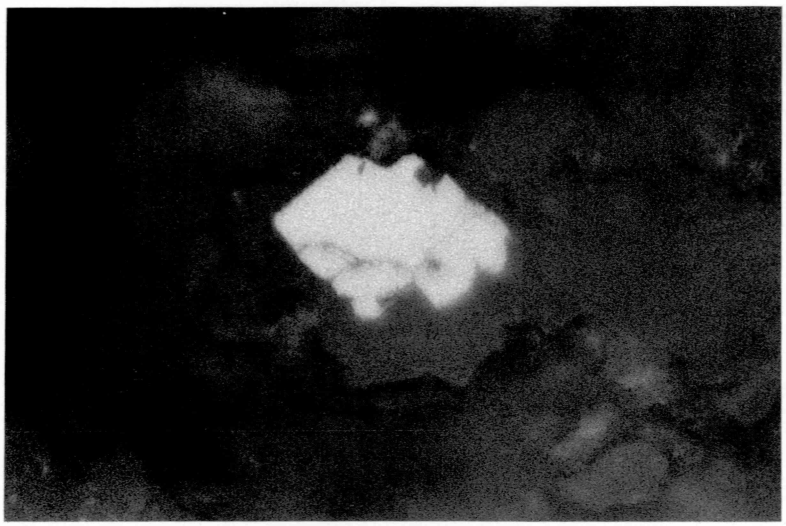

(A)

0 1 mm

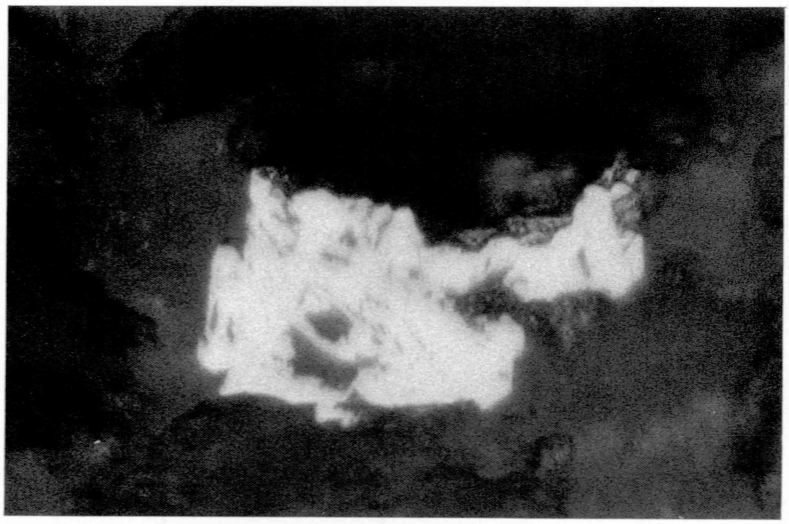

(B)

Plate VI

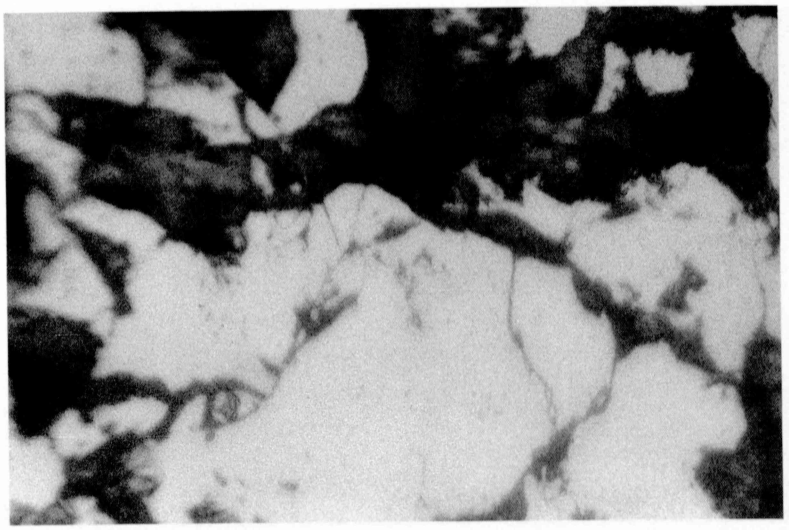

(A)

0 1 mm

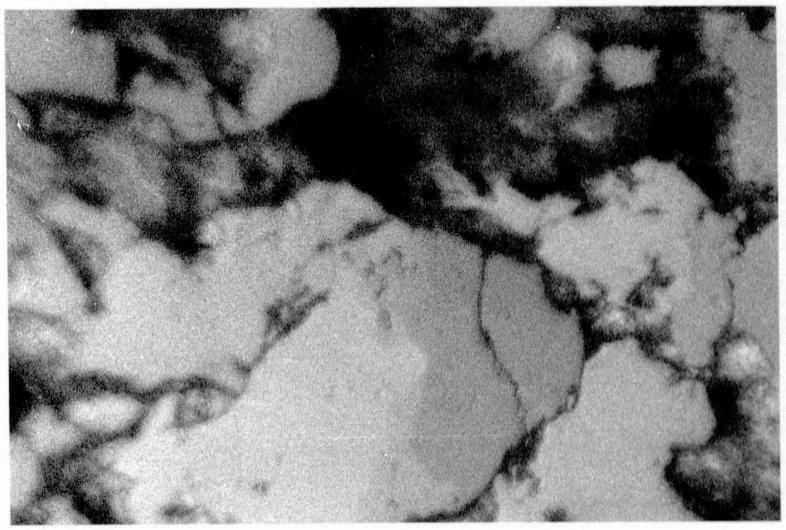

(B)

Plate VII

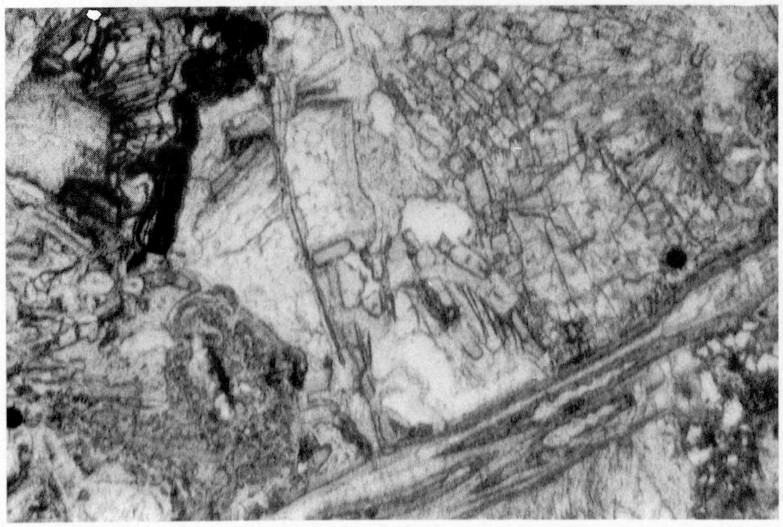

(A)

0 2 mm

(B)

Plate VIII

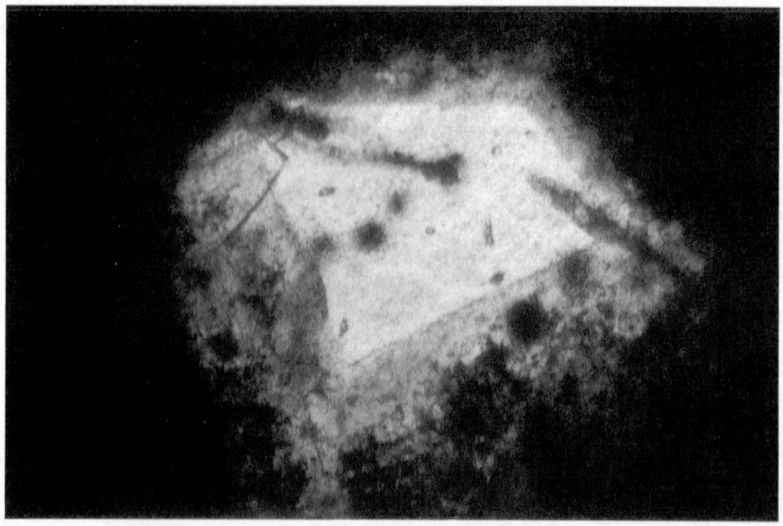

(A)

0 1 mm

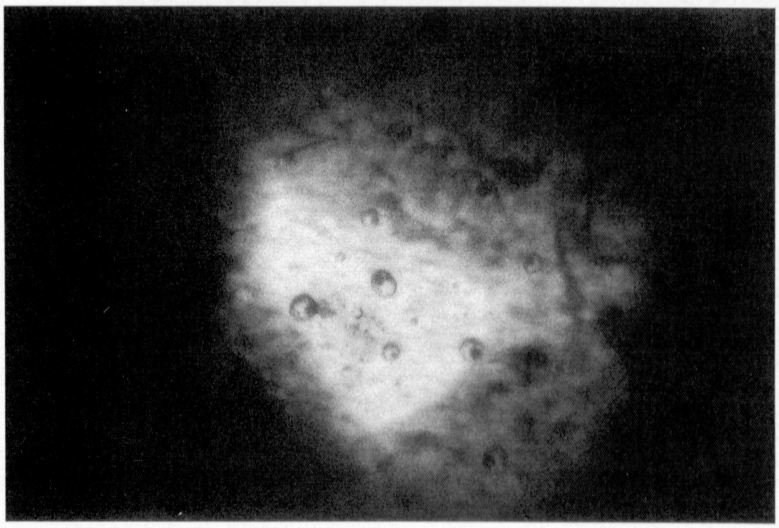

(B)